

AD-A034 552

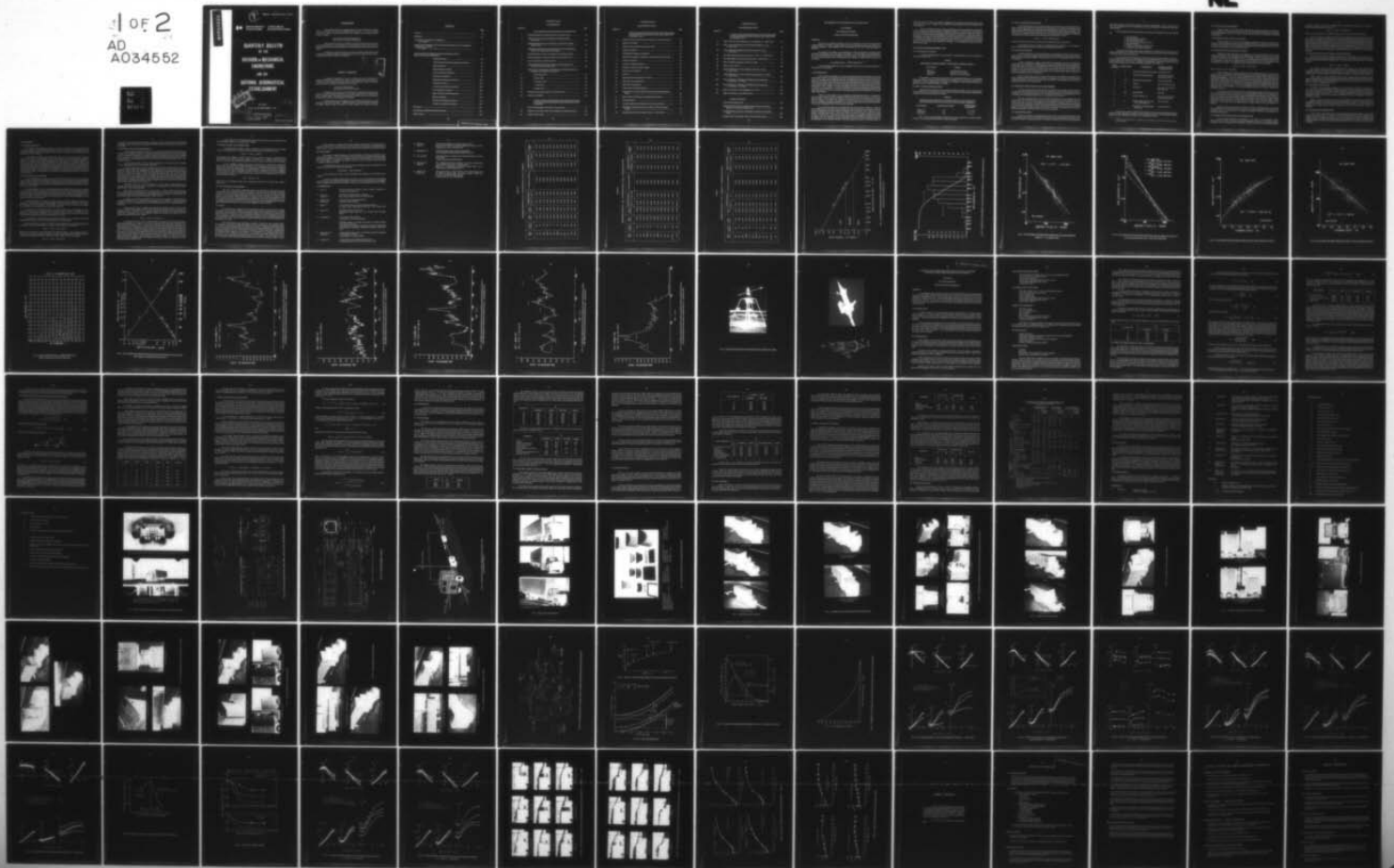
NATIONAL RESEARCH COUNCIL OF CANADA OTTAWA (ONTARIO) --ETC F/G 13/6
QUARTERLY BULLETIN OF THE DIVISION OF MECHANICAL ENGINEERING AN--ETC(U)
SEP 76

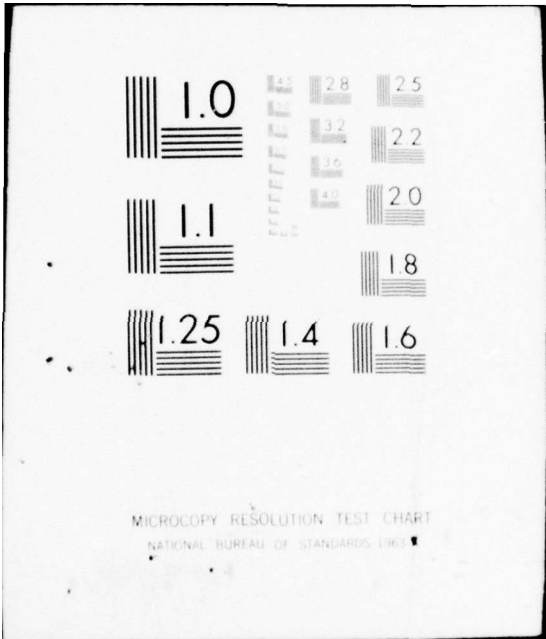
UNCLASSIFIED

DME/NAE-1976(3)

NL

1 of 2
AD
A034552





MICROCOPY RESOLUTION TEST CHART
NATIONAL BUREAU OF STANDARDS-1963-A

ADA 034552

7

REPORT NO. DME/NAE-1976(3)



National Research Council Canada

Conseil national de recherches Canada

6

QUARTERLY BULLETIN
OF THE
DIVISION OF MECHANICAL
ENGINEERING
AND THE
NATIONAL AERONAUTICAL
ESTABLISHMENT

DDC
RECEIVED
JAN 19 1977

OTTAWA

1 JULY TO 30 SEPTEMBER, 1976

12/13 pp.

11 30 Sep 76

DISTRIBUTION STATEMENT A
Approved for public release:
Distribution Unlimited

244 050 LB

ISSN 0047-9055

FOREWORD

The Quarterly Bulletin is designed primarily for the information of Canadian industry, Universities, and Government Departments and agencies. It provides a regular review of the interests and current activities of two Divisions of the National Research Council of Canada:

The Division of Mechanical Engineering
The National Aeronautical Establishment

Some of the work of the two Divisions comprises classified projects that may not be freely reported and contractual projects of limited general interest. Other work, not generally reported herein, includes calibrations, routine analysis and the testing of proprietary products.

Comments or enquiries relating to any matter published in this Bulletin should be addressed to: *DME/NAE Bulletin, National Research Council of Canada, Ottawa, Ontario, K1A 0R6*, mentioning the number of the Bulletin.

DISTRIBUTION AVAILABILITY CODES	
DME AVAIL. and SPECIAL	
A	

AVANT-PROPOS

Le Bulletin Trimestriel est conçu en premier lieu pour l'information de l'Industrie Canadienne, des Universités, des Agences et des Départements Gouvernementaux. Il fournit une revue régulière des intérêts et des activités actuelles aux quels se consacrent deux Divisions du Conseil National de Recherches du Canada:

Division de Génie Mécanique
Etablissement Aéronautique National

Quelques uns des travaux des deux Divisions comprennent des projets classifiés qu'on ne peut pas rapporter librement et des projets contractuels d'un intérêt général limité. D'autres travaux, non rapportés ci-après dans l'ensemble, incluent des étalonnages, des analyses de routine, et l'essai de produits de spécialité.

Veuillez adresser tout commentaire et toute question ayant rapport à un sujet quelconque publié dans ce Bulletin à: *DME/NAE Bulletin, Conseil National de Recherches du Canada, Ottawa, Ontario, K1A 0R6*, en faisant mention du numéro du Bulletin.

CONTENTS

	Page
Foreword	(i)
Illustrations	(iv)
The Airborne Concentration of Falling Snow, J.R. Stallabrass	1
A Wind Tunnel Investigation into the Fuel Savings Available from the Aerodynamic Drag Reduction of Trucks K.R. Cooper	31
 <i>Current Projects of the Division of Mechanical Engineering and the National Aeronautical Establishment:</i>	
Analysis Laboratory	89
Control Systems and Human Engineering Laboratory	91
Engine Laboratory	92
Flight Research Laboratory	94
Fuels and Lubricants Laboratory	96
Gas Dynamics Laboratory	99
High Speed Aerodynamics Laboratory	102
Hydraulics Laboratory	104
Low Speed Aerodynamics Laboratory	107
Low Temperature Laboratory	109
Marine Dynamics and Ship Laboratory	111
Railway Laboratory	112
Structures and Materials Laboratory	114
Unsteady Aerodynamics Laboratory	116
Publications	117
Aeronautical and Mechanical Engineering Library	124
Uplands Library	125

CONTENTS (Cont'd)

ILLUSTRATIONS

Figure No.		Page
THE AIRBORNE CONCENTRATION OF FALLING SNOW		
1	Relationship Between Visibility and Snow Accumulation Rate	15
2	Frequency of Occurrence and Exceedance Probability of Snow Concentration	16
3	Relationship Between Snow Concentration and Observed Visibility — All Snow Types	17
4	Relationship Between Snow Concentration and Observed Visibility for Various Snow Crystal Types and Groupings	18
5	Relationship Between Snow Concentration and Videograph Output	19
6	Relationship Between Observed Visibility and Videograph Output	20
7	Snow Concentration vs Temperature Plot	21
8	Relationship Between Snow Concentration and Precipitation Rate, and Visibility and Precipitation Rate	22
Record of Snow Concentration as Deduced from Videograph Output, and Comparison with Measured Concentration —		
9	20 December 1973	23
10	21 March 1974	24
11	16 December 1974	25
12	7 March 1975	26
13	19 March 1976	27
14	Whirling Arm Apparatus Mounted on Laboratory Roof	28
15	Cyclone Snow Sampler	29
A WIND TUNNEL INVESTIGATION INTO THE FUEL SAVINGS AVAILABLE FROM THE AERODYNAMIC DRAG REDUCTION OF TRUCKS		
1	Wind Tunnel Installation with Model on Ground Plane	51
2a	Details of Ground Plane, Wind Tunnel Installation and Model Mounting	52
2b	Details of Model Trailer	53

CONTENTS (Cont'd)

ILLUSTRATIONS (Cont'd)

Figure No.		Page
	A WIND TUNNEL INVESTIGATION INTO THE FUEL SAVINGS AVAILABLE FROM THE AERODYNAMIC DRAG REDUCTION OF TRUCKS (Cont'd)	
3	Definition of Forces, Moments and the Body Axis Co-Ordinate System	54
4	Baseline Truck Models	55
5	Add-On Devices and Trailer Nose Shapes Tested	56
6	Airglide Air Deflector	57
7	General Motors Dragfoiler Air Deflector	58
8	Rudkin-Wiley Airshield Air Deflectors, Vortex Stabilizer and Gap Seal	59
9	Uniroyal Air Deflector	60
10	University of Maryland Deflector	61
11	Original and Improved Deflector Angles	62
12	Aeroboost Corner Fairings	63
13	Nose Cone	64
14	Systems Science and Software (S ³) Airvane	65
15	Trailer Front Face Modifications	66
16	Trailer Skirt Configurations	67
17	Corner Radius and Tail Modifications	68
18	Exploded View of Variable Radius Corners and Removable Separation Blocks	69
19	Speed at Which Aerodynamic and Rolling Drags are Equal	70
20	Fuel Requirements	70
21	Average Canadian Wind Probabilities at 10 Ft. Above the Road	71
22	Probability of Exceeding a Given Yaw Angle for a Truck Travelling 55 Mph	72
23	Characteristics of the Three Baseline Trucks (V = 225 Ft./Sec.)	73

CONTENTS (Cont'd)

ILLUSTRATIONS (Cont'd)

Figure No.		Page
	A WIND TUNNEL INVESTIGATION INTO THE FUEL SAVINGS AVAILABLE FROM THE AERODYNAMIC DRAG REDUCTION OF TRUCKS (Cont'd)	
24	Effect of Tractor-Trailer Separation for the Freightliner (V = 225 Ft./Sec.)...	74
25	Effect of Reynolds Number for the IHC 1800 Loadstar (X = 53 In., V = 225 Ft./Sec.)	75
26	White Freightliner WFT8664 with Add-On Devices (X = 53 In., V = 225 Ft./Sec.)	76
27	IHC 1800 Loadstar with Add-On Devices (X = 53 In., V = 225 Ft./Sec.)	77
28	IHC 1600 Straight Truck with Add-On Devices (V = 225 Ft./Sec.)	78
29	Effect of Deflector Inclination at Zero Yaw Angle	79
30	Effect of Corner Radius	80
31	Trailer Modifications with the Freightliner Tractor (X = 53 In., V = 225 Ft./Sec.)	81
32	Trailer Modifications with the IHC 1800 Loadstar Tractor (X = 53 In., V = 225 Ft./Sec.)	82
33a	Flow Visualization of Baseline and Modified Trucks Using Smoke (V = 50 Ft./Sec., $\psi = 0$ Deg.)	83
33b	Flow Visualization of Baseline and Modified Trucks Using Smoke (V = 50 Ft./Sec., $\psi = 0$ Deg.)	84
34	Effect of Turbulence on the Freightliner (X = 53 In.)	85
35	Effect of Turbulence on the Straight Truck	86

CURRENT PROJECTS

Self De-Icing Navigation Buoy	98
Internal Flow Studies for Low Energy Losses at Extreme Geometries: Application to a Specific Industrial Duct	100
Aeroelastic Model of the Lions' Gate Bridge in the 30-Ft. X 30-Ft. Wind Tunnel	106
Proposed Polar VII Icebreaker in the 15-Ft. Vertical Wind Tunnel	108

THE AIRBORNE BY CONCENTRATION OF FALLING SNOW

J.R. Stallabrass

Low Temperature Laboratory

Division of Mechanical Engineering

SUMMARY

The need for a greater knowledge of the mass concentration of snow in the atmosphere became apparent as the result of engine malfunctions in helicopters and resulted in the initiation of a programme designed to derive statistical snow concentration data for use in engineering design applications.

The results of five winters of data gathering at Ottawa are presented and indicate a 50% probability of exceeding a mass concentration of 0.15g/m^3 , a 10% probability of exceeding 0.6g/m^3 and a 1% probability that the concentration will exceed 1.2g/m^3 . The measurements also show that the snow mass concentration may be estimated from the visibility to within a factor of about 2 by the relation:

$$\text{Concentration (g/m}^3\text{)} = 1900 (\text{Visibility (m)})^{-1.27}$$

A back-scattering visibility meter (the Videograph) was shown to be a useful instrument for estimating snow concentration.

1.0 INTRODUCTION

Until recently there appears to have been little practical need for information on the mass concentration of snow in the atmosphere, at least at heights greater than that to which blowing snow occurs. In particular, aircraft flight through snow has presented few problems because the dry snow crystals did not adhere to the surfaces on which they impinged. However, in recent years, malfunctions of the gas turbine engines of certain helicopters have occurred as a result of snow accumulations in the engine intakes, usually as a result of stray engine heat within the intakes melting the snow just sufficiently to make it adhere; the subsequent release of these snow accumulations into the engine can have serious consequences. As a result a need exists for a statistical quantitative knowledge of the snow mass content of the air to allow the meaningful design, testing and qualification of aircraft engine intake systems.

Further, such knowledge of snow concentration finds application where it is necessary to know the snow mass flux under circumstances where the horizontal component of the flux is significant relative to the vertical flux, whether that horizontal flux is due to movement of an object (such as a surface or air vehicle), the induction of air and snow into an air intake system (such as that of a stationary gas turbine installation), or as a result of wind action (such as the accumulation of wet snow on transmission lines or communication antennae).

The vertical flux is given by the precipitation rate, data for which is based on, at best, an hourly average, but more usually a 6-hourly average. The mass concentration can, in theory, be derived from the precipitation rate but requires a knowledge of the fall velocities of the spectrum of snow particles comprising the snowfall. Unlike rain, where the terminal velocity of a drop is a known function of its size (Ref. 1) and where the drop size spectrum is reasonably correlated with rainfall rate (Refs. 2 and 3) so that liquid water content may be derived with reasonable confidence from the precipitation rate, the derivation of snow concentration from snowfall rate is unreliable because of the dependence of the terminal velocities of the snow particles not only on their size but also on

their form (Refs. 4, 5 and 6), their degree of aggregation into flakes, and their liquid water content in the case of wet snow. In addition the size spectrum is usually unknown and not necessarily related to snowfall rate.

Thus an independent and direct means of measuring snow mass concentrations was required to derive reliable snow mass concentration probability statistics. This report presents a tentative concentration probability distribution based on measurements made in the Ottawa area over a period of five years, and thus extends the preliminary data presented in Reference 11. Since the method of measurement used does not lend itself readily to routine measurements, the relationships between the concentration measurements and observed visibility and between the concentration and the output of a back-scatter visibility meter (Videograph) are given, so that concentration may be estimated either from the routinely recorded parameter of visibility, or if a Videograph visibility meter is available, from its output.

2.0 EXISTING SNOW MEASUREMENT DATA

2.1 Snow Intensity and Visibility

In present observing practice, snow intensity is normally defined in terms of visibility as presented in Table I below:

TABLE I
DEFINITION OF SNOW INTENSITY AS RELATED TO VISIBILITY (REF. 7)

Snow Intensity	Visibility
light (S-)	5/8 statute mile or more
moderate (S)	reduced to 1/2 or 3/8 mile.
heavy (S+)	reduced to 1/4, 1/8 or 0 mile.

This definition of snow intensity, apart from being somewhat arbitrary, is of a qualitative nature only and has no basis in terms of either snow accumulation rate or snow concentration in the atmosphere. It has the advantage that in arriving at an estimate of snow intensity it employs the regularly measured or estimated variable of visibility.

2.2 Snow Accumulation Rate and Intensity

Using the above definition of snow intensity, Wasserman and Monte (Ref. 8), using 20 years of snow depth data for LaGuardia Field, New York City, derived the relation between average hourly snowfall and snow intensity presented in Table II:

TABLE II
AVERAGE HOURLY SNOWFALL (INCHES PER HOUR) VS. SNOW INTENSITY
(Data for LaGuardia Field, New York City, Dec. 1949 through Mar. 1969)(Ref. 8)

Snow Intensity	Average Hourly Snowfall	Probable Range of Snowfall Rate
light (S-)	0.2	0 - 0.45
moderate (S)	1.0	0.5 - 1.4
heavy (S+)	1.6	> 1.4

This is a much more meaningful interpretation of snow intensity since it relates the degree of intensity to an actual quantitative measure of the snowfall itself.

2.3 Snow Accumulation Rate and Visibility

By combining Tables I and II a tentative relation between visibility and snowfall rate may be deduced. This relation agrees with that derived by Richards (Ref. 9) for light snow intensity, but for heavy intensity suggests hourly accumulation rates approximately double those of Richards' curve which was based on twelve years of data from 1941 to 1952 for Toronto International Airport. This data has been re-analysed on the assumption that a linear relationship exists between the logarithms of visibility and snow accumulation rate, resulting in the following best fit relation:

$$\text{Log}_{10} V = -0.419 - 0.607 \text{Log}_{10} R$$

where R is Visibility in statute miles, and R is Snow Accumulation Rate in inches/hour.

This relation is shown in Figure 1. Comparing Table II with Figure 1, no discrepancy is seen to exist between the data of Richards and that of Wasserman and Monte.

2.4 Snow Mass Concentration

As already indicated, no body of data already exists pertaining to the mass concentration of snow in the air. It might be supposed that intensity and concentration are synonymous; however, intensity, being a subjective qualitative assessment, lends no clue to the quantitative measure of mass concentration.

It seems reasonable to suppose that neither the accumulation rate nor the visibility by itself is likely to be a particularly reliable indicator of snow concentration unless the prevailing snow crystal type and size are known. A knowledge of the terminal velocity of the particles and the density of the snow cover is necessary if accumulation rate is to be used, while the use of visibility which depends on the scattering of light from the snow particles (and from dust, smoke, aerosol, etc.) requires a knowledge of the scattering characteristics of ice crystals which in turn also depends on their size and type as well as their orientation.

Thus it appears that, initially at least, data on snow concentration must depend on the actual measurement of this parameter. It may then be determined, by correlation with other meteorological measurements, whether concentration data can reliably be deduced from any of these other parameters, either alone or in combination.

3.0 METHOD OF SNOW CONCENTRATION MEASUREMENT

The basic approach used to measure snow concentration was to sample a known volume of the atmosphere and to separate from it the snow for measurement of its mass. The apparatus (Fig. 14) consisted of a sampling device mounted at the end of an arm rotating in a horizontal plane at sufficient height above the surrounding surface as to be unaffected by blowing snow.

The type of sampling device used for the bulk of the data was a cyclone separator (Fig. 15) mounted with its axis aligned with the radial arm. Flow through the device ensured high catch efficiency while both cyclone and centrifugal action ensured efficient separation of the snow from the air with little chance of particle re-entrainment in the exhausting air. The separated snow was retained in the device and weighed after a given collection period (in the order of 2 to 6 minutes depending largely on intensity), so giving a measure of the average concentration during that period. A mechanical shutter was used to close the cyclone entry when not sampling.

3.1 Associated Measurements

The snow concentration measurements alone are useful in providing statistical data suitable for establishing design and test criteria applicable to aircraft (and other) apparatus sensitive to snow encounters. However, as already indicated, it is desirable to correlate the snow content measurements

with other relevant meteorological parameters recorded simultaneously, so that a means may be found for determining the snow concentration from some combination of these more easily measured parameters.

The following associated measurements were therefore made adjacent to the snow sampling site:

1. Air temperature
2. Dew point (relative humidity)
3. Wind speed and direction
4. Snow crystal type and estimate of size
5. Observed visibility
6. Output of a Videograph visibility meter*
7. Precipitation rate (water equivalent).

The heated precipitation gauge proved unreliable in its original form, and only after considerable development did it provide a few readings of precipitation rate that could be compared with concentration and visibility measurements.

Snow crystal type was observed by allowing a number of crystals or flakes to fall onto a velvet covered board. This snow crystal classification scheme of Magono and Lee (Ref. 10) was used in recording crystal type. However, for the purposes of correlating the data, many of these types were grouped together reducing the number of individual categories to 9, as follows:

TYPE CATEGORY	DESIGNATION	DESCRIPTION	MAGONO AND LEE CLASSIFICATION
1	P	Plates and Broad Branched Crystals	P1a, P1b, P1c, P7a
2	D	Dendritic and Stellar Crystals	P1d, P1e, P1f, P2a, P2b, P2c, P2d, P7b, CP1b
3	RD	Rimmed Plates and Dendrites	R1c, R1d, R2a, R2b
4	G	Graupel	R3b, R3c, R4a, R4b, R4c
5	N	Needles, etc.	N1a, N1b, N1c, N1d, N1e, N2a, N2b, N2c
6	RN	Rimmed Needles	R1a, R1b
7	C	Columns, Bullets, etc.	C1b, C1c, C1d, C1e, C1f, C2a, C2b, CP1a, CP2a
8	S	Multiple Capped Columns, Side Plane Assemblages, etc.	CP1c, S1, S2, S3
9	I	Miscellaneous, including Broken Crystals, etc.	I1, I2, I3a, I3b, I4

In most cases a variety of crystal types co-existed, but one type usually predominated; the snowfall was then categorized according to the predominant type. Where it was impossible to assign a predominant type, the sample was included in the miscellaneous (I) type.

* A back-scatter meter developed by Dr. F. Fruengel of Germany and presently manufactured in Canada by Sperry Gyroscope Ottawa Division.

4.0 ANALYSIS OF MEASUREMENTS

Because certain of the measurements were manual, requiring the agency of a human observer working normal working hours, only about 20% of the actual snowfall during the five winters was sampled. However, there is no reason to believe that this 20% did not constitute a reasonably random sample.

4.1 Probability Distribution of Snow Concentration

Figure 2 presents the frequency and probability distribution of 666 concentration measurements. It demonstrates that there is a 50% probability that during a snowfall the mass concentration will exceed 0.15g/m^3 , a 10% probability of the concentration exceeding 0.6g/m^3 , and that 1% of the time the concentration may exceed about 1.2g/m^3 .

4.2 Correlation Between Concentration and Visibility

Regression analysis techniques were applied to the snow concentration and the other measured quantities, but the only relations showing significant correlation were those between mass concentration, visibility, and Videograph output. The relation between concentration and visibility is shown in Figure 3 for snow of all types. As is to be expected from physical reasoning (Ref. 11), this relationship conforms to a log-log relationship. The regression curve of the logarithm of the concentration as a function of the logarithm of the visibility is also shown. Its equation is:-

$$\text{Log}_{10} C = 3.277 - 1.272 \text{Log}_{10} V$$

where C is in g/m^3 , and V is in metres.

Table III presents the regression results for each individual snow type, for all types combined, and for two groupings of snow types that appear to have similar regression equations. These groupings are of types 1, 7 and 8 (i.e. plates and broad branched crystals, columns and bullets, and side plane assemblages, etc.) and of all the rimed types (i.e. types 3, 4 and 6). (Type 9 (miscellaneous) matched the rimed types almost exactly but is not shown combined for consistency's sake.) The other two snow types did not combine well with any other type, although type 5 (needles) has insufficient data points (6 only) to be certain that its characteristic differs so markedly from those of the other types. The regression equations for the two groupings (and here for clarity the rimed and miscellaneous types are combined), the two nonconforming types, and for all types combined are illustrated in Figure 4.

An attempt to take relative humidity into multiple regression with visibility and concentration was not successful since it proved not to be an independent variable, but to be influenced by snow concentration. It had been thought that by taking humidity into regression that the effect of haze on the visibility observation would be largely accounted for. However, it seems likely that haze forming particles will be scoured by higher intensity snowfalls, which incidentally result in higher humidities, so that haze effects are only likely to be evident at lower snow concentrations. This would seem to be borne out by the greater degree of scatter evident at lower concentrations in Figure 3.

Except for some cases of minute ice crystals ($< 0.5 \text{ mm}$) no systematic effect due to crystal size was observed. It is likely that any effect due to size was masked by uncertainties in measurement, particularly those due to directional (i.e. spatial) and temporal variations in concentration and visibility during the sample.

4.3 Correlation Between Concentration and Videograph Output

All data points relating snow concentration to the output of the Videograph visibility meter are shown in Figure 5. Several functional relationships between the concentration and the Videograph output were attempted in the regression analysis, and of these the one giving the highest

correlation coefficient and the lowest standard error of the estimate was found to be a log-log relationship. The resulting regression equation is:-

$$\text{Log}_{10} C = 0.252 + 4.263 \text{Log}_{10} Vg$$

where C is in g/m^3 , and Vg is the Videograph output in mA. This is shown plotted in Figure 5.

Table IV presents the regression results for all the data points and for those of each individual snow type. Unlike the visibility results, there is little differentiation between the various snow types with the possible exception of type 1 (i.e. plates). Although the regression equation for snow type 4 (graupel) differs appreciably from those of the other snow types, the data points mesh moderately well with the other rimed types and so this type has not been treated separately. Accordingly, Table IV also presents the regression results for the two groupings of snow types, viz. types 2, 5, 7, 8 and 9 (all the unrimed types except plates), and types 3, 4 and 6 (the rimed types). The regression equation curves for these two groups do not differ significantly from that for all the snow types combined.

4.4 Correlation Between Observed Visibility and Videograph Output

The data collected also permitted calibration of the Videograph output in terms of observed visibility under conditions of falling snow. Data for all snow types are presented in Figure 6. Of various functional relationships attempted, the one fitting best the data points was the log/linear equation:-

$$\text{Log}_{10} V = 4.615 - 2.420 Vg$$

This equation, however, tends to underestimate the visibility at low output currents, while the log/log regression relationship (which fitted the data only slightly less well) rather seriously overestimates the visibility at high Videograph readings (i.e. the more critical low visibility end of the visibility range). Hence the log/linear relation above is considered to provide the better calibration.

Table V presents the linear regression results for Log. Visibility against Videograph Output. Again two groupings of snow types having reasonably consistent sets of data have been subjected to regression analysis. These are all the unrimed types with the exception of needles, and the two rimed types (i.e. 3 and 6) excluding graupel (type 4).

4.5 Concentration and Temperature

In Figure 7 the temperature dependence of the concentration is shown in the form of a scatter plot. No discernible relationship between maximum snow concentration and temperature is seen to exist. However, over one half of the data points (and hence half of the time that snow occurs) are within the temperature range 0 to -8°C . The highest concentrations measured occurred with a temperature between -10 and -12°C ; however, considerable filling in of the diagram is expected as more data is collected.

Figure 7 includes 19 cases of wet snow (i.e. temperature $> 0^{\circ}\text{C}$) that were not included in the regression analysis of concentration and visibility because the presence of liquid water in the snowflake matrix placed the point well outside the main body of points on the concentration vs. visibility plot. In many cases the degree of melting was such that the crystal type could not be discerned.

4.6 Concentration and Precipitation Rate

A few results were obtained from the heated precipitation gauge during the last winter covered by this report. These are shown in Figure 8 plotted against both snow concentration and visibility. The three readings of 0.39 mm/hr. were with snow type 8, whilst the remainder were obtained during a snowfall of miscellaneous type (type 9). Because of the scarcity of points and the rather large amount of scatter, little weight should be afforded the least squares relationships shown in Figure 8.

5.0 DISCUSSION

5.1 Probability Distribution

The frequency and probability statistics of snow mass concentration close to ground level are presented in Figure 2. Although the measurements were made a few feet above the ground, it is not considered that the statistics of the measured values of mass concentration will vary greatly between ground level and the cloud base.

This distribution applies to the Ottawa region over the five winters (1971-75) of measurements. A smoothing of the distribution curve is to be expected as the sampling period increases. It might also be expected that the distribution will differ with location, for example it might be expected to be biased toward higher concentrations in coastal regions and in areas in the lee of the Great Lakes, and to lower concentrations in colder sub-arctic and arctic regions. The correlation of snow concentration with other parameters such as visibility should permit the derivation of snow concentration distributions from existing meteorological records for any desired station. However, until statistical data for other regions can be amassed, it is suggested that the data for Ottawa is typical of many regions of Canada and the United States with the possible exception of those areas mentioned above.

5.2 Snow Concentration and Visibility

It seems evident from the results presented in Table III and Figures 3 and 4 that the differing light scattering characteristics of different ice crystal types do have an effect on the visual range as might be expected. However, other modifying influences, as yet not positively identified and isolated, appear to be as significant as the crystal form in causing variation in the observed visibility for a given snow mass concentration.

A marked difference in the concentration-visibility relationship between unrimed and rimed snow of the same type (cf. types 2 and 3) is evident. Two factors are probably operative, the added mass relative to the crystal dimensions resulting from the accreted rime, and the modification of the basic hexagonal form of the crystal and the resulting effect on scattering characteristics. In spite of this, the degree of riming (i.e. from snow crystals with a few frozen droplets to graupel) did not appear to have any consistent effect.

Rather surprising is the consistency evident between the widely differing crystal types 1 (plates), 7 (columns) and 8 (side plane assemblages). The large scatter (as evidenced by the value of the standard error of the estimate) in the dendritic crystal type (type 2) is thought to arise largely from unreliable visibility estimates during snow flurry conditions.

In none of the correlations was there any marked indication that the aggregation of individual snow crystals into snowflakes had any consistent effect, although it is possible that the generally poorer correlation exhibited by the stellar and dendritic type crystals (the type most commonly forming flakes) may have resulted in part from this cause.

It is perhaps not surprising that the miscellaneous category (type 9) exhibited such a high standard error of estimate in view of the portmanteau nature of this category.

If the snow type is not known, the regression results suggest that the mass concentration may be estimated from the observed visibility to within a factor of about 2.2 by the relation:

$$\text{Log}_{10} C = 3.278 - 1.272 \text{Log}_{10} V$$

However, if the snow type can be determined, an improved estimate of the concentration may in most cases be obtained. For example, if the snow type is identified as columnar (type 7) the concentration can be estimated with 95% confidence to within a factor of 1.85 by the relation:

$$\text{Log}_{10} C = 3.673 - 1.410 \text{Log}_{10} V$$

In this case, if the visibility were 1000 metres, the equation predicts a most likely snow concentration of 0.28g/m^3 , while the standard error suggests that it almost certainly will lie between the values 0.15 and 0.51g/m^3 .

5.3 Snow Concentration and Videograph Output

From the results presented in Table IV it is obvious that in the relation between mass concentration and Videograph output the snow type has less significance than when observed visibility is used to predict the concentration. One might conjecture, for example, that in the case of graupel there is an increase in the back-scatter relative to unrimed crystals while at the same time the density of the particle is correspondingly greater with the result that the mass/back-scatter ratio is substantially the same.

Also noticeable in Table IV is how well the miscellaneous snow category (type 9) correlates with the Videograph reading. This rather defies explanation!

The data points for snow type 5 (needles) lie below the mean calibration line for the remaining unrimed crystal forms, suggesting that the back-scatter from needles is lower than for the other type. This accords with Reference 12 which suggests that back-scattering from randomly oriented ice needles and columns is small, while plates and irregular types of crystals have strong back-scattering returns. It might, however, be argued that plates, in particular, are not randomly oriented but tend to fall essentially flat so that only their edges are presented to the Videograph beam, thus resulting in low back-scatter relative to their overall size. This may in fact explain why plate type crystals (type 1) generally demonstrated a lower Videograph output for a given mass concentration than other snow types (Section 4.3 and Table IV).

Conversely, rimed snow types demonstrated on the average somewhat greater back-scattering than unrimed crystals, while for graupel the Videograph output was generally slightly greater still for a given observed visibility.

The regression equation for all snow types, $\text{Log}_{10} C = 0.252 + 4.263 \text{Log}_{10} \text{Vg}$, demonstrates a slightly, but not very significantly, lower standard error in its estimate of concentration than the equation relating observed visibility to concentration. This would seem to be due mainly to the lower scatter evident at low snow concentrations (cf. Figs. 3 and 5).

Nevertheless, in spite of the possible factor of 2 error in its estimate, it is evident that the Videograph visibility meter is a useful device for estimating snow concentration. In deriving statistical distributions of snow concentration these errors will largely cancel out with a sufficient number of data points.

Close scrutiny of Figure 5 suggests that the regression equation $\text{Log}_{10} C = 0.252 + 4.263 \text{Log}_{10} \text{Vg}$ somewhat overestimates low snow concentrations and generally underestimates high concentrations. To try to adjust for this, the regression equation using concentration as the independent variable and Videograph output as the dependent variable was computed. An average of the two regression equations resulted in the relation:

$$\text{Log}_{10} C = 0.337 + 4.614 \text{Log}_{10} \text{Vg}$$

This equation has been used to compute the snow concentration from the recorded Videograph output readings for a number of snow storms showing a fairly wide range of intensities. The results are shown in Figures 9, 10, 11, 12 and 13. The short horizontal bars in these figures show the actual measured snow concentration and the period over which the measurement was made. The Videograph output was recorded each minute except for certain periods when the observer was not on duty -- at these times a 10-minute sampling interval was used. Because of the discrete sampling of this quantity, certain peaks and troughs will have been lost; however, the relatively short duration of such extremes and the relatively long response time (about 15 seconds) of the instrument to a step change in back-scatter result in very little significant information being lost by the one-minute sampling interval, and comparisons with the measured concentrations (which are averages over several minutes) should be reasonably valid.

Indeed, Figures 9 to 13 demonstrate generally good prediction of snow concentration even when fairly rapid changes in concentration are occurring.

5.4 Observed Visibility and Videograph Output

The data presented in Figure 6 allow a calibration of the Videograph in terms of visibility for snow of undefined type. The regression equation best fitting these data was found to be:

$$\text{Log}_{10} V = 4.615 - 2.420 Vg$$

which estimates the visibility to within a factor of about 2. With the exception of graupel and the miscellaneous snow category, improved estimates of visibility may be obtained if the snow type is known, or even if it can be determined whether the snow is rimed or unrimed, as Table V indicates.

In the Videograph calibration experiment conducted by the Atmospheric Environment Service (Ref. 13) a similar linear relationship between the Videograph output and the logarithm of visibility was obtained in snow (Graph 3), but with progressive deviation from linearity for visibilities greater than about 3 miles (5000 metres) in a similar manner to the present results. Direct comparison of the two sets of results is complicated by the fact that the instruments involved used different basic calibrations; however, if a simple transformation is applied to the Videograph output (Vg) from the present results as follows:

$$Vg^* = 1.23 (Vg - .16)$$

where Vg^* is the transformed output, close correspondence between the AES and NRC results is found to exist.

5.5 Snow Concentration and Temperature

The lack of any definite relationship between the measured air temperature and snow concentration is not unexpected since the temperature at ground level may bear little relationship to that at those levels at which formation and growth of the snow crystals took place. The great variation of crystal types falling concurrently on many occasions, the frequent complex crystal forms, and the occurrence of riming all attest to the variations in temperature and saturation of the air encountered by the snow particles during their lifetime. The only certain things that can be said with regard to temperature are that wet snow occurs at 0°C and above, and that the higher the temperature, the greater is the tendency for snow crystals to aggregate to form snowflakes.

5.6 General

An automatic snow sampler has been constructed in which the collected snow is melted and allowed to flow dropwise through a hypodermic needle under the influence of the centrifugal acceleration. The droplet flow is monitored photoelectrically and the resulting pulses counted over a given time period to obtain the snow concentration. Calibration of the device against the existing "manual" sampler is currently underway and indications are that the device underestimates the snow concentration by a factor of about 1.2 when a theoretical calibration based on the data of Harkins and Brown (Ref. 14) is used.

This underestimation may result from a number of causes, the most probable being: (a) evaporation: this would be particularly significant at low concentrations; (b) incomplete separation: because of heating requirements, the design of this sampler is considerably simpler than that of the cyclone separator used for manual measurements, and consequently separation of smaller snow particles from the air may not be as efficient; (c) production of small satellite drops: under the high centrifugal acceleration (approx. 40 g.) conditions of drop formation, it is possible that drop formation may not be as consistent as under static (1 g.) conditions, and small satellite drops may be produced that are not detected by the photo-detector. This is thought to be more likely to occur at low concentrations when the droplet-forming needle may not receive a continuous supply of water.

When calibration is complete, this automatic sampler will provide not only continuous concentration histories of all snowfall events at its location, but also, because its sampling period is shorter (about 1 minute), more fine detail of these events than is possible with the manual method.

6.0 CONCLUSIONS

The results of statistical analysis on the measurements of snow mass concentration over a 5-winter period suggest, at least for the Ottawa region, a modal mass concentration of about $0.2\text{g}/\text{m}^3$, although the frequency of occurrence is relatively constant for all concentrations from about $0.06\text{g}/\text{m}^3$ to about $0.6\text{g}/\text{m}^3$. The median concentration is shown to be about $0.15\text{g}/\text{m}^3$, and the maximum concentration approaches $2.0\text{g}/\text{m}^3$.

The measurements also show that snow mass concentration may be estimated from the visibility to within a factor of about 2 by the relation:

$$\text{Concentration} \approx 1900 (\text{Visibility})^{-1.27}$$

If the particular snow type is known, generally better estimates of concentration can be obtained.

Use of the Videograph visibility meter has shown it to be a useful instrument for estimating snow concentration. By appropriately scaling the read-out meter, a direct indication of concentration could be obtained, with about the same degree of accuracy as that obtained from observed visibility.

7.0 REFERENCES

1. Gunn, R. *The Terminal Velocity of Fall for Water Droplets in Stagnant Air.* J. Meteor. 6, 1948, 243-248.
2. Laws, J.O.
Parsons, D.A. *The Relation of Raindrop-Size to Intensity.* Trans. Amer. Geophys. Union, 24, 1943, 452-460.
3. Marshall, J.S.
Palmer, W.M. *The Distribution of Raindrops with Size.* J. Meteor. 5, 1948, 165-166.
4. Magono, C. *On the Falling Velocity of Solid Precipitation Elements.* Sci. Repts. of the Yokohama Nat. Univ., Sec. 1, No. 3, 1954, 33-40.
5. Brown, S.R. *Terminal Velocities of Ice Crystals.* Atmospheric Science Paper No. 170, Colorado State University, 1970.
6. Heymsfield, A. *Ice Crystal Terminal Velocities.* J. Atmos. Sci., V. 29, 1972, 1348-1357.
7. *MANOBS. Manual of Standard Procedures for Surface Weather Observing and Reporting.* Sixth Edition, incorporating Amendments 1 through 5. Department of Environment, Atmospheric Environment Service, Toronto, Ont., 1974.
8. Wasserman, S.E.
Monte, D.J. *A Relationship between Snow Accumulation and Snow Intensity as Determined from Visibility.* J. Appl. Meteor., 11, 1972, 385-388.
9. Richards, T.L. *An Approach to Forecasting Snowfall Amounts.* Canadian Met. Branch, Technical Circular 2421, 1954.

10. Magono, C.
Lee, C.W. *Meteorological Classification of Natural Snow Crystals.*
Journal of the Faculty of Science, Hokkaido University, Ser. VII
(Geophysics), 11, No. 4, 1966, 321-335.
11. Stallabrass, J.R. *Preliminary Measurements of Snow Concentration.*
N.R.C. Laboratory Technical Report LTR-LT-42, 1972.
12. Liou, Kuo-nan *Light Scattering by Ice Clouds in the Visible and Infrared: A Theoretical Study.*
J. Atmos. Sciences, 29, 1972, 524-526.
13. Sheppard, B.E.
Clink, W.L. *The Videograph Calibration Experiment at Toronto International Airport 23 November 1970 to 31 October 1971.*
Report TR 1, Atmospheric Environment Service, Dept. of the Environment, Toronto, February 1974.
14. Harkins, W.D.
Brown, F.E. *The Determination of Surface Tension (Free Surface Energy), and the Weight of Falling Drops: The Surface Tension of Water and Benzene by the Capillary Height Method.*
J. Amer. Chem. Soc., 41, 1919, 499-524.

TABLE III
REGRESSION RESULTS: LOG₁₀ CONCENTRATION VS. LOG₁₀ VISIBILITY

Snow Type	No. of Samples	Mean Log ₁₀ C	Mean Log ₁₀ V	Standard Deviation		Correlation Coefficient r	Regression Equation		Standard Error
				Log ₁₀ C	Log ₁₀ V		Coefficient	Constant	
ALL	647	-0.847	3.241	0.477	0.349	-0.932	-1.272	3.278	0.173
1(P)	38	-1.059	3.389	0.460	0.309	-0.970	-1.442	3.827	0.112
2(D)	60	-1.243	3.437	0.474	0.272	-0.920	-1.601	4.257	0.186
3(RD)	139	-0.805	3.206	0.508	0.403	-0.954	-1.202	3.049	0.151
4(G)	52	-1.106	3.525	0.388	0.303	-0.889	-1.140	2.913	0.178
5(N)	6	-0.866	3.090	0.482	0.458	-0.972	-1.022	2.292	0.114
6(RN)	53	-0.800	3.268	0.419	0.315	-0.915	-1.218	3.180	0.169
7(C)	57	-0.878	3.229	0.463	0.315	-0.958	-1.410	3.673	0.133
8(S)	160	-0.738	3.171	0.359	0.248	-0.926	-1.341	3.513	0.136
9(I)	82	-0.582	3.050	0.460	0.366	-0.916	-1.154	2.936	0.185
1,7,8	255	-0.817	3.217	0.415	0.283	-0.946	-1.389	3.650	0.134
3,4,6	244	-0.868	3.287	0.481	0.386	-0.939	-1.170	2.979	0.165

TABLE IV
REGRESSION RESULTS: LOG₁₀ CONCENTRATION VS. LOG₁₀ VIDEOGRAPH OUTPUT

Snow Type	No. of Samples	Mean Log ₁₀ C	Mean Log ₁₀ Vg	Standard Deviation		Correlation Coefficient r	Regression Equation		Standard Error
				Log ₁₀ C	Log ₁₀ Vg		Coefficient	Constant	
ALL	634	-0.857	-0.260	0.475	0.104	0.937	4.263	0.252	0.167
1(P)	39	-1.059	-0.350	0.460	0.109	0.919	3.891	0.302	0.181
2(D)	60	-1.243	-0.354	0.474	0.098	0.945	4.570	0.372	0.155
3(RD)	136	-0.810	-0.237	0.512	0.110	0.951	4.442	0.241	0.159
4(G)	52	-1.106	-0.297	0.388	0.095	0.931	3.794	0.020	0.142
5(N)	6	-0.866	-0.281	0.482	0.107	0.932	4.211	0.315	0.174
6(RN)	52	-0.808	-0.247	0.420	0.091	0.938	4.318	0.261	0.145
7(C)	57	-0.878	-0.263	0.463	0.097	0.909	4.314	0.257	0.193
8(S)	160	-0.738	-0.235	0.359	0.072	0.922	4.604	0.346	0.139
9(I)	73	-0.622	-0.213	0.465	0.100	0.951	4.395	0.316	0.144
2,5,7,8,9	356	-0.824	-0.256	0.467	0.099	0.945	4.451	0.316	0.153
3,4,6	240	-0.874	-0.252	0.483	0.105	0.946	4.338	0.219	0.157

TABLE V
REGRESSION RESULTS: LOG₁₀ VISIBILITY VS. VIDEOGRAPH OUTPUT

Snow Type	No. of Samples	Mean Log ₁₀ V	Mean Vg	Standard Deviation		Correlation Coefficient r	Regression Equation		Standard Error
				Log ₁₀ V	Vg		Coefficient	Constant	
ALL	634	3.248	0.565	0.348	0.129	-0.900	-2.420	5.615	0.151
1(P)	38	3.389	0.460	0.309	0.110	-0.901	-2.546	4.560	0.134
2(D)	60	3.437	0.455	0.272	0.108	-0.909	-2.302	4.483	0.113
3(RD)	136	3.209	0.598	0.407	0.147	-0.952	-2.646	4.792	0.125
4(G)	52	3.525	0.517	0.303	0.117	-0.819	-2.128	4.626	0.174
5(N)	6	3.090	0.538	0.458	0.131	-0.980	-3.435	4.936	0.092
6(RN)	52	3.275	0.578	0.314	0.120	-0.918	-2.407	4.665	0.125
7(C)	57	3.229	0.559	0.315	0.121	-0.911	-2.374	4.555	0.130
8(S)	160	3.171	0.589	0.248	0.091	-0.861	-2.363	4.564	0.126
9(I)	73	3.073	0.627	0.367	0.126	-0.912	-2.657	4.738	0.150
1,2,7,8,9	388	3.224	0.558	0.317	0.123	-0.906	-2.326	4.522	0.134
3,6	188	3.227	0.593	0.384	0.140	-0.945	-2.600	4.768	0.125

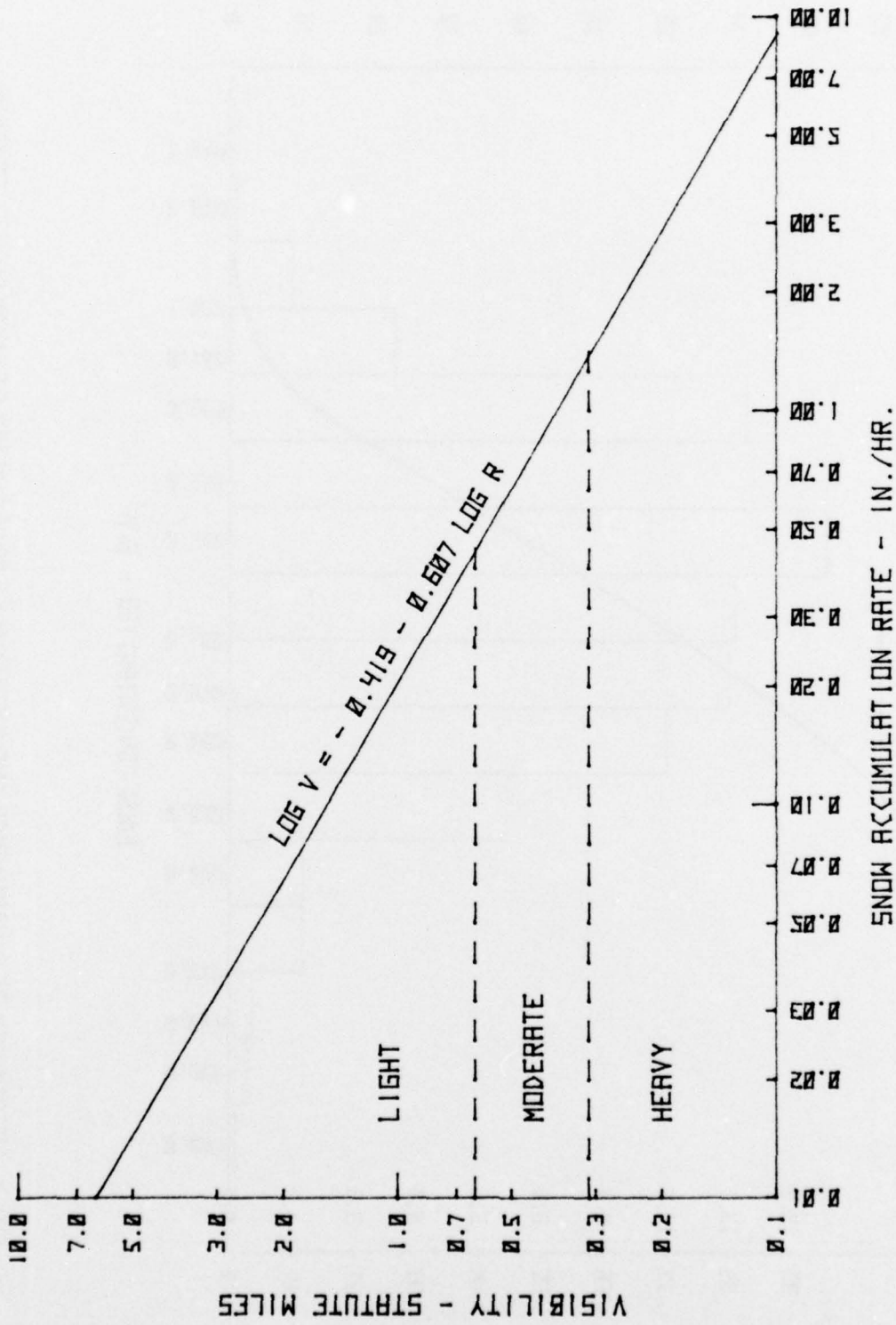


FIG. 1: RELATIONSHIP BETWEEN VISIBILITY AND SNOW ACCUMULATION RATE

(BASED ON DATA OF RICHARDS, REF. 9)

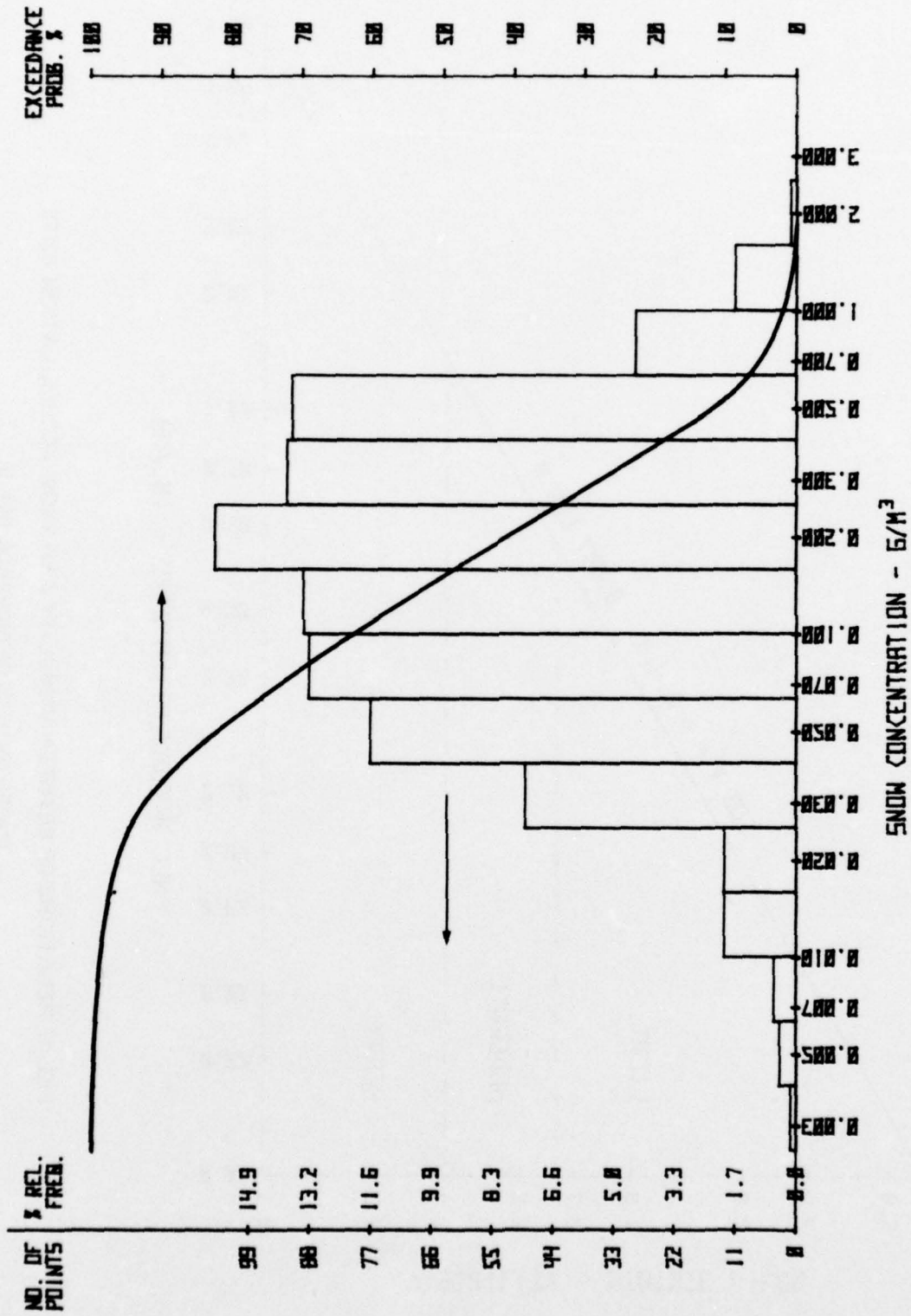


FIG. 2: FREQUENCY OF OCCURRENCE AND EXCEEDANCE PROBABILITY OF SNOW CONCENTRATION

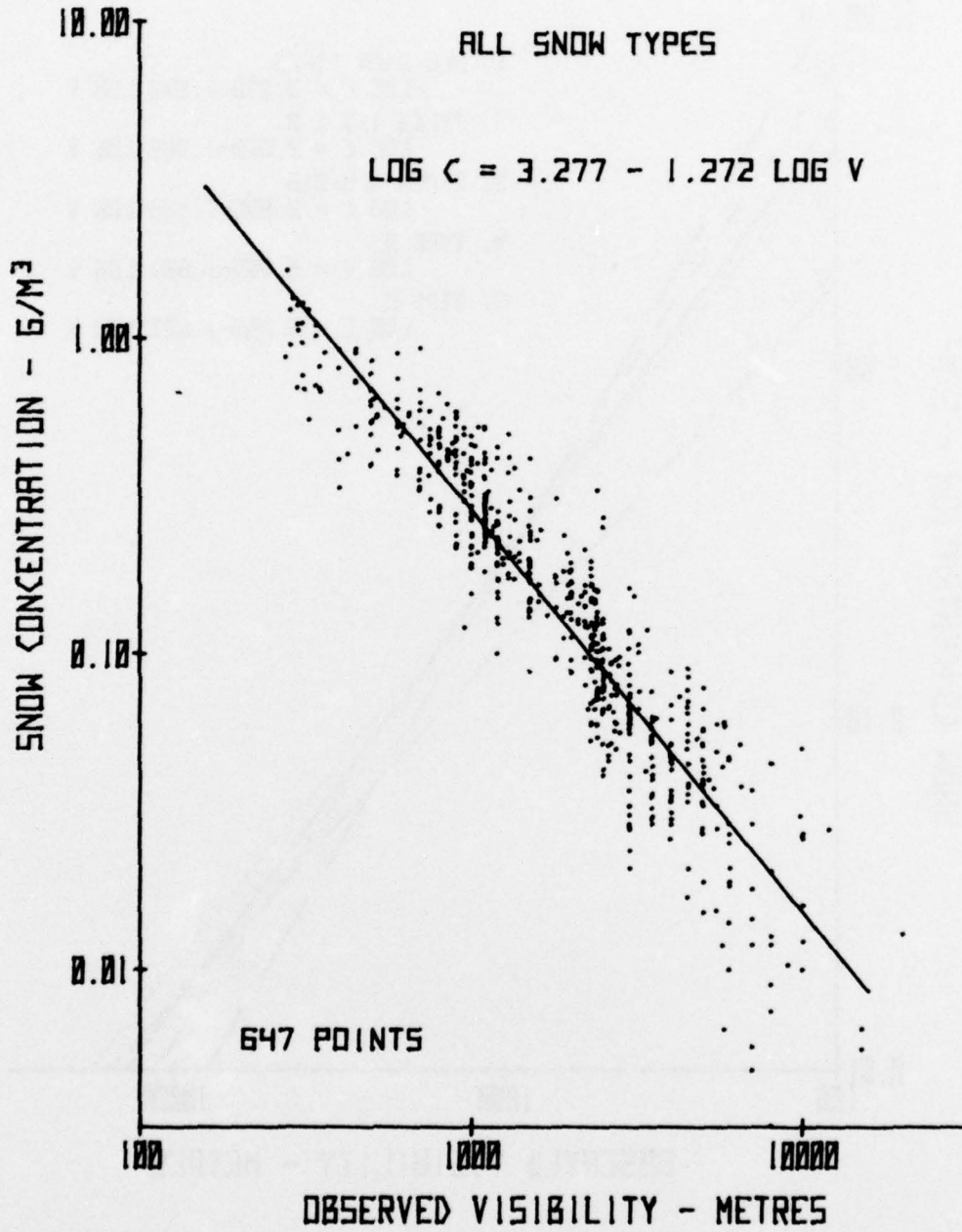


FIG. 3: RELATIONSHIP BETWEEN SNOW CONCENTRATION AND OBSERVED VISIBILITY - ALL SNOW TYPES

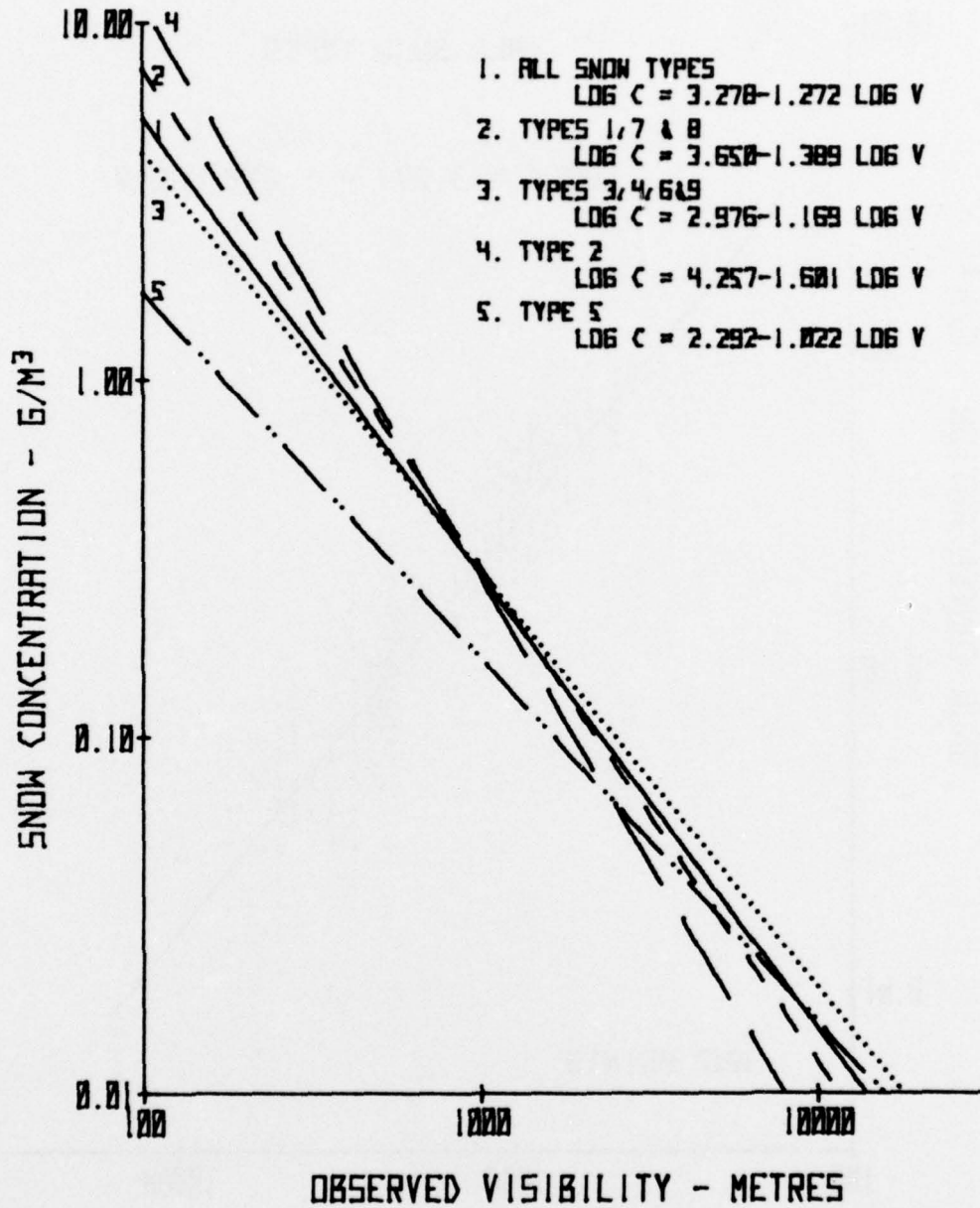


FIG. 4: RELATIONSHIP BETWEEN SNOW CONCENTRATION AND OBSERVED VISIBILITY FOR VARIOUS SNOW CRYSTAL TYPES AND GROUPINGS

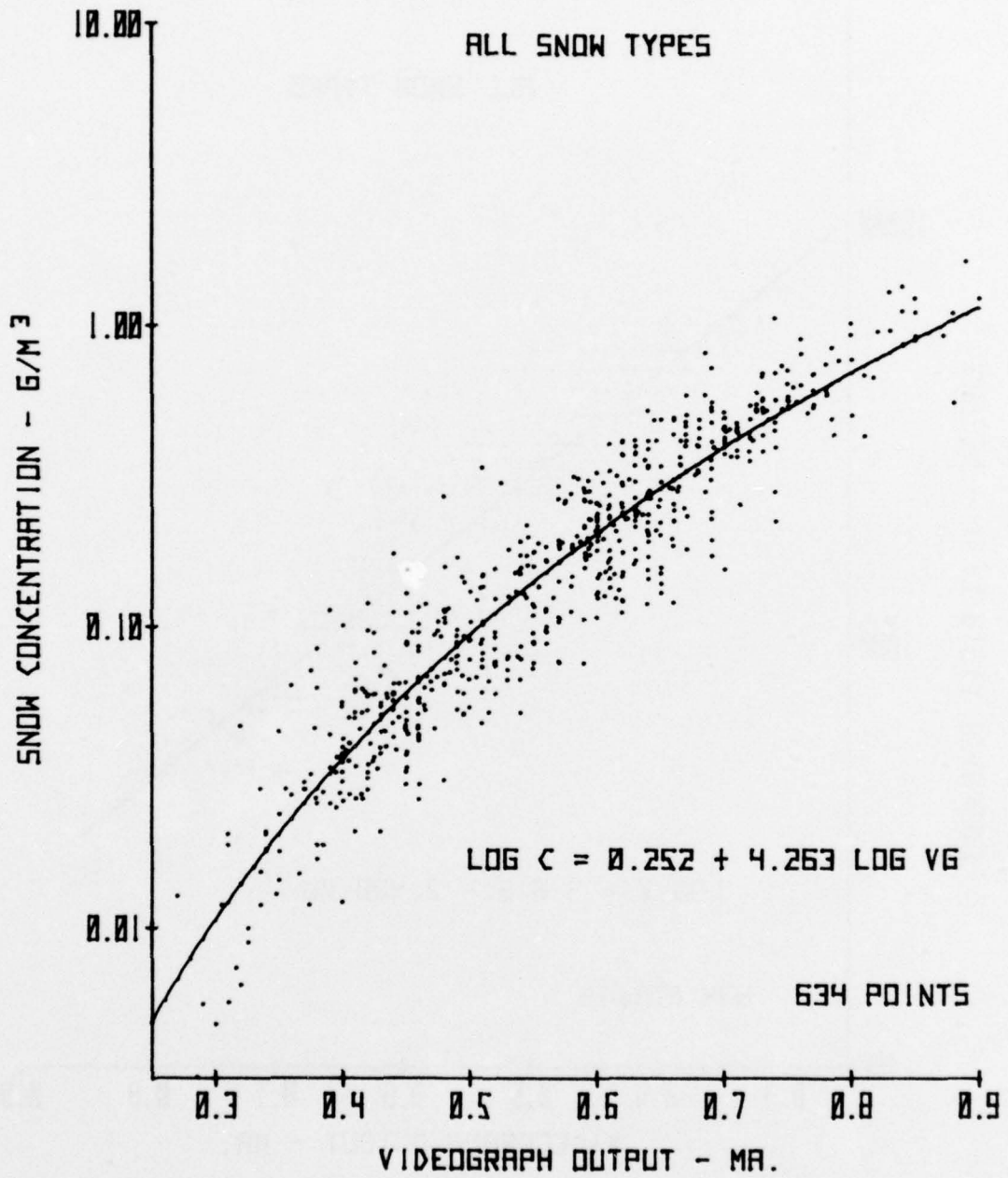


FIG. 5: RELATIONSHIP BETWEEN SNOW CONCENTRATION AND VIDEOGRAPH OUTPUT

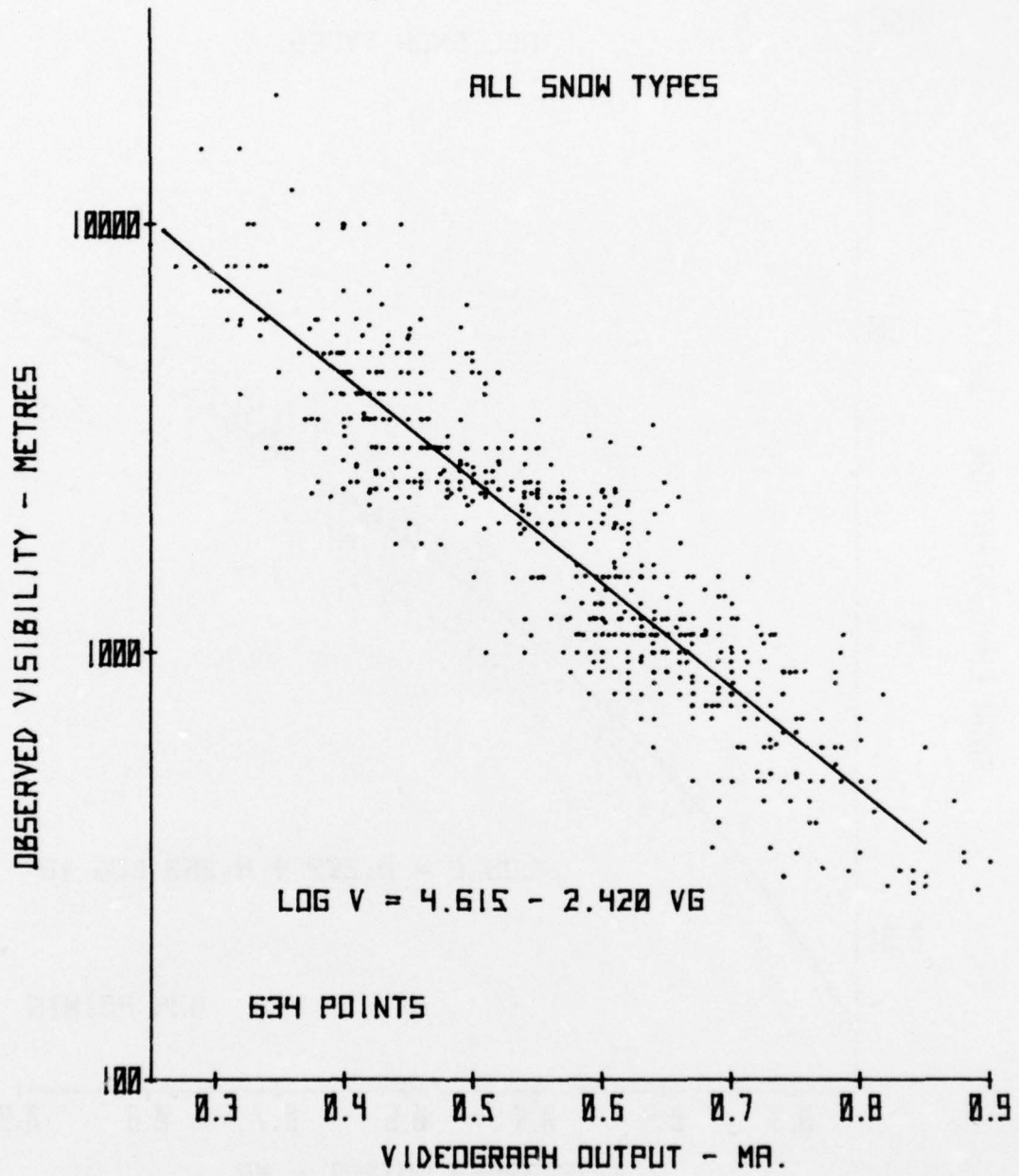


FIG. 6: RELATIONSHIP BETWEEN OBSERVED VISIBILITY AND VIDEOGRAPH OUTPUT

TOTAL NO. OF OBSERVATIONS = 666

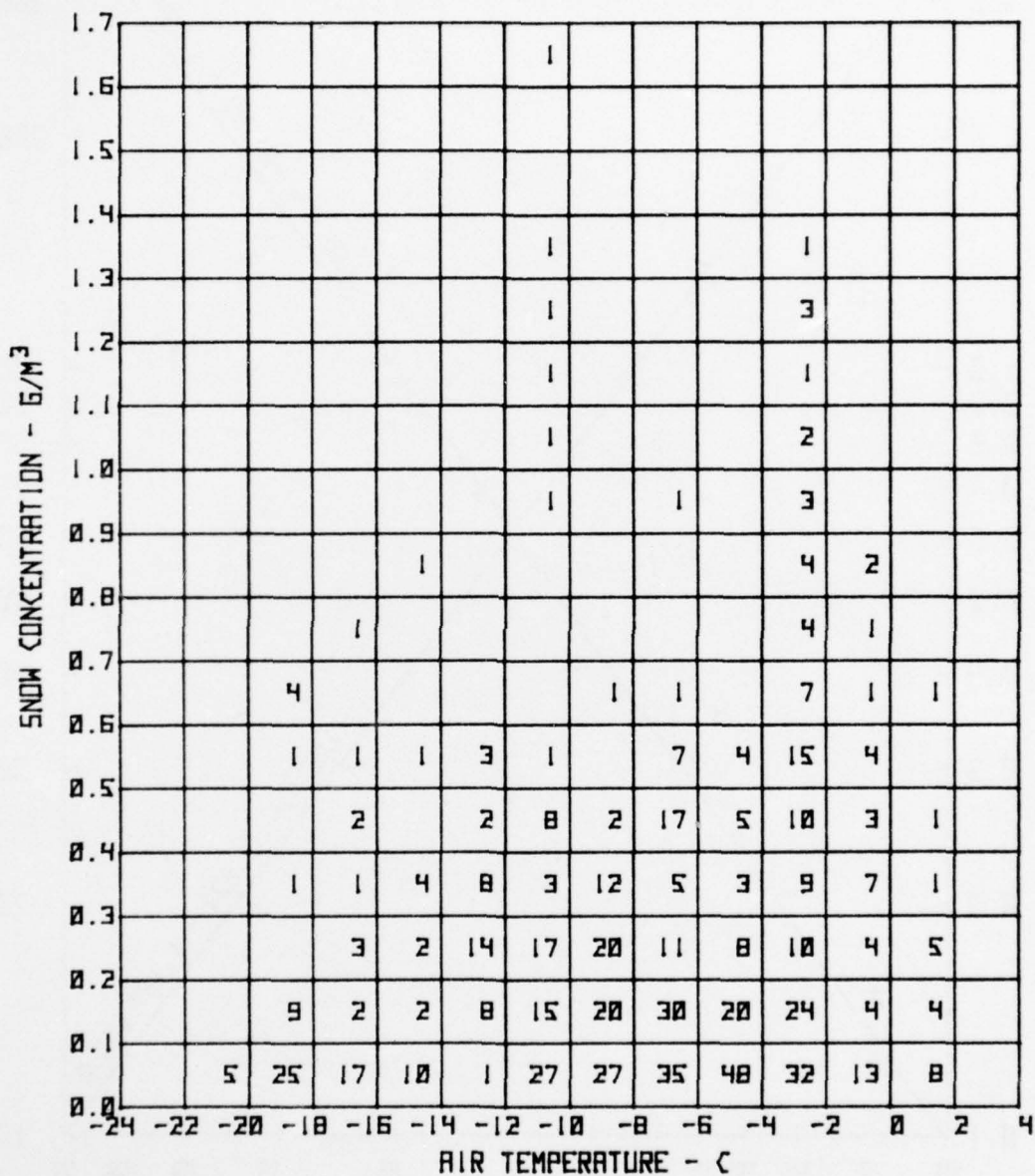


FIG. 7: SNOW CONCENTRATION vs TEMPERATURE PLOT
 (Numbers in Squares indicate Number of Observations)

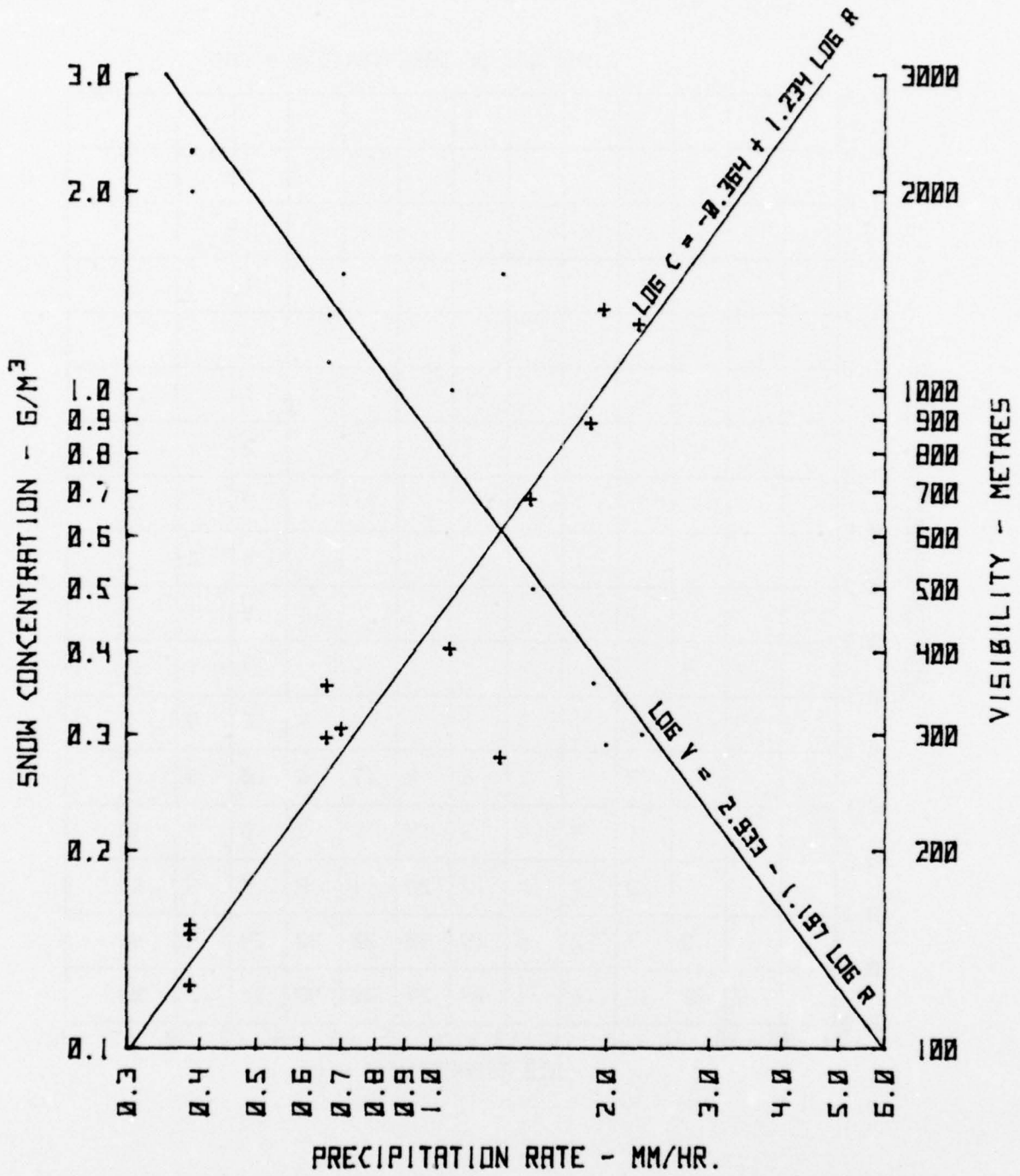


FIG. 8: RELATIONSHIP BETWEEN SNOW CONCENTRATION AND PRECIPITATION RATE, AND VISIBILITY AND PRECIPITATION RATE

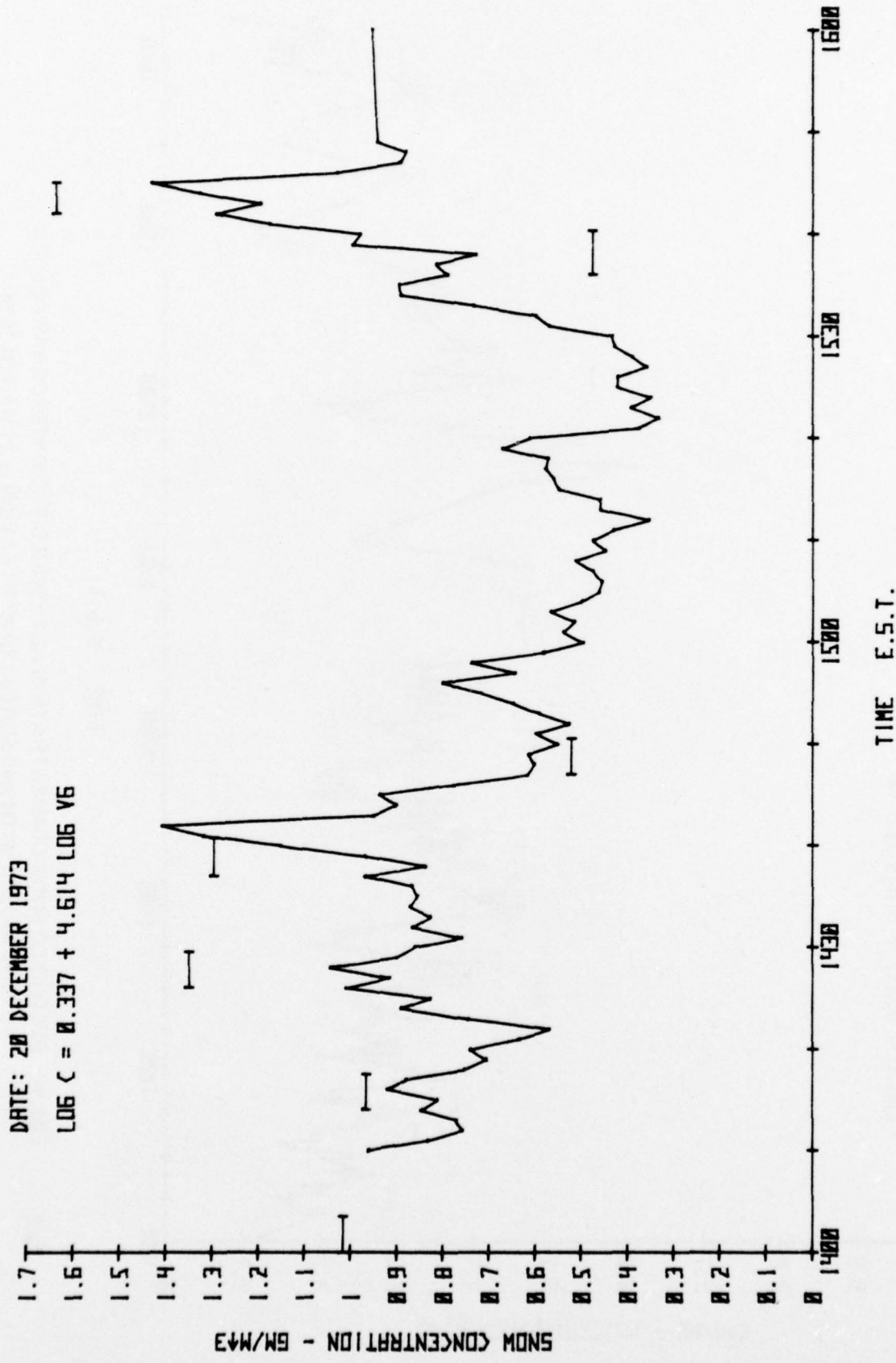


FIG. 9: RECORD OF SNOW CONCENTRATION AS DEDUCED FROM VIDEOGRAPH OUTPUT, AND COMPARISON WITH MEASURED CONCENTRATION - 20 DECEMBER 1973

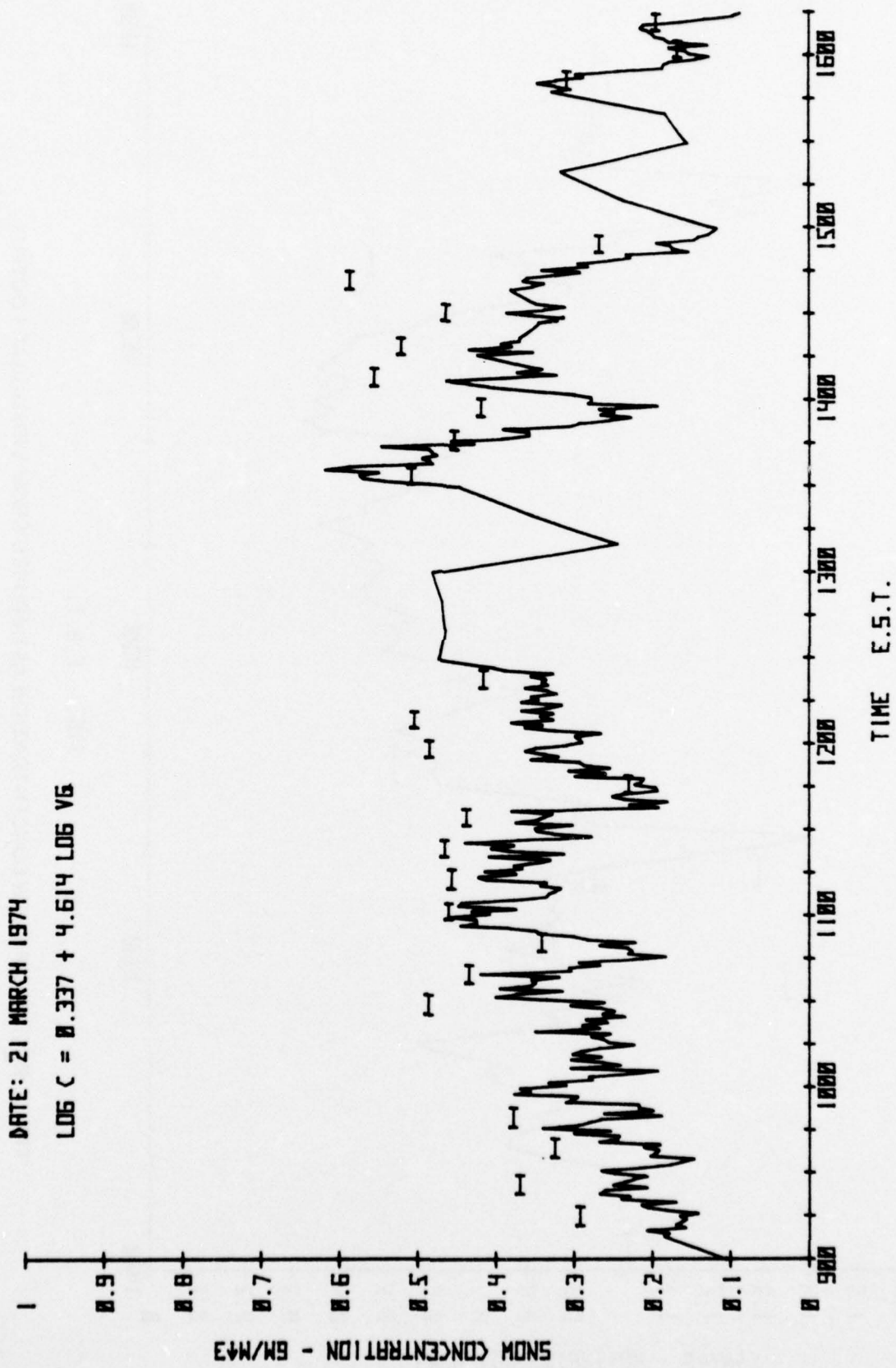


FIG. 10: RECORD OF SNOW CONCENTRATION AS DEDUCED FROM VIDEOGRAPH OUTPUT,
AND COMPARISON WITH MEASURED CONCENTRATION - 21 MARCH 1974

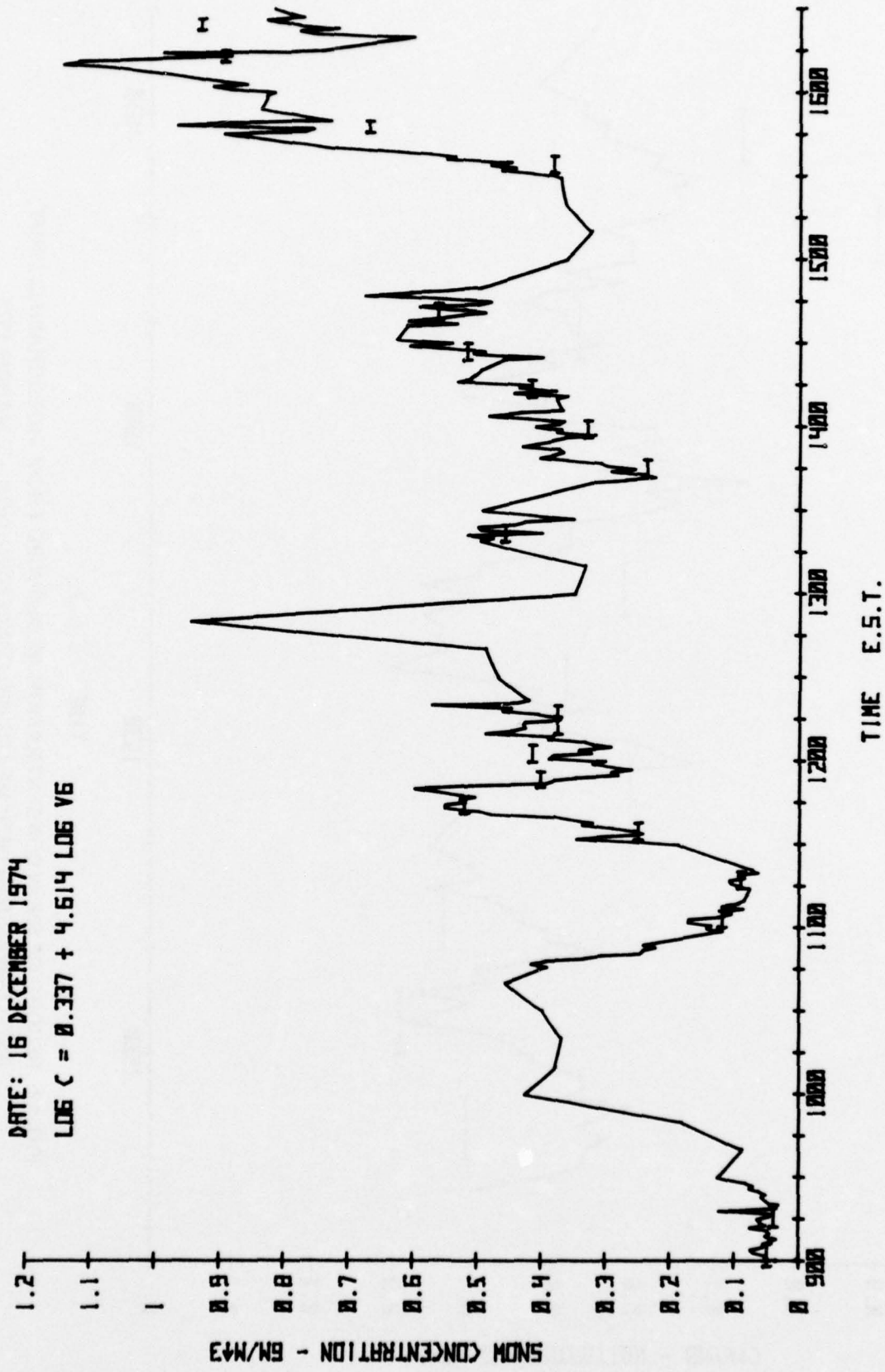


FIG. 11: RECORD OF SNOW CONCENTRATION AS DEDUCED FROM VIDEOGRAPH OUTPUT, AND COMPARISON WITH MEASURED CONCENTRATION - 16 DECEMBER 1974

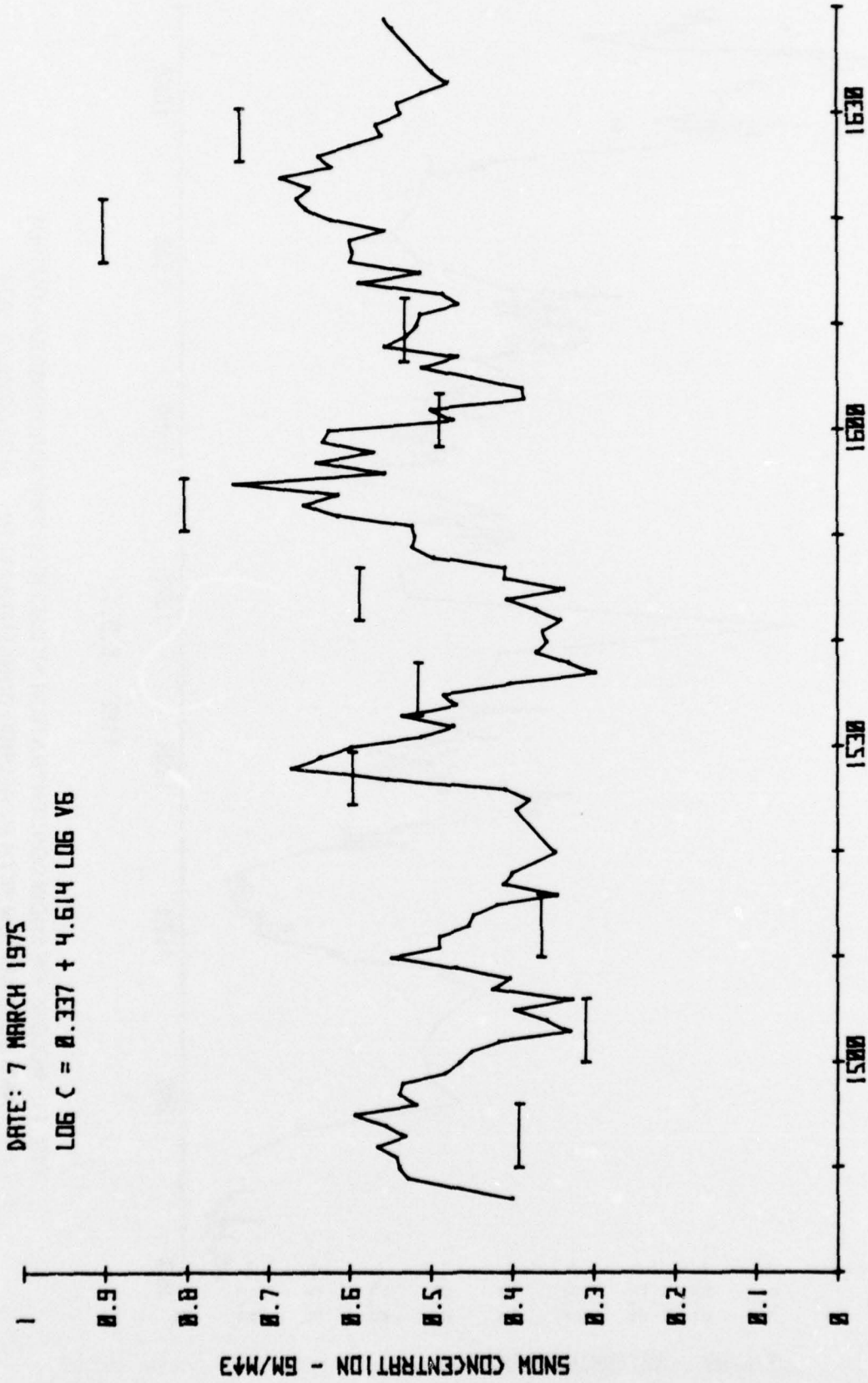


FIG. 12: RECORD OF SNOW CONCENTRATION AS DEDUCED FROM VIDEOGRAPH OUTPUT, AND COMPARISON WITH MEASURED CONCENTRATION - 7 MARCH 1975

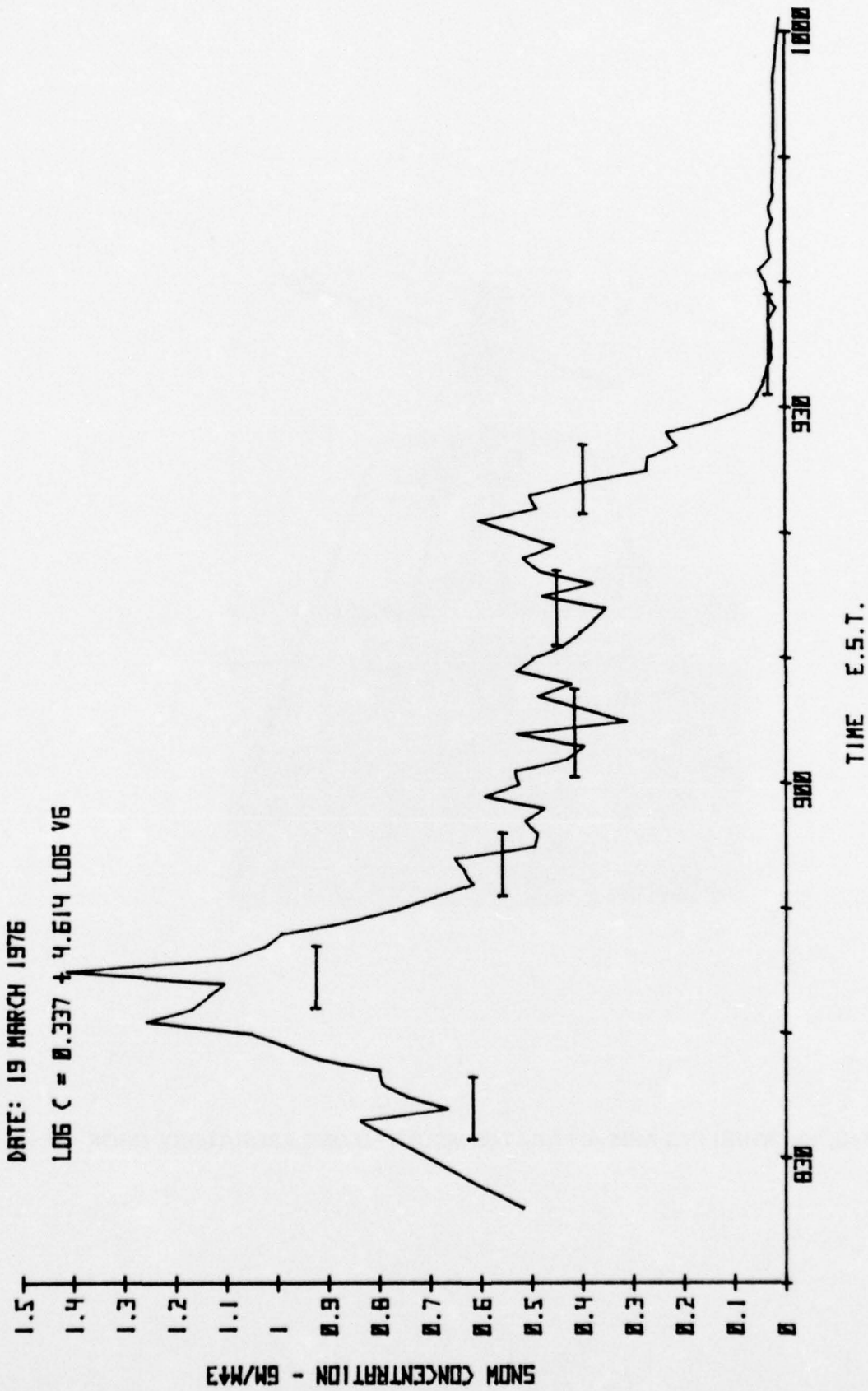


FIG. 13: RECORD OF SNOW CONCENTRATION AS DEDUCED FROM VIDEOGRAPH OUTPUT, AND COMPARISON WITH MEASURED CONCENTRATION - 19 MARCH 1976



FIG. 14: WHIRLING ARM APPARATUS MOUNTED ON LABORATORY ROOF

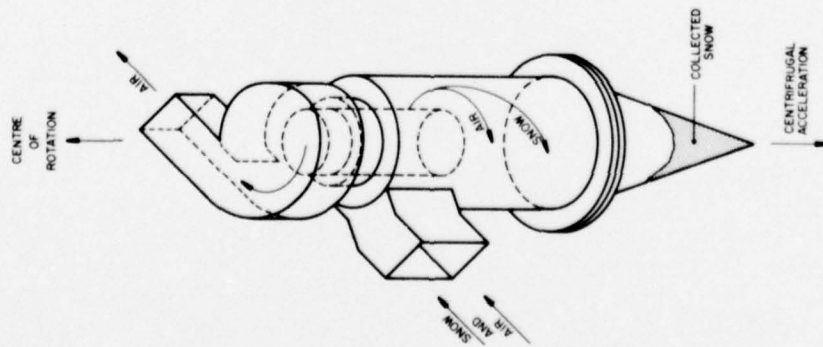
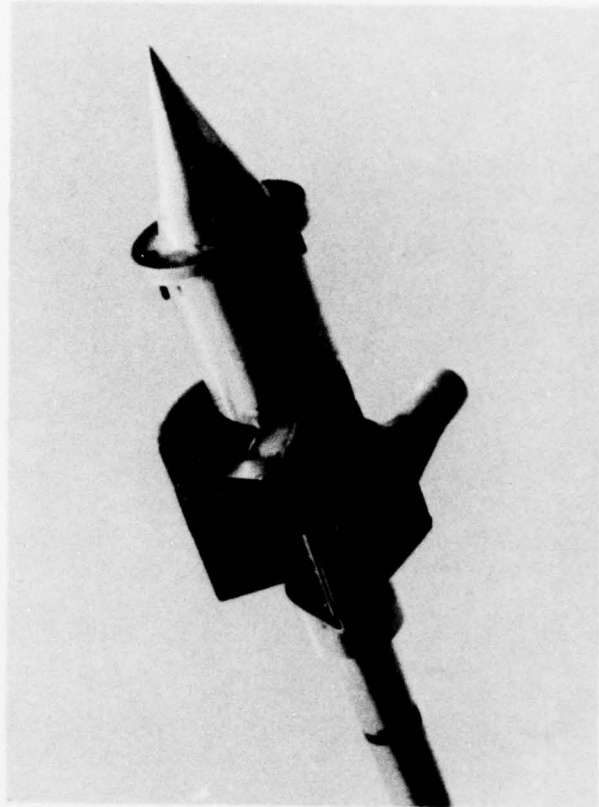


FIG. 15: CYCLONE SNOW SAMPLER

A WIND TUNNEL INVESTIGATION INTO THE FUEL SAVINGS AVAILABLE FROM THE AERODYNAMIC DRAG REDUCTION OF TRUCKS

K.R. Cooper

Low Speed Aerodynamics

National Aeronautical Establishment

ABSTRACT

An investigation of the aerodynamic drag of trucks and the drag reductions possible through the use of commercially available add-on devices was made on three 1:10 scale models in the National Aeronautical Establishment's 6-ft. X 9-ft. working section wind tunnel. A series of tests were also performed to determine the effect of trailer modifications which could be implemented by the trailer manufacturer. Both the use of add-on devices and trailer modifications produced drag reductions which could provide fuel savings of up to 10 percent for a tractor-trailer and 18 percent for a straight truck at 55 mph.

1.0 INTRODUCTION

A range of products is currently available to truck operators (Ref. 1) to reduce the aerodynamic drag of a truck and so improve fuel consumption. These devices are not usually provided by the manufacturer, but are "add-ons" purchased later by the owner. The devices fall into two basic categories - cab mounted deflectors, and additions to a trailer or box to provide the effect of corner rounding.

The wind tunnel test program (Refs. 2, 3) was initiated at the National Research Council at the request of Canadian Pacific Transport Ltd. who desired some impartial, controlled test information which would assist in the selection of aerodynamic drag reducing equipment for their fleet. Since the most recently published information concerning the general aerodynamics of trucks was published more than twenty years ago (Refs. 4, 5, 6) a general study of truck and trailer aerodynamic was incorporated into the program.

2.0 TEST PROGRAM

Three detailed 1:10 scale model trucks were tested in the 6-ft. X 9-ft. wind tunnel of the Low Speed Aerodynamics Laboratory. The tractor models and the straight truck model were originally funded by the National Science Foundation (USA) and were provided by Dr. Jeffrey Kirsch of Systems, Science and Software, La Jolla, California. The trailer model was made in one of NRC's shops.

The models were mounted on a separate ground plane, as shown in Figure 1, providing an adequate simulation of a truck moving through the air and over the ground (Ref. 7). Details of the wind tunnel installation are shown in Figure 2.

Three components of the total force and three components of the total moment, defined in Figure 3 were measured. While it may seem that only the drag is important in a discussion of fuel saving aerodynamic devices, it must be kept in mind that these devices should not cause any degradation in the truck's handling characteristics which are affected by the lateral forces and moments.

Details of the vehicles tested, two tractor-trailer combinations and a straight truck, are given below. Photographs of these vehicles are shown in Figure 4.

Cab-over-Engine (COE) Tractor-Trailer

White Freightliner WFT 8664, 8.5-ft. X 13.5-ft. X 45-ft. Trailmobile Trailer
10-in. radii on front side posts of trailer
10.00 X 20 tires all around
Tractor-trailer separation variable from 23 in. to 83 in.
Tractor-trailer height differential of 47 in.
Frontal area of 107 ft.².

Conventional (CONV) Tractor-Trailer

IHC 1800 Loadstar, 8.5-ft. X 13.5-ft. X 45-ft. Trailmobile trailer
10-in. radii on front side posts of trailer
9.00 X 20 tractor tires
10.00 X 20 trailer tires
Tractor-trailer separation variable from 23 in. to 73 in.
Tractor-trailer height differential of 70 in.
Frontal area of 103 ft.².

Straight Truck (Unarticulated)

IHC 1600 Loadstar
8-ft. X 8-ft. X 20-ft. box van
217-in. wheelbase
131-in. height
9.00 X 20 front tires and 10.00 X 20 rear tires
Cab-box roof height differential of 51.2 in.
Frontal area of 90 ft.².

In all, eight commercially available cab and trailer mounted devices were tested, as well as two prototype devices of considerable promise. The following list (in alphabetical order) summarizes the devices tested and they are shown in Figures 5 to 17.

Cab Mounted Devices

Airglide air deflector
General Motors Dragfoiler air deflector (modified for use with the Freightliner)
Rudkin-Wiley Airshield air deflector
Rudkin-Wiley Gap Seal (prototype, used with a deflector)
Uniroyal air deflector
University of Maryland fairing (prototype).

Trailer Mounted Devices

Aeroboost
Nose Cone
Rudkin-Wiley Vortex Stabilizer (used with a deflector)
Systems Science and Software (S³) Airvane.

The wind tunnel balance weighbeams have the capability of measuring applied forces or moments, which are steady, to an accuracy of 0.2 percent. Because of the truck model's bluffness, the forces and moments are not steady, especially when at large yaw angles. In order to provide better measurements under these circumstances three data points were taken and averaged for each yaw position. The measuring accuracy should be about 0.2 percent near zero yaw angle, increasing to 0.5 percent at 25 degrees. Thus accuracy to two decimal places should be equalled or exceeded for all force and moment coefficients.

The trailer model was provided with removable corners (Fig. 18) so that the effects of corner radius on the front and rear side and top corners and the top longitudinal corners could be investigated. Radii of 0 in. (square), 2 in., 6 in., 10 in., 12 in. and 18 in. were tested. Radii of 2 in. and 10 in. are commonly found on contemporary trailers. The straight truck corners were all square.

The baseline tractor-trailer measurements were made for separations of 23 in. to 83 in. full scale in 10-in. increments. The measurements using add-on devices or corner radii were made at 33-in., 53-in. and 73-in. separations. The separation was changed by inserting one to six spacer blocks between the trailer face and the trailer body, each representing a 10-in. width full scale. The trailer model length represented 45 ft. full scale with no spacers (83" separation simulation) and 50 ft. with all spacers in place.

The many possible truck-device combinations were tested over a range of windspeeds to investigate scale effects and over a range of yaw angles (caused by side winds) of from -4 degrees to +20 degrees in all cases and to +40 degrees in a few special instances. This exceeds the range of practical concern.

The aerodynamic force and moment coefficients are presented in a body axis co-ordinate system as shown in Figure 3 and are defined in the notation. The origin of co-ordinates is at ground level below the fifth wheel for the two tractor trailers and at ground level below the front of the box for the straight truck.

The solid and wake blockage correction used is that of Maskell (Ref. 8). This may not be a completely satisfactory correction, but is the best currently available. The correction to the dynamic pressure has the form

$$q_c = q (1 + 2.5 C_{D_{uc}} A/S) \quad \text{lb/ft}^2 \quad (1)$$

Typical correction factors for the baseline freightliner and the IHC 1600 straight truck are given below.

Yaw Angle (deg)	q_c/q	
	Freightliner	IHC 1600
0	1.06	1.05
5	1.07	1.05
10	1.10	1.06
15	1.13	1.07
20	1.16	1.08

3.0 EFFECT OF AERODYNAMICS ON FUEL CONSUMPTION

The total drag on a truck which must be overcome by the engine can be broken down into several main components — aerodynamic drag, due to air flow over the truck, and rolling resistance due to rolling losses in the tires. In addition there are some smaller parasitic losses due to accessories and friction in the drive line which can all be included in a power transfer efficiency. Grade resistance is ignored in the following discussions as the trucks will be assumed to travel at constant speed on a flat road.

The aerodynamic drag arises primarily from aerodynamic pressures acting on the vehicle due to its motion through the air. Positive pressure forces on the front of the tractor and the exposed portion of the trailer front in addition to negative, suction forces on the rear of the trailer cause about 80 percent of the aerodynamic drag. The rest of the drag is due to flow over individual components such as wheels, axles, etc. The aerodynamic skin friction drag of the tractor and trailer surfaces is negligible.

The total engine power required is that needed to overcome rolling and aerodynamic drag corrected by the power transfer efficiency, and is given by

$$P_c = \frac{1}{\eta} [P_r + P_a] \quad \text{hp} \quad (2)$$

The term in parentheses on the right-hand side is the power required at the driving wheels. The factor η , about 0.80 to 0.85, accounts for the parasitic losses. The rolling power, assuming a rolling resistance coefficient of 0.01 (10 lb of rolling drag per 1000-lb weight) is given by

$$P_r = \frac{0.01 VW}{550} \quad \text{hp} \quad (3)$$

The aerodynamic power is given by

$$P_a = \frac{VD}{550} = \frac{\frac{1}{2} \rho A C_D V^3}{550} \quad \text{hp} \quad (4)$$

Using (3) and (4) in (2) gives

$$P_c = \frac{1}{550\eta} \left[0.01 WV + \frac{1}{2} \rho A C_D V^3 \right] \quad \text{hp} \quad (5)$$

The power required to overcome rolling resistance is proportional to truck speed and weight while that required to overcome aerodynamic drag is proportional to the cube of speed, the truck size as represented by the frontal area, and the drag coefficient. Initially, at low speed, the rolling resistance is the larger, but as truck speed increases, the V^3 term predominates and the aerodynamic power is larger. The speed at which the rolling power and aerodynamic power requirements cross over (aerodynamic drag greater than rolling resistance) is a function of the square root of the density of the truck defined as the weight per unit frontal area. This speed can be computed from Equation (5) by equating the terms in the right-hand side and solving for V to obtain

$$V_{\text{cross}} = \left[\left(\frac{0.02}{\rho C_D} \right) \left(\frac{W}{A} \right) \right]^{1/2} \quad \text{ft/sec} \quad (6)$$

For a given drag coefficient the cross-over speed increases with (W/A) as is shown in Figure 19.

The fuel saving provided by a given drag reduction depends on the fraction of the total power required to satisfy the aerodynamic drag. At the cross-over speed the fractional change in fuel consumption would be one-half the fractional drag reduction.

The fuel consumed by a truck can be estimated using the engine specific fuel consumption and power requirements (Eq. (5)) giving

$$\mu = \left(\frac{1.467 \text{ SFC}}{\sigma V} \right) P_c \quad \text{Imp. gal./m.} \quad (7)$$

Assuming a specific fuel consumption $\text{SFC} = 0.38 \text{ lb/hp-hr}$ (diesel engine) and a fuel density of $\sigma = 8.5 \text{ lb/Imperial gallon}$, Equations (7) and (5), can be combined to give

$$\mu = \frac{1.19 \times 10^{-4}}{\eta} \left[0.01 W + \frac{1}{2} \rho A C_D V^2 \right] \quad \text{gal/mi} \quad (8)$$

The two expressions in parentheses in Equation (8), each multiplied by the leading term ($\mu = 0.85$), are shown in Figure 20 for the three trucks tested at 55 mph. The truck's characteristics are summarized in the following table. The drag coefficient values are representative of those measured for the three truck types.

TRUCK TYPE	W (lb)	A (ft ²)	C _D	W/A (lb/ft ²)	μ (gal/mi)
COE Tractor-Trailer	70,000	107	0.90	680	20.8
Conventional Tractor-Trailer	55,000	103	0.90	533	18.3
Straight Truck	18,000	90	0.90	200	11.8

The fuel consumed to overcome rolling resistance is constant with speed and increases with truck weight. The fuel used to counter aerodynamic drag increases with velocity squared. Because the product of frontal area and drag is nearly the same for each truck type, the dominance of the aerodynamic fuel requirements occurs at lower speeds for the lower density trucks. The curves would suggest that the fractional fuel savings available through aerodynamic drag reduction would be as large for a pick-up-and-delivery straight truck at city speeds as for a tractor-trailer at highway speeds. While the annual mileage of the city or highway delivery truck is much less than for the intercity tractor-trailers, they are far more numerous and so the overall contribution to fuel conservation would be significant. At highway speeds the straight truck can save as much fuel per mile as the much larger combination vehicles.

The incremental change in fuel consumption for a given incremental change in drag coefficient is (from (8))

$$\Delta \mu = 5.95 \times 10^{-5} \frac{\rho A \Delta C_D V^2}{\eta} \quad \text{gal/mi} \quad (9)$$

Thus a 0.10 reduction in drag coefficient would result in a fuel saving of 1.22×10^{-2} gal/mi at 55 mph for the freightliner, or 1220 gallons for one year assuming 100,000 miles travelled annually. The fuel saving is usually quoted in gallons per hundred miles (gphm) and this standard will be used from now on (Eq. (9) \times 100).

A drag reduction can be achieved by lowering the pressures on the front of the tractor or trailer, or by raising the trailer's base pressure. All the add-on devices tested act to reduce the positive pressures on the front of the trailer, especially the part exposed above the tractor roof.

The cab-mounted air deflectors, moderately curved plates placed on the cab roof, are all variations on the principle originally introduced by Rudkin-Wiley with the Airshield. This device deflects the airflow, which previously would have struck the front face of the trailer, smoothly onto the roof and sides of the trailer. The front face now is exposed to lowered pressures in the wake of the deflector, while the pressures on the inclined and curved deflector are also low. The sum of the deflector and trailer face pressures is lower than those on the trailer without the deflector and this pressure reduction results in the drag reduction. Since the path of the flow separating from the deflector is curved, adjustment must be made to the height and/or location or angle of inclination of the deflector to cater for changes in tractor-trailer height differential or separation. Some of the deflectors provide this variability, others do not.

Most of the trailer mounted devices reduce trailer front face pressures by rounding, or effectively rounding some or all of the top and side corners. Others attempt to counter cross-winds by modifying or blocking flows across the gap between the tractor and the trailer.

4.0 EFFECTS OF THE NATURAL WIND ON AERODYNAMIC DRAG

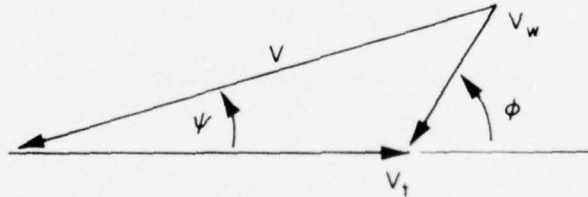
The wind tunnel simulation should provide a good representation of a truck moving through still air. However, a real vehicle is usually exposed to a variable, gusty wind. This wind continuously changes in speed and direction. At any instant in time the wind velocity vector can be considered as the sum of a mean and a fluctuating component. The steady, mean wind increases in speed from zero at ground level to a maximum value hundreds of feet above the ground. The unsteady fluctuating part consists of a series of gusts distributed approximately normally about this mean value. If the wind is blowing at an angle ϕ to the direction of the truck's motion it will produce an air speed different from the road speed and will cause a resultant wind direction which is yawed relative to the truck's direction of motion. The magnitude of the mean yaw angle is given by

$$\psi = \tan^{-1} \left[\frac{(V_w/V_t) \sin \phi}{1 + (V_w/V_t) \cos \phi} \right] \quad \text{deg.} \quad (10)$$

and the resulting mean air speed is given by

$$V = V_t \left[1 + (V_w/V_t)^2 + 2 (V_w/V_t) \cos \phi \right]^{1/2} \quad \text{ft/sec} \quad (11)$$

as shown by the following vector diagram.



Since the mean wind speed varies with height above ground in a fashion which depends on the local terrain, the yaw angle and speed defined in Equations (10) and (11) will increase over the height of the truck. It is common practice to use a power-law variation of mean wind speed with height of the form

$$V_w(h) = V_w(h_{ref}) (h/h_{ref})^\alpha \quad (12)$$

where $0.14 \leq \alpha \leq 0.40$ (Ref. (9)), the lower values being for smoother terrain. Although the mean wind may vary appreciably over the height of the vehicle the deviation of the resultant speed and direction would be only a few percent above and below the mean values at the trailer mid-height (about 10 ft. above the ground) at highway speeds. Thus it is probably a reasonable approximation to simulate the wind-endured yaw angle by rotating the model, in uniform flow, about a vertical axis as is usually done.

The wind velocity profile given by Equation (12) is only valid for uniform terrain roughness. If the truck is travelling downwind of a wind-break like a line of trees the velocities will probably be somewhat less than given by Equation (12) at 10 ft. On the other hand many roads are raised above the surrounding ground level and this will lead to a local flow acceleration at road level. It is expected that these two effects will cancel to some extent so that the simple power law profile should be satisfactory on the average.

The effects of wind gusts on the truck aerodynamics, if any, are not understood and are difficult to represent at model scale. The gusts occur in the horizontal plane (longitudinal gusts in the wind direction and lateral gusts perpendicular to it) and in the vertical plane. These gusts can be considered as eddies of varying size swept along by the mean wind. Some of the eddies are smaller than the truck size, some are of similar size and some are several times larger.

The lateral gusts will cause the resultant wind angle to fluctuate about its mean value in a random fashion. The variation would be of the order of ± 2 or ± 3 degrees for a 10-mph wind at 10 ft. above the ground perpendicular to a truck travelling 55 mph.

The effect of wind gusts can, perhaps, be separated into two parts — firstly, the averaging effect due to fluctuating angles induced by the gusts and secondly, unsteady aerodynamic effects.

The averaging effect results from the drag in a turbulent flow being the average drag over a range of fluctuating yaw angles about the mean value. This would cause a drag increase near zero yaw angle, reducing to no change at yaw angles greater than about 15 degrees. The averaging effect would also occur in the vertical plane since vertical gusts would induce a fluctuating non-zero pitch angle. In these instances the instantaneous aerodynamic drag coefficient for a given approach velocity vector would equal that for the steady state condition. When the yaw and pitch dependences are known it should be possible to average the force data measured in a wind tunnel in smooth flow and obtain the turbulent flow behaviour.

It is also possible that the higher frequency gusts (wavelength of the order of truck length) could induce instantaneous forces which differ considerably from those measured for the same approach velocity vector in steady flow. Such unsteady effects could only be simulated by introducing the "correct" gusts. Unfortunately, while the distribution, or spectrum, of gust sizes is known, this distribution cannot be properly simulated with any current technique at the size scaling required. It is only possible to readily generate gusts of the order of the truck width or less.

If one could determine which range of gust sizes were most important it might be possible to simulate just these and so allow for the unsteady effects of the full turbulent flow. In the present test some experiments were performed using turbulence generated by a square array of flat bars.

The variability of the wind with time of day, season and location within a country is not so much a problem of the wind's effect on aerodynamics, but rather a problem of data interpretation. As a truck travels throughout the country it will encounter mean winds of changing magnitude and direction. These winds, in turn, cause large variations in aerodynamic drag, and will result in an average drag which is a function of the wind climate and the vehicle's aerodynamic characteristics. The following table indicates the magnitude of the drag change produced by mean winds of different strengths and directions using the Freightliner travelling at 55 mph as an example ($X = 53$ in.).

V_w (mph)	ϕ (deg.)	ψ (deg.)	V (mph)	D (lb)	% Increase
0	—	0	55.0	760	—
5	90°	5.2	55.2	897	18.0
10	45°	6.5	62.5	1229	61.7
10	90°	10.3	55.9	1110	46.1
10	135°	8.4	48.4	798	5.0
10	180°	0	45.0	509	-33.0

The large variations in drag force demonstrate that the only meaningful fashion in which the model measurements can be extrapolated to full scale for long-term, country-wide operation is to average the measured drag force distribution over the expected range of yaw angles.

5.0 WIND AVERAGED DRAG COEFFICIENT

A first approach to this problem was proposed by Buckley and Sekscienski (Ref. (10)) in an attempt to account for the average effects due to wind. They assumed that the national average wind for the United States, 9.5 mph at a 30-ft. height above ground, could blow equally probably from all directions and used this fact to compute an average drag coefficient. Essentially, the direction of the 9.5-mph wind vector was varied from head-on to the truck to tail-on, through 180° , using a finite number of angle increments. For each increment in wind direction the drag value is interpolated from the measured drag versus yaw angle curve for the yaw angle induced. The average of these drag values provides the "wind-averaged" drag coefficient.

As the wind direction is changed through 180° the resultant yaw angle at first increases to a maximum of $\psi = 10.0^\circ$ (for $\phi = 100^\circ$) and then decreases to zero at $\phi = 180^\circ$.

While this analysis allows the inclusion of yaw effects due to wind it does so incompletely. The wind speeds in real life are distributed about the yearly mean value, sometimes being lower and sometimes higher. When the winds blow above the yearly average value, the yaw angle induced could be considerably greater than the 10-degree maximum allowed by the analysis. In addition, the trucks will be travelling through rougher terrain than found at most airports on the average, requiring a reduction in the wind speeds measured at airports sites. Finally, a further reduction would be required to adjust the measured winds to a more representative height of truck operation.

A more realistic approach, then, would be to apply the average wind probability density distribution over a whole country, adjusted to an appropriate reference height, the trailer mid-height. The wind data are available in the form of hourly wind summaries from meteorological stations, usually at airports. The data have been recorded over many years and come in the form of tables which log the numbers of hours during which the mean hourly wind blew from a specific band of wind directions within a given range of speed.

The data are usually taken at a height of 33 ft. (10 m) in open terrain. In order to correct the data to 10 ft., the trailer mid-height, and to account for rougher terrain than found at airports, the wind velocities are reduced by a factor of 2 based on current descriptions of surface wind profiles (Refs. (9), (11)).

The winds from the airport sites were taken from the measurement levels of 33 ft. and transferred to the top of the boundary layer, 900 ft. above ground using $\alpha = 0.15$ in Equation (12). These winds were then applied at the greater boundary layer depth of 1300 ft. over the rougher terrain representative of truck operation, and then transferred back down to 10 ft. using $\alpha = 0.25$ in Equation (12). Thus

$$V_w(10) = V_w(33) (900/33)^{1.5} (10/1300)^{2.5} = 0.5V_w(33)$$

The choice of exponents and depth of the earth's boundary layer is somewhat arbitrary. However, if the most extreme ranges are used $0.4 \leq V_w(10)/V_w(33) \leq 0.6$ so the value of 0.5 represents a median value.

Wind records for a twenty-year period were collected for 30 sites in Canada and were averaged to produce one master wind distribution. The data showed nearly uniform probabilities of occurrence for any wind speed irrespective of direction, except for a slight bias to winds from the West. Preliminary computations showed that no matter what direction a truck was chosen to be moving the wind averaged drag coefficients were always within one percent of each other.

The wind averaged drag coefficients computed (Freightliner) using the full directional wind statistics for a truck travelling North, East, South and West at 55 mph were 0.99, 0.98, 0.99, 1.00 respectively. Use of the average velocity distribution for each direction gave $\bar{C}_D = 0.99$. In comparison the use of a single average Canadian yearly speed (not a distribution of speeds) of 10.2 mph at 33-ft. height gave $\bar{C}_D = 1.13$.

The wind averaged drag coefficient is defined as

$$\bar{C}_D = \int_0^{2\pi} \int_0^{V_w^{\max}} C_D(\psi) \left[1 + (V_w/V_t)^2 + 2(V_w/V_t)\cos\phi \right] p(V_w, \phi) dV_w d\phi \quad (13)$$

where the wind probability ($\text{mph}^{-1} \text{rad}^{-1}$) is normalized such that

$$\int_0^{2\pi} \int_0^{V_w^{\max}} p(V_w, \phi) dV_w d\phi = 1.0 \quad (14)$$

If the distribution is assumed to consist of only one speed — the yearly average value, V_a , occurring with equal probability from all wind directions — then $p(V_w, \phi)$ can be replaced by $p(V_w) \delta(V_w - V_a)$ in Equations (13) and (14). Equation (14) becomes

$$\int_0^{2\pi} \int_0^{V_w^{\max}} p(V_w) \delta(V_w - V_a) dV_w d\phi = p(V_a) \int_0^{2\pi} d\phi = 2\pi p(V_a) = 1.0$$

Thus

$$p(V_a) = \frac{1}{2} \pi$$

and Equation (13) reduces to the form used by Buckley (Ref. (10)), which is

$$\bar{C}_D(V_a) = \frac{1}{2\pi} \int_0^{2\pi} C_D(\psi) \left[1 + (V_a/V_t)^2 + 2(V_a/V_t) \cos\phi \right] d\phi$$

Since the directional characteristics of the mean hourly winds had little effect on the wind averaged drag coefficient it was decided to use the same distribution for all wind directions. This distribution is the probability density function shown in Figure 21. The probability has been normalized such that the area under the density curve is 1.0. The curve shown is a Weibull fit of the observed data and has the form

$$p(V_w) = \frac{k V_w^{k-1}}{c^k} \exp \left\{ -(V_w/c)^k \right\} \quad (15)$$

where $c = 6.97$ and $k = 1.73$. This probability density must be multiplied by $\frac{1}{2}\pi$ for use in Equation (13). For each direction the probability of 0 mph wind speed is 0, the probability reaches a maximum at about 4.5 mph and decreases to very low values by 20 mph. The cumulative probability distribution is related to the density function and is the fraction of the time that the wind equals or exceeds any speed from all directions. Obviously it must begin at 1.0 since all winds equal or exceed 0 mph. From this curve it can be seen that a 10-mph wind is equalled or exceeded only 14 percent of the time from all directions. For a truck driving in any direction, then, it is likely to see a wind angle of more than 10 degrees only for a fraction of the time that the wind is at or above 10 mph.

It is possible to calculate the probability of exceeding any given wind angle using the density distribution given in Figure 21 where

$$P(> \psi) = \frac{\int_0^{V_w^{\max}} \int_{\phi_1(V_w)}^{\phi_2(V_w)} p(V) d\phi dV_w}{\int_0^{V_w^{\max}} \int_0^\pi p(V) d\phi dV_w} \quad (16)$$

$\phi_1(V_w)$ and $\phi_2(V_w)$ are the wind angle bounds within which the yaw angle is just equal to or greater than the particular value of ψ for which the cumulative probability is required. Due to symmetry considerations only the range $0^\circ \leq \phi \leq 180^\circ$ is required. The yaw angle cumulative distribution calculated from this relationship is shown in Figure 22. The wind angle is equal to or exceeds five degrees 120 days per year, ten degrees 25 days per year and fifteen degrees 3.5 days per year, about one percent of the time. Thus it would seem that the performance of add-ons is of most significance, on the average in Canada, for yaw angles of ten degrees or less.

6.0 TEST RESULTS

A selection of the experimental results are presented below that outline the trends found throughout the tests. No attempt will be made to discuss the detailed aerodynamic behaviour and the main emphasis will be on drag and the fuel saving available through drag reduction. The remainder of this section will be devoted to discussions of drag and the following section will summarize the expected fuel savings.

6.1 General Remarks

The trends in all the aerodynamic force and moment coefficients with yaw angle are similar for the three truck types tested (Fig. 4) as shown in Figure 23. The tractor-trailer separation used was 53 in.

The side force, yawing moment and rolling moment coefficients are all nearly linear with yaw angle and pass through zero at 0 degrees (anti-symmetrical about 0 degrees). The slopes of the side force and rolling moment coefficient curves are positive while the slope of the yawing moment curve is negative. The straight truck has the lowest side force slope and the highest rolling moment slope suggesting that the lateral centre of pressure is higher for the straight truck than for the tractor-trailers. No differences in these coefficients were observed between the two tractor-trailers.

The lift and pitching moment coefficients are symmetrical about zero yaw angle. The lift coefficients are always positive with the lift curve slopes for the tractor-trailers increasing from zero at 0 degrees yaw to a maximum by 10 degrees and then decreasing again. The lift curve slope for the straight truck varies only slightly over most of the yaw angle range and has a value equal to about one-fifth that for the tractor-trailers. The pitching moment is nearly constant with yaw angle for the straight truck but has an increasing negative slope for the tractor-trailers, leading to negative (i.e., nose-down) pitching moments beyond about 10 degrees. It is probable that the majority of the lift increase with yaw angle is due to lift on the trailer which would lead to the negative moments.

The drag coefficient curve is symmetrical about zero yaw angle with the lowest drag values found at zero. The cab-over-engine tractor-trailer combination has higher drag than the conventional tractor-trailer. Both curves are approximately parallel and show a large increase in drag with yaw angle up to 20 degrees.

The straight truck has a drag at 0 degrees which lies between the values for the other two vehicles, and a much slower drag rise with yaw angle which may be attributed to no gap between the cab and the box and reduced underbody ground clearance. Flows through the tractor-trailer gap and under the trailer at non-zero yaw angles may induce flow separations on the downstream side of the trailer which cause the drag rise seen. The wind averaged drag coefficients and estimated fuel consumptions for the three trucks at 55 mph are ($X = 53$ in.).

Vehicle	\bar{C}_D	μ (gphm)
COE	0.99	22.0
CONV	0.92	18.6
Truck	0.88	11.6

The separation between a tractor and trailer varies with tractor and trailer type and axle loading regulations. Typical changes in aerodynamic forces and moments which occur with changing separation are shown for the Freightliner in Figure 24. The greatest effects are seen at large yaw angles, and drag is most effected. In general the drag increases with separations up to about 40 in. and then becomes constant or decreases slightly as shown in the inset figure. The following table gives this behaviour for both tractor types and suggests that it is worth using a small separation whenever possible.

Separation, In.	\bar{C}_D			
	Freightliner	μ (gphm)	IHC 1800	μ (gphm)
23	0.91	20.9	0.90	18.3
33	0.94	21.3	0.93	18.7
43	0.98	21.8	0.94	18.8
53	0.99	21.9	0.92	18.6
63	1.00	22.0	0.94	18.8
73	1.00	22.0	0.96	19.0
83	0.98	21.8	—	—

The effects of small changes to the tractors' configurations were also investigated and are summarized below for a separation of 53 in.

Modification	\bar{C}_D			
	Freightliner	μ (gphm)	IHC 1800	μ (gphm)
Baseline	0.99	21.9	0.92	18.6
Radiator louvres closed	0.98	21.8	0.92	18.6
Exhaust pipe removed	0.98	21.8	—	—
Double bumper	1.02	22.3	—	—
Roof-mounted air conditioner	—	—	0.96	19.0
Sun visor	1.01	22.2	—	—
Trailer mounted refrigeration unit	0.94	21.3	0.91	18.4
Mud flaps removed	0.94	21.3	—	—

The effect of test Reynolds number is shown in Figure 25 for the IHC 1800 conventional tractor-trailer and typifies the results for the other trucks. There are some changes in the force and moment coefficients with increasing Reynolds number. In particular, the drag drops from its values at low speed, becoming constant above $Re = 6.5 \times 10^6$. This Reynolds number ($V = 225$ ft./sec.) was used for the majority of the test.

6.2 Commercially Available and Prototype Devices

Some typical results with commercially available and prototype devices are shown for the Freightliner, the IHC 1800 loadstar and the IHC 1600 straight truck in Figures 26, 27 and 28 respectively (53 in. separation for tractor-trailers). The only significant change in the forces and moments other than drag can be seen in the lift and pitching moment coefficients for the two tractor-trailers (Figs. 26, 27). The presence of a cab-mounted deflector leads to a general reduction in the lift coefficients producing two parallel families of curves. This is reflected in a negative shift on the pitching moment coefficients.

The drag coefficients showed the greatest changes and several clear trends can be observed. The deflectors produce the greatest drag reductions near zero yaw angle, however the reduction

decreases as the yaw angle increases and a drag increase above baseline can occur. The angle at which this cross-over occurs depends on the tractor roof to trailer roof height differential and on whether the deflector is properly sized and correctly mounted. The airshield deflector increases the drag beyond 13 degrees on the Freightliner (Fig. 26) by a small amount ($H = 47$ in.) while it increases the drag beyond 7 degrees on the IHC 1800 Loadstar (Fig. 27) suggesting that the deflector is less effective with the more exposed trailer ($H = 70$ in.). The loss of deflector performance with increasing yaw angle is less for the straight truck than for the tractor-trailer and no cross-over was observed for any deflector.

It was found during the tests that most of the simple flat-plate deflectors were mounted too vertically for best performance. Tilting them farther from the vertical could result in considerably improved performance and eliminated this cross-over problem. An example of this is provided by the Dragfoiler-type deflector which shows a drag reduction even at 20 degrees for the Freightliner. The use of a gap sealing element between tractor and trailer greatly enhances the performance of a deflector as does the use of trailer skirts. The trailer skirts also offer the potential for reducing spray in wet weather.

The trailer rounding modifications are characterized by the results for the nose cone. It produces the best drag reductions of the commercially available devices for the straight truck and conventional tractor-trailer and is as good as most presently available deflectors for the Freightliner. The drag reduction produced with this device is almost constant with yaw angle. Similar results are shown for the Aeroboost and Airvane in Figure 28. The Airvane was only fitted to the top corner of the box and should perform about as well as the Nose Cone if used on the front side corners.

Prototype devices such as a preliminary version of the University of Maryland Deflector and Gap Seal, or trailer skirts used with a deflector indicate the increased performance which will be realized through the use of improved deflectors employed in combination with other devices.

Figure 29 shows the effect of changing the angle of a deflector on the drag reduction available and it is evident that one should make sure, as is so often not the case, that the deflector is properly adjusted to match the tractor and trailer used. It also shows that the departure from minimum drag is less for a deflector too vertical than for one inclined too much. The proper setting can be determined by using a piece of light rope taped to the top centre of the deflector to indicate when the airflow is just coming onto or slightly above the trailer roof, or a total head tube mounted just above the trailer roof can be used to detect the separating flow from the deflector.

6.3 Trailer Modifications

While the use of add-on devices can provide useful drag reductions, modifications to future equipment can also be used to obtain fuel savings. There are many areas on contemporary trailers where modest changes could lead to reduced drag at little or no cost to payload. Many trailers today have rounded side corners at the trailer front, some have various amounts of corner bevel and, in one instance, a rounded front face.

The effect of different corner radii used on various combinations of corners was investigated for the tractor-trailers and the results are summarized in Figure 30. The fuel savings possible compared to the baseline trailer configuration are given for the cab-over-engine and conventional tractors at $X = 53$ in. and 55 mph in the following table. All three front corners were radiused with the value given.

Corner Radius (In.)	$\Delta \mu$ (gphm, X = 53 In.)	
	Freightliner	IHC 1800
0	-1100	-2472
6	611	471
12	856	942
18	856	942
52	1590	1412

It was found that the top longitudinal corner radius had no effect on drag and that a 10-in. corner radius on the front corners was sufficient to obtain a majority of the drag reduction available through large radius. Adding this radius to the top front corner reduced the wind averaged drag coefficient by 0.07 for the Freightliner and 0.08 for the IHC 1800 Loadstar (53-in. separation). Rounding the rear top and sides using an 18-in. radius with the Freightliner reduced \bar{C}_D by an additional increment of 0.12. This latter modification would interfere with the door operation and would reduce the trailer volume and so would probably not be acceptable to the industry.

Various front face shapes were tried on the trailer and the results found are summarized in the table below. The bevelled nose is the unit used with tandem trailers. The shapes are defined in the photographs of Figure 15.

Trailer Configuration	\bar{C}_D					
	X (In.)	Freightliner	μ (gphm)	X (In.)	IHC 1800 Loadstar	μ (gphm)
10 in. radius front sides	23	0.91	20.9	23	0.90	18.3
Nose cone	35	0.84	20.1	35	0.82	17.4
Bevelled nose	21	0.91	20.9	21	0.93	18.7
Cylindrical nose	21	0.88	20.6	21	0.84	17.6
Faired cylindrical nose	21	0.86	20.3	21	0.80	17.1
Faired cylindrical nose + streamlined tail	21	0.74	18.8	—	—	—

The last entry is for a completely impractical configuration but seems to illustrate the maximum available gains through modifications to the trailer rear face.

Figures 31 and 32 present full data sets for some of these configurations. Again the drag coefficient shows the greatest change of all the force and moment coefficients. The drag curves do not cross, and remain approximately parallel over the yaw range tested. In Figure 32 it is interesting to note that the drag at large yaw angles with the faired cylindrical trailer nose barely exceeds the zero yaw drag with a square cornered trailer.

6.4 Flow Visualization

Some of the effects of the add-on devices on the flow over two of the trucks can be seen in the photographs of Figure 33. A stream of smoke released ahead of the model at a test speed of 50 ft./sec. was used to trace the flow. Only side elevations are shown for the two truck types tested — the tractor-trailer and the straight truck.

The down flow behind the tractor, the stagnation point on the trailer, and the separated flow pocket just behind the trailer top front corner can be seen. All the deflectors provide improved flow over the trailer roof. The inclined Uniroyal deflector can be seen to provide better flow than when more vertical. The Nose Cone removed the flow separation on the top of the trailer but still permits some flow to go down behind the tractor while the deflectors do not.

A large separated flow region can be seen behind to front top corner for the baseline straight truck. None of the deflectors bring the flow cleanly onto the box roof as they did for the tractor-trailer. The Airshield is seen to provide the least separated flow of all the deflectors as would be expected on the basis of the drag measurements. The Nose Cone allows the flow to remain attached, which explains its effectiveness. The Airvane is probably not remounted properly (the truck was not attached to the balance for these photographs so it was not possible to adjust the Airvane to give minimum drag) for the smoke photograph.

6.5 Effects of Turbulence at Model Scale

A preliminary investigation into the effect of turbulence on the truck's aerodynamics was undertaken using the turbulent flow field behind a uniform, bi-planar grid across the inlet of the wind tunnel test section. The grid was constructed from an array of 4 in. wide plywood plates placed vertically and horizontally on 16-in. centres providing a square lattice (Fig. 1). The centre of the turntable was located 12 ft. (36 bar diameters) downstream of the grid. The longitudinal turbulence intensity behind the grid was about 7 percent of the test speed and the integral longitudinal scale of the turbulence was about 7 in. — less than the model trailer width. The lateral turbulence intensity was 4 percent and the lateral scale was 4 in., nearly one-half the model trailer width.

The expected longitudinal turbulence intensity at the trailer mid-height at a truck speed of 55 mph would be about 3 percent of the resultant airspeed for a 10-mph wind and the lateral intensity would be about 2 percent. The longitudinal scale in the atmosphere might be of the order of 50-100 ft. (Ref. (11)) (1 to 2 trucklengths) and the lateral scale would be about 10 to 15 ft. (Ref. (11)), 1 or 2 truck widths. Thus the turbulent field used was of too high an intensity and of too short a scale length to properly simulate the average atmospheric turbulence. The lateral scales and intensities, those of most importance, come close enough to modelled full scale values that the grid flow should provide an indication of the possible effects of turbulence.

Measurements were made behind the grid for both the Freightliner and the IHC 1600 straight truck, and the drag data are presented in Figures 34 and 35, respectively. The test speed was only 50 ft./sec. because the large pressure drop across the grid precluded use of a higher speed. It appears, however, that the Reynolds number is sufficient since the presence of the turbulence serves to cause early boundary layer transition on the model. More scatter was present in the data than for the main experiment due to the small loads and the unsteadiness in the flow.

The most noticeable trend for the tractor-trailer in the presence of turbulence (Fig. 34) is that the drag near zero yaw angle is increased. This result supports some of the turbulence averaging arguments presented in Section 4.0 although it is not possible to separate these effects and any due to unsteady aerodynamics. The increase in drag is greatest when the deflector is present, as would be expected, because its yaw curve shows the steepest drag rise. With turbulence the Nose Cone shows a small drag rise near zero yaw but otherwise the drag curve is almost identical to the uniform flow result. While the wind averaged drag coefficients are within a few percent of each other in smooth and turbulent flow, this small change represents a significant fraction of the drag reduction achieved in many cases. The effects of turbulence on the wind averaged drag coefficient is given for the Freightliner ($X = 53$ in.) in the following table.

Configuration	Smooth Flow		Turbulent Flow		$\overline{\Delta C_{D_T}} / \overline{\Delta C_D}$
	$\overline{C_D}$	$\overline{\Delta C_D}$	$\overline{C_{D_T}}$	$\overline{\Delta C_{D_T}}$	
Baseline	0.99	—	1.01	—	—
Uniroyal Deflector	0.86	0.13	0.90	0.11	0.85
Uniroyal Def. + Gap Seal	0.82	0.17	0.86	0.14	0.88
Nose Cone	0.89	0.10	0.91	0.10	1.00

The right-hand column shows that the deflector performance is reduced with turbulence present by 15 percent and by 12 percent when the Gap Seal is also used. The Nose Cone showed no performance change.

These results are in qualitative agreement with the work of Buckley et al (Ref. (12)) and Marks et al (Ref. (13)) who showed that the drag measured on a full scale tractor-trailer in the gusty wind was higher for the unmodified vehicle in turbulence than for a wind tunnel model of it, in smooth flow. It was also found that deflector performance at full scale was reduced compared to the results found in a wind tunnel, and that the amount of this difference was reduced by a Gap Seal.

Wind tunnel tests on the IHC 1600 straight truck in smooth and turbulent flow (Fig. 35) showed differences similar to those found for the Freightliner. The baseline results for both flows were closer than in the case of the Freightliner although there was a small trend to increased drag near zero yaw with turbulence. The importance of the averaging effect of turbulence is small because the drag curve slopes are small for the straight truck. The deflector suffers a considerable drag increase in turbulent flow while the Nose Cone, again, shows no change. The Airvane generally shows a drag reduction in turbulence which could be related to the effective Reynolds number being changed by the presence of turbulence. The wind averaged drag coefficients measured are given below.

Configuration	Smooth Flow		Turbulent Flow		$\overline{\Delta C_{D_T}} / \overline{\Delta C_D}$
	$\overline{C_D}$	$\overline{\Delta C_D}$	$\overline{C_{D_T}}$	$\overline{\Delta C_{D_T}}$	
Baseline	0.88	—	0.89	—	—
Airshield Deflector	0.73	0.15	0.79	0.10	0.67
Nose Cone	0.68	0.20	0.69	0.20	1.00
S ³ Airvane	0.80	0.08	0.79	0.10	1.25

These preliminary data would suggest that the general force levels are not greatly effected by the presence of turbulence but that differences between configurations can be. Thus smooth flow in a wind tunnel can provide an effective technique for developing drag reducing devices. However, comparisons of the exact magnitudes of the drag reductions from various devices may be subject to errors of the magnitude of the differences noted above. It may be possible to include adequate turbulence inputs through the correct uniform grid choice, and it may also be possible to adjust the data measured in smooth flow in a wind tunnel using averaging techniques over the range of fluctuating pitch and yaw angles encountered by full scale trucks.

7.0 SUMMARY OF RESULTS

The graphical presentation of results is useful for defining the aerodynamic characteristics of different trucks and of changes to them, but is not convenient for comparisons of large numbers of modifications. A more effective format is obtained through use of the wind averaged drag

TABLE 1

WIND AVERAGED DRAG COEFFICIENTS AND ESTIMATED FUEL USAGE
AT 55 MPH FOR DATA AVERAGED OVER THREE TRACTOR-TRAILER
SEPARATIONS (33 in., 53 in., 73 in.)

Configuration		White Freightliner WFT8664 GCVW = 70,000 lb.			I.H.C. 1800 Loadstar GCVW = 55,000 lb.			I.H.C. 1600 Straight Truck 20 ft. Box, GVW = 18,000 lb.		
		\bar{C}_D	mpg	Fuel Savings Per Year** (Imp. gal.)	\bar{C}_D	mpg	Fuel Savings Per Year** (Imp. gal.)	\bar{C}_D	mpg	Fuel Savings Per Year** (Imp. gal.)
Baseline		0.98	4.58	—	0.94	5.32	—	0.88	8.62	—
TRAILER MODIFICATIONS	Square corners	1.07	4.36	- 1102	1.13*	4.75	- 2240	—	—	—
	Refrigeration unit	0.94*	4.69	490	0.91	5.42	354	—	—	—
	Bevelled nose	0.91 ⁺	4.77	856	0.93 ⁺	5.35	118	—	—	—
	12 in. Radius — front top and side corners	0.91	4.77	856	0.84*	5.68	1179	—	—	—
	12 in. front radii and 18 in. rear radii	0.80*	5.11	2201	—	—	—	—	—	—
	Cylindrical nose	0.88 ⁺	4.85	1225	0.84 ⁺	5.68	1179	—	—	—
	Rounded cylindrical nose	0.86 ⁺	4.91	1470	0.80 ⁺	5.83	1651	—	—	—
TRACTOR MOUNTED DEVICES	Airglide	0.91	4.77	856	0.92	5.39	236	0.86	8.78	31
	Airshield (old setting)	0.91	4.77	856	0.90	5.46	472	—	—	—
	Airshield (new setting)	0.86*	4.91	1470	—	—	—	—	—	—
	Airshield (old setting + Gap Seal)	0.86	4.91	1470	0.86	5.60	943	0.73	9.95	232
	Airshield (new setting + Gap Seal)	0.82*	5.03	1960	—	—	—	—	—	—
	Uniroyal (old setting)	0.90	4.80	980	0.92	5.39	236	0.78	9.46	155
	Uniroyal (new setting)	0.86	4.91	1470	0.90	5.46	472	0.75*	9.75	201
	Uniroyal (new setting) + 6 in. radius on 3 front corners	0.84*	4.98	1712	—	—	—	—	—	—
	G.M. Dragfoiler	0.87	4.89	1347	—	—	—	—	—	—
	G.M. Dragfoiler (+ Gap Seal) [#]	0.83	5.00	1837	—	—	—	—	—	—
U of M Fairing (+ Gap Seal) ^z	0.81	5.08	2079	—	—	—	—	—	—	
TRAILER MOUNTED DEVICES	Vortex stabilizer (+ Airshield, old setting)	0.90	4.80	980	0.88	5.23	708	—	—	—
	Trailer skirts	0.91*	4.77	856	—	—	—	—	—	—
	Trailer skirts (+ Airshield, old setting)	—	—	—	0.78*	5.92	1883	—	—	—
	Skirts and Gap Seal (+ Airshield, old setting)	—	—	—	0.75*	6.05	2236	—	—	—
	Nosecone	0.87	4.88	1347	0.83	5.71	1297	0.68	10.48	309
	Aeroboost [†]	—	—	—	—	—	—	0.76	9.65	186
	S ³ Airvane (top only)	0.92*	4.74	735	0.87*	5.56	825	0.80	9.28	124
S ³ Airvane (top + sides)	—	—	—	—	—	—	0.69*	10.37	294	

NOTES: ** Based on 100,000 mi. for combinations and 15,000 mi. for straight truck

* Data taken at 53 in. separation only

⁺ Data taken at 21 in. separation only

[#] Modified version constructed for the Freightliner and not the optimum, but close to it

^z An approximation using cylindrical corner fairings

[†] Estimate based on limited data

^x Preliminary version

coefficient. Table 1 provides this information for a wide range of truck configurations. The data are presented in three groups — trailer modifications, tractor or cab mounted devices, and trailer mounted devices. Fuel consumption (obtained by inverting Eq. (8)) and the estimated annual fuel saving for each device are given.

Corner rounding is an effective drag reducing technique and it would seem reasonable to expect trailer manufacturers to radius the top front trailer (or box) corner on future equipment. Large rounded trailer noses provide some improvement over 10 or 12 in. corner radii, especially at larger yaw angles, and allow closer coupling. If this nose shape could be added to the current 45 ft. maximum trailer length without exceeding over-all truck length limits they should be attractive to operators because of the volume increase. These shapes may be most effective when used with a deflector. Square front corners are to be avoided.

The advantages of tilting the deflector back more and using a variable angle mounting to maintain best performance at any separation is clearly apparent. The changes found in the wind tunnel test using the new deflector settings have been confirmed in engineering road and fleet testing by both manufacturers who have adopted this technique. It can also be seen that the use of a deflector when the top front trailer corner is radiused gives a better drag reduction than when a square corner is present. It is possible that the effects of wind turbulence will be reduced by such a combination. Also, the sensitivity to deflector angle would be reduced making the deflector easier to set. The use of a gap sealing device with a deflector would seem both practical and worthwhile.

The trailer mounted devices generally give drag reductions which are similar to those obtained through trailer modifications. Trailer skirts are seen to be effective. Little extra drag reduction is achieved when both skirts and a Gap Seal are used together.

8.0 CONCLUSIONS

The fuel saving potentials for a wide range of currently available and prototype add-on drag reducing devices have been assessed in a comprehensive wind tunnel investigation. It has been shown that all the devices tested provide useful fuel savings and most would pay for themselves within one year. Improved devices, and combinations of devices, seem to offer the prospect for greater fuel savings than are now achieved. Modifications to current trailer designs can also offer significant fuel savings.

In general the trends predicted at model scale in a wind tunnel provide a useful, qualitative prediction of full scale truck aerodynamics as demonstrated by limited correlation with field experience. However quantitative extrapolation of the wind tunnel data to full scale should be performed with some caution until the effects of wind turbulence are better understood and more complete correlation with full scale can be established. Preliminary investigations of the effect of turbulence in the wind tunnel simulation, when compared to some full scale data, suggest that turbulence effects might be accounted for by a simplified turbulence simulation, or by the appropriate data interpretation.

ACKNOWLEDGEMENT

The author would like to thank all those who supported this program — the National Science Foundation and Systems Science and Software who provided the tractor models, the manufacturers who freely provided a wide range of design information, and Canadian Pacific Transport who provided some financial support and much-needed background information.

REFERENCES

1. Schenck, P. *Reducing Air Drag.*
Motor Truck Magazine, Nov. 1975.

2. Cooper, K.R. *Wind Tunnel Investigations of Eight Commercially Available Devices for the Reduction of the Aerodynamic Drag on Trucks.*
Roads and Transportation Association of Canada, Quebec City, September 1976.
3. Cooper, K.R. *An Article on the Reduction of Fuel Consumption of Trucks Through Aerodynamic Drag Reduction.*
Motor Truck Magazine, Waldham Publications, Toronto, September 1976.
4. Sherwood, W.A. *Wind Tunnel Test of Trailmobile Trailers.*
University of Maryland Wind Tunnel Rept. No. 85, 1953.
5. Wandson, R.I. *Wind Tunnel Test of Trailmobile Trailers, 2nd Series.*
University of Maryland Rept. No. 98, 1953.
6. Gross, D.S. *Wind Tunnel Tests of Trailmobile Trailers, 3rd Series.*
University of Maryland Rept. No. 150, 1955.
7. Beauvais, F.N.
Tignor, S.C.
Turner, T.R. *Problems of Ground Simulation in Automotive Aerodynamics.*
SAE 680121.
8. Maskell, E.C. *A Theory of the Blockage Effects on Bluff Bodies in a Closed Wind Tunnel.*
RAE Rept. No. 2685, 1963.
9. Davenport, A.G. *Rationale for Determining Design Wind Velocities.*
ASCE Transactions, Paper No. 3123.
10. Buckley, F.T.
Sekscienski, W.S. *Comparisons of Effectiveness of Commercially Available Devices for the Reduction of Aerodynamic Drag on Tractor-Trailers.*
SAE 750704.
11. Teunissen, H.W. *Characteristics of the Mean Wind and Turbulence in the Planetary Boundary Layer.*
UTIAS Review No. 32, 1970.
12. Buckley, F.T.
Marks, C.H.
Walston, W.H. *An Analysis of Coast-Down Data to Assess Aerodynamic Drag Reduction of Full-Scale Tractor-Trailer Trucks in Windy Environments.*
SAE 760107.
13. Marks, C.H.
Buckely, F.T.
Walston, W.H. *An Evaluation of the Aerodynamic Drag Reduction Produced by Various Cab Roof Fairings and a Gap Seal on Tractor-Trailer Trucks.*
SAE 760105.

NOTATION

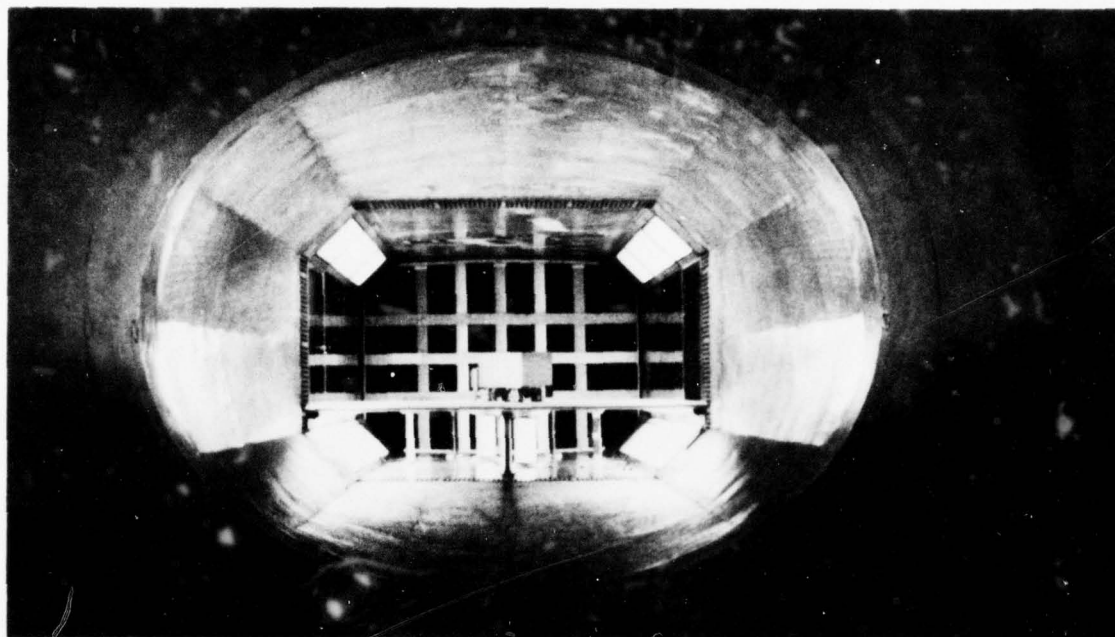
A	projected frontal area, ft ²
B	reference length, ft. (nominal trailer length for tractor-trailers, 45-ft. full scale; wheelbase for straight truck, 18-ft. full scale)
c	} constants in the Weibull function
k	

NOTATION (Cont'd)

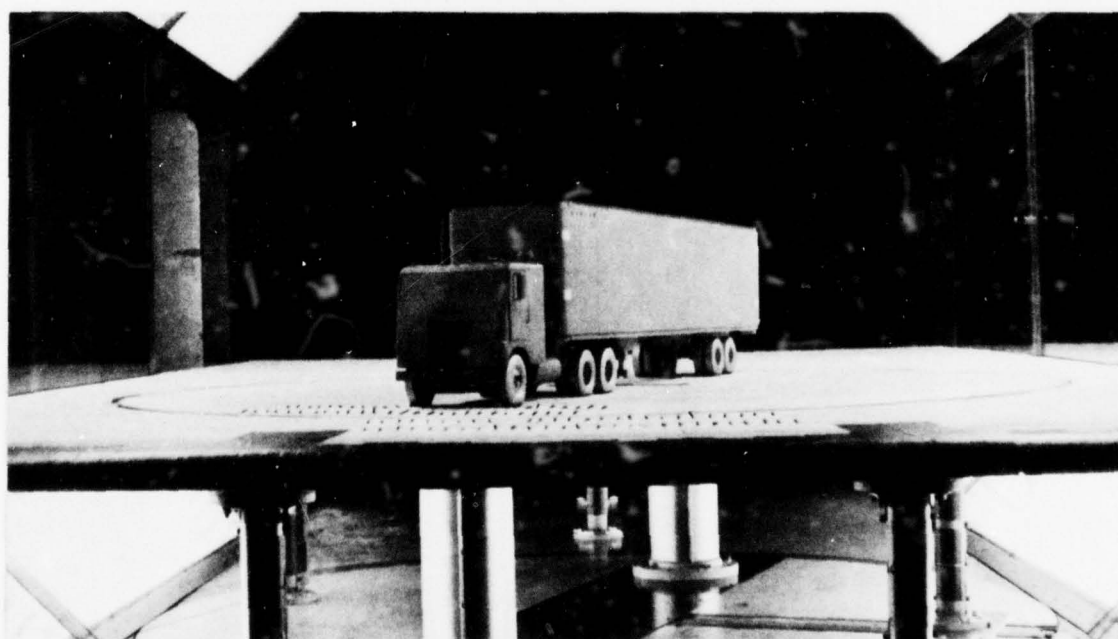
D	body axis drag force, lb
L	body axis lift force, lb
Y	body axis side force, lb
M	body axis pitching moment, lb ft.
N	body axis yawing moment, lb ft.
R	body axis rolling moment, lb ft.
C_D	drag coefficient, $D/q_c A$
$C_{D_{uc}}$	wind axis drag coefficient uncorrected for blockage
\bar{C}_D	wind averaged drag coefficient
\bar{C}_{D_T}	wind averaged drag coefficient in turbulent flow
C_L	lift coefficient, $L/q_c A$
C_Y	side force coefficient, $Y/q_c A$
C_M	pitching moment coefficient, $M/q_c AB$
C_N	yawing moment coefficient, $N/q_c AB$
C_R	rolling moment coefficient, $R/q_c AB$
h	height above ground, ft.
H	height differential between the tractor or cab and trailer roofs, in.
$P(> \xi)$	cumulative probability (probability of exceeding ξ)
$p(\xi)$	probability density (probability of occurrence of ξ)
P_a	power required to overcome aerodynamic drag, hp
P_e	total engine power required, hp
P_r	power required to overcome rolling drag, hp
q	dynamic pressure, $\frac{1}{2} \rho V^2$ lb/ft ²
q_c	dynamic pressure corrected for blockage, lb/ft ²
Re	Reynolds number based on trailer length or wheelbase, 6380 B V
S	wind tunnel test section area above the ground plane, ft ²
SFC	engine specific fuel consumption, lb/hp-hr

NOTATION (Cont'd)

V	resultant air speed approaching the truck, ft./sec. or mph
V_w	wind speed, ft./sec. or mph
V_t	truck speed, ft./sec. or mph
W	truck weight, lb
X	separation between rear face of tractor and front face of trailer, in.
α	exponent in wind power law profile
Δ	indicates the difference between two quantities
η	efficiency of power transmission (power delivered at drive wheels divided by total engine power)
θ	angle of cab-mounted deflector from the vertical
μ	fuel consumption, gal/mi or gal/100 mi (gphm)
ρ	air density, .00238 at STP (.00251 used for fuel calculations)
σ	fuel density, lb/Imperial gallon
ϕ	direction of wind relative to direction of truck motion (0 deg head on)
ψ	yaw angle between resultant wind direction and the direction of truck motion (deg)



VIEW UPSTREAM WITH MODEL YAWED AND TURBULENCE GENERATING GRID IN PLACE.



VIEW DOWNSTREAM WITH THE FREIGHTLINER INSTALLED. THE GROUND PLANE, TURNTABLE AND FAIRINGS SHIELDING THE LOAD CARRYING STRUTS CAN BE SEEN.

FIG. 1: WIND TUNNEL INSTALLATION WITH MODEL ON GROUND PLANE.

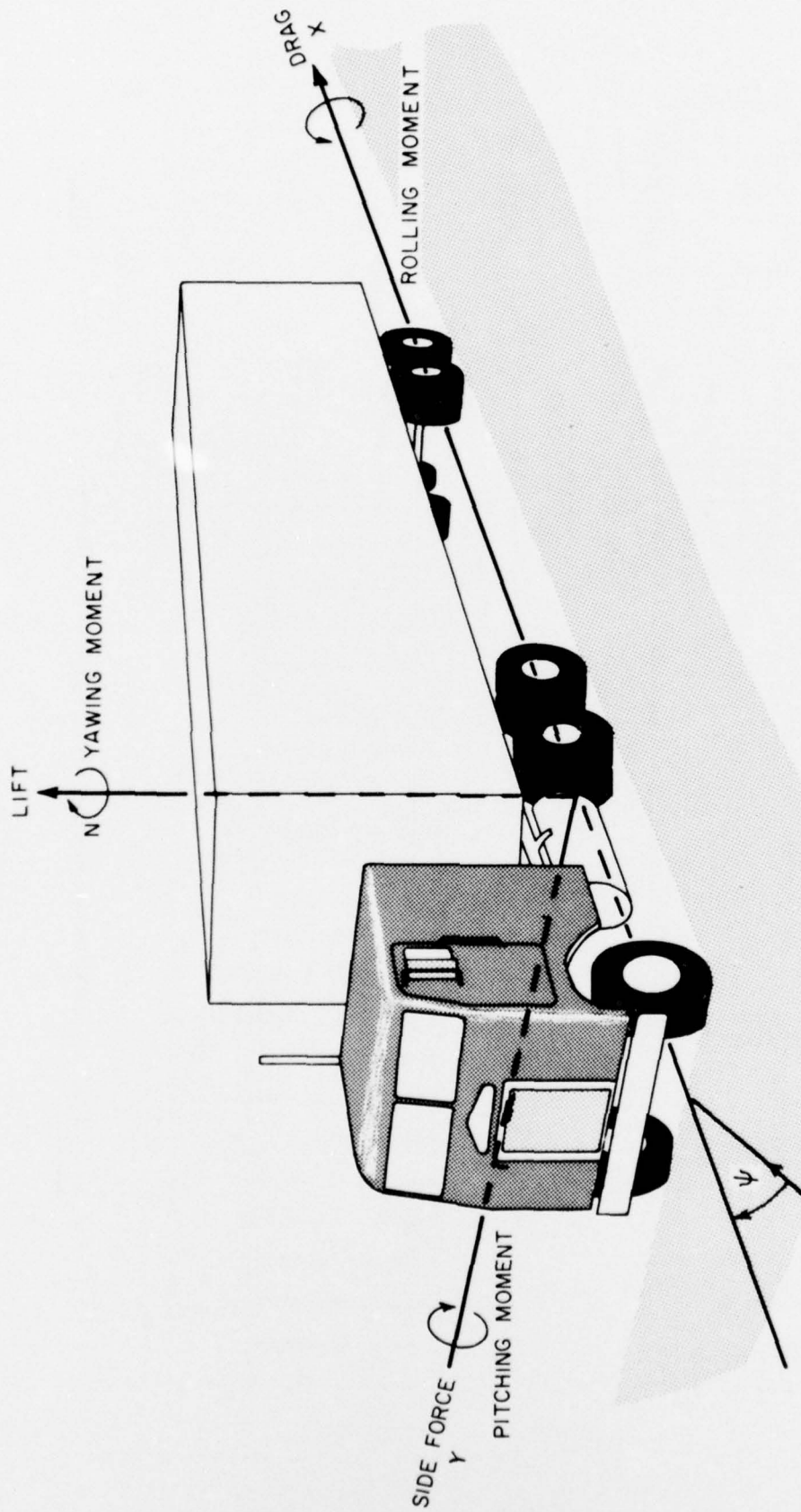
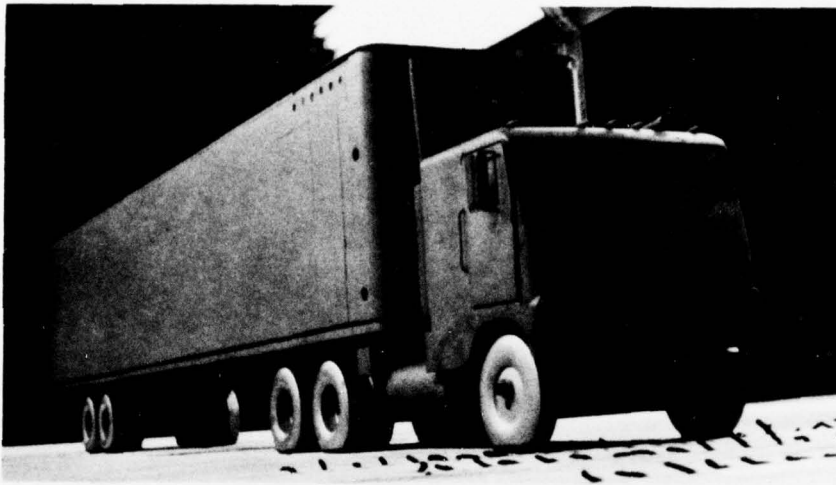
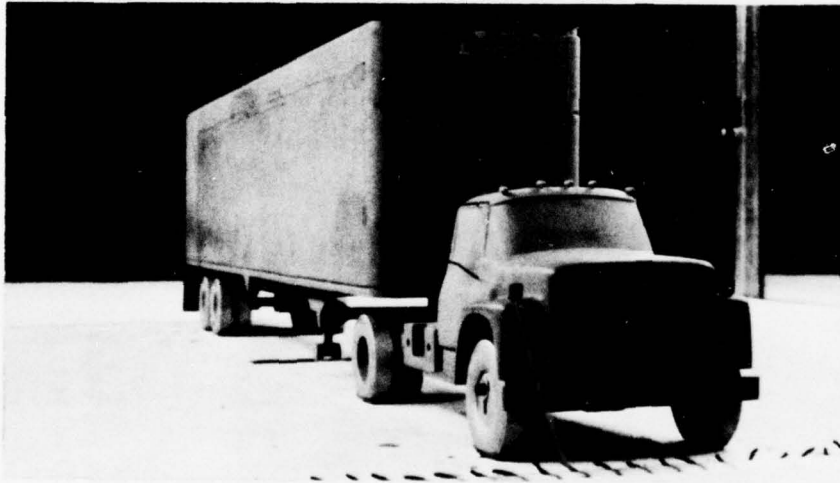


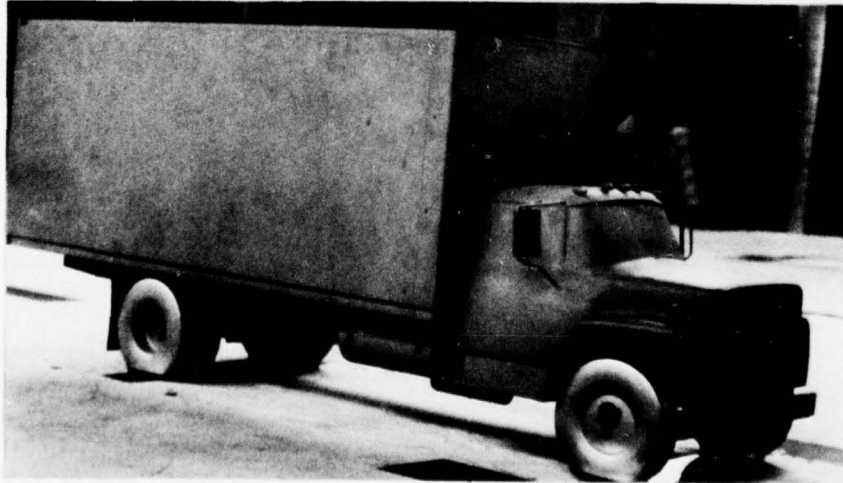
FIG. 3: DEFINITION OF FORCES, MOMENTS AND THE BODY AXIS CO-ORDINATE SYSTEM



a WHITE FREIGHTLINER WFT8664

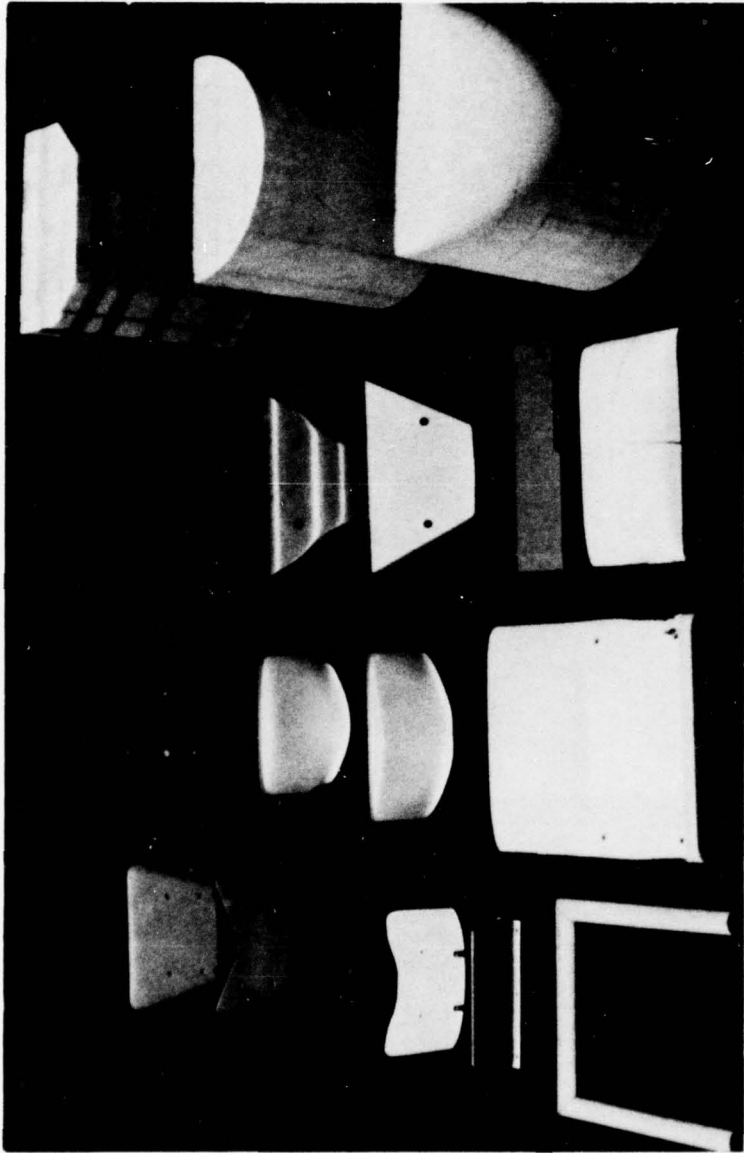


b IHC 1800 LOADSTAR



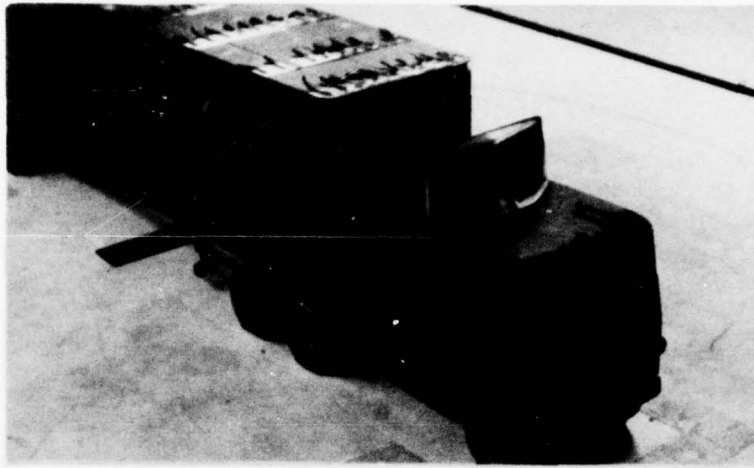
c IHC 1600 STRAIGHT TRUCK

FIG. 4: BASELINE TRUCK MODELS.

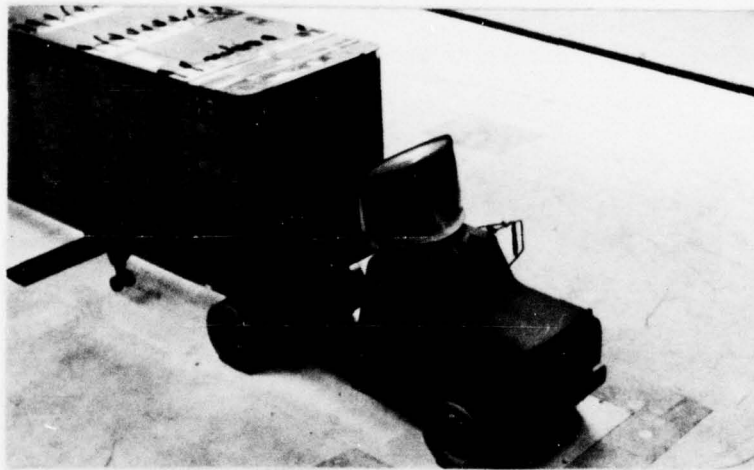


- | | | | |
|-----------------------------------|--------------------------|------------------------|-------------------------|
| FIBERGLASS AIRSHIELD | UNIROYAL DEF. | U. OF MARYLAND FAIRING | BEVELLED NOSE |
| AIRSHIELD FOR IHC 1600 | AIRGLIDE DEF. (IHC) | DRAGFOILER DEF. | CYLINDRICAL NOSE |
| CORLITE AIRSHIELD | AIRGLIDE DEF. (WFT 8664) | DRAGFOILER DEF. | FAIRED CYLINDRICAL NOSE |
| AIRSHIELD FOR IHC 1600 + GAP SEAL | NOSE CONE (TRAILER) | GAP SEAL | |
| VORTEX STABILIZER | | NOSE CONE (IHC 1600) | |
| AEROBOOST | | | |

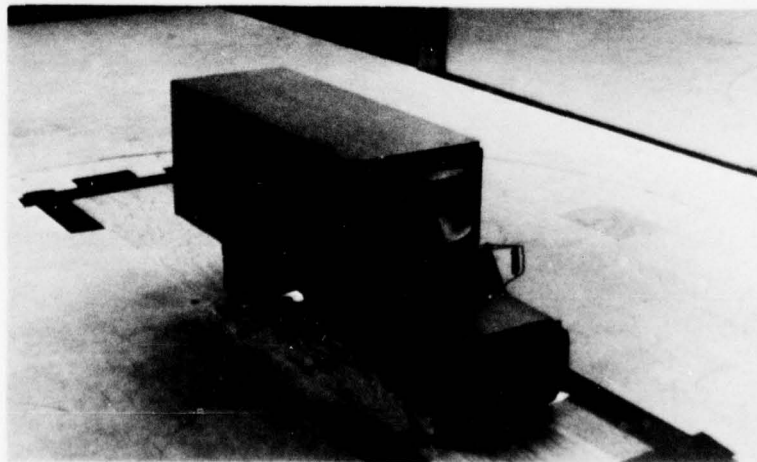
FIG. 5: ADD-ON DEVICES AND TRAILER NOSE SHAPES TESTED.



FREIGHTLINER

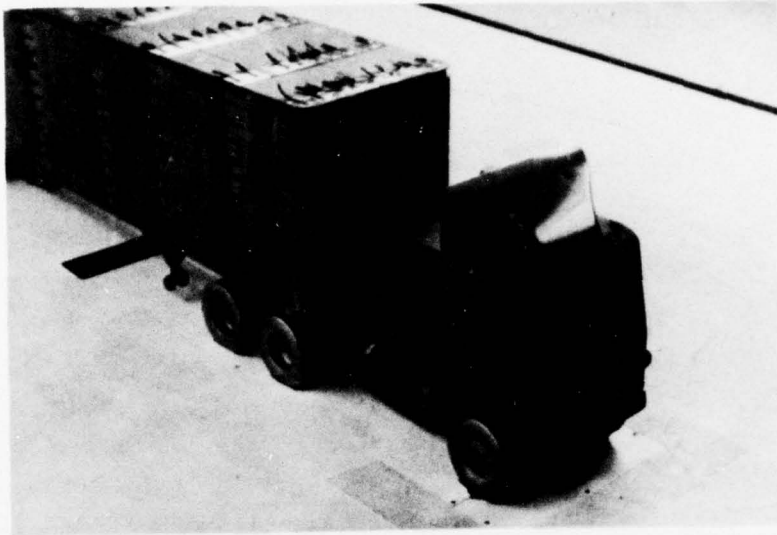


IHC 1800

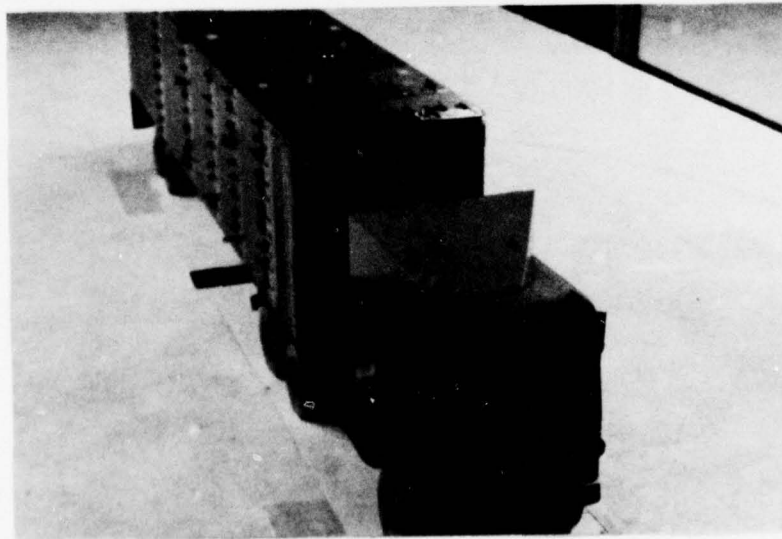


STRAIGHT TRUCK

FIG. 6: AIRGLIDE AIR DEFLECTOR

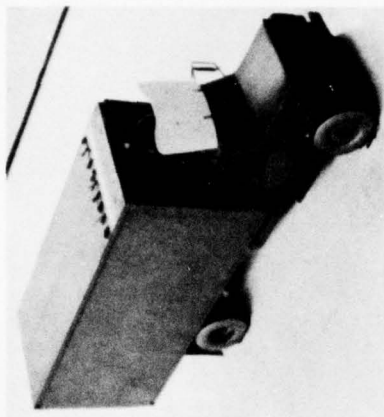


CURVED SIDE ELEVATION
AND PLANFORM.

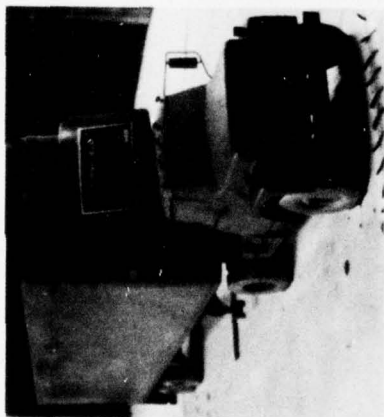


STRAIGHT SIDE ELEVATION
AND PLANFORM.

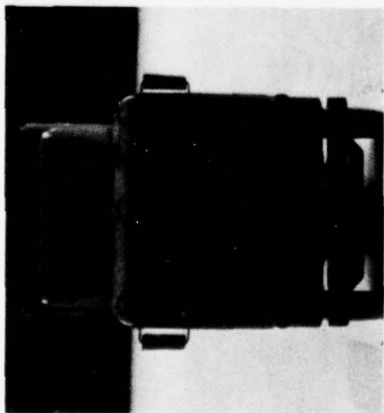
FIG. 7: GENERAL MOTORS DRAGFOILER AIR DEFLECTOR.



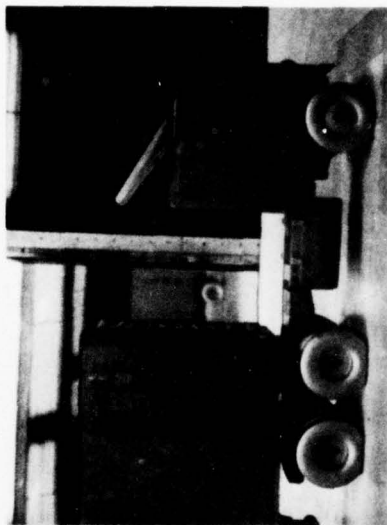
STRAIGHT TRUCK,
CORLITE DEFLECTOR
+ GAP SEAL



IHC 1800
CORLITE DEFLECTOR



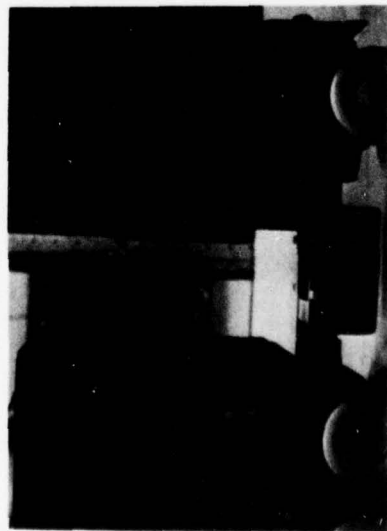
FREIGHTLINER
FIBREGLASS DEFLECTOR



IMPROVED AIRSHIELD

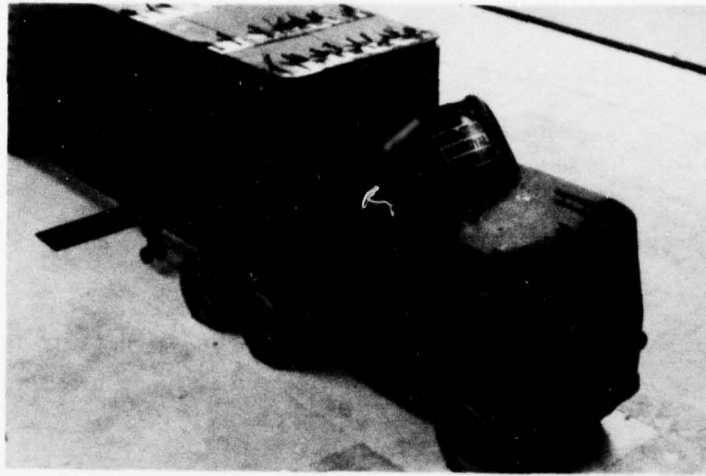


GAP SEAL

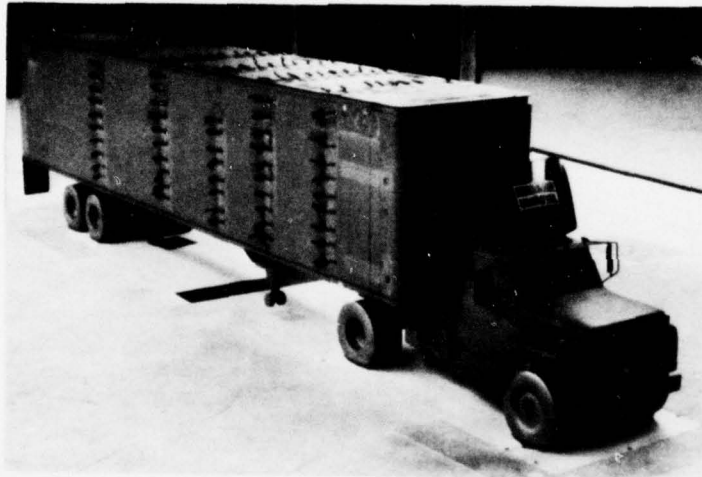


VORTEX STABILIZER

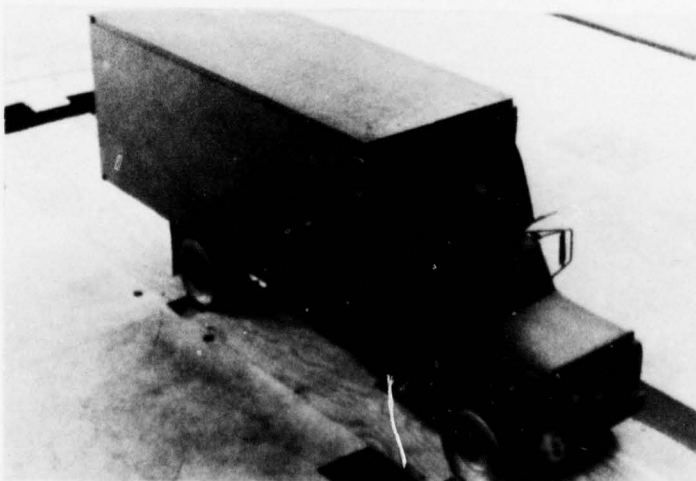
FIG. 8: RUDKIN-WILEY AIRSHIELD AIR DEFLECTORS, VORTEX STABILIZER AND GAP SEAL.



FREIGHTLINER



IHC 1800



STRAIGHT TRUCK

FIG. 9: UNIROYAL AIR DEFLECTOR.

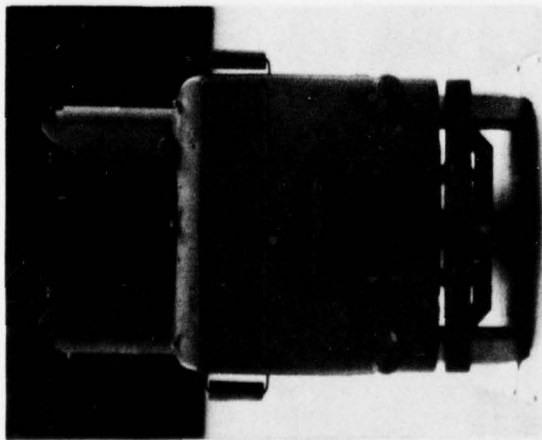
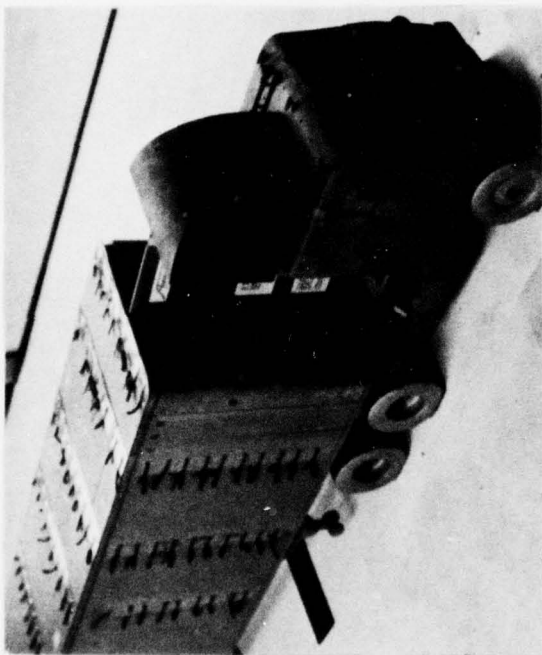
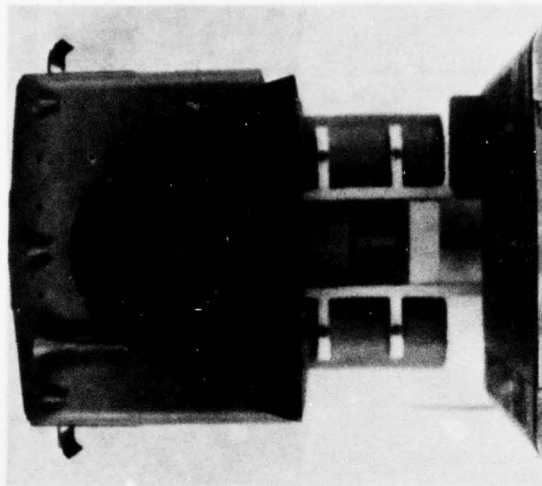
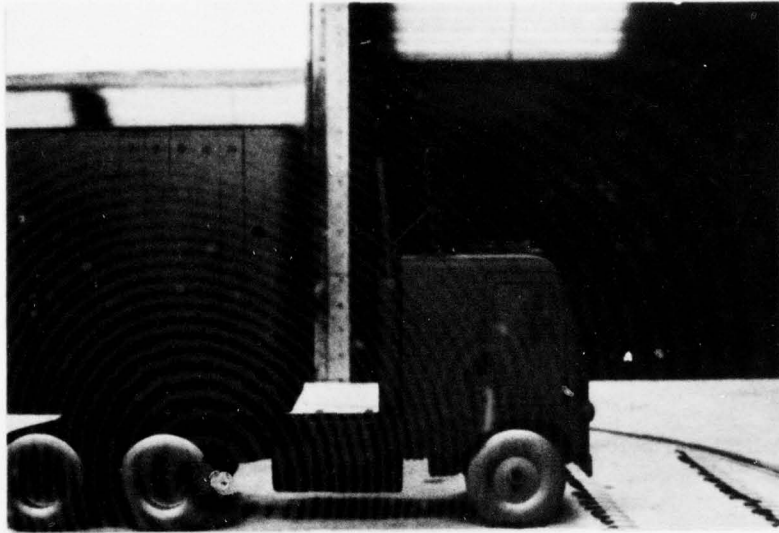
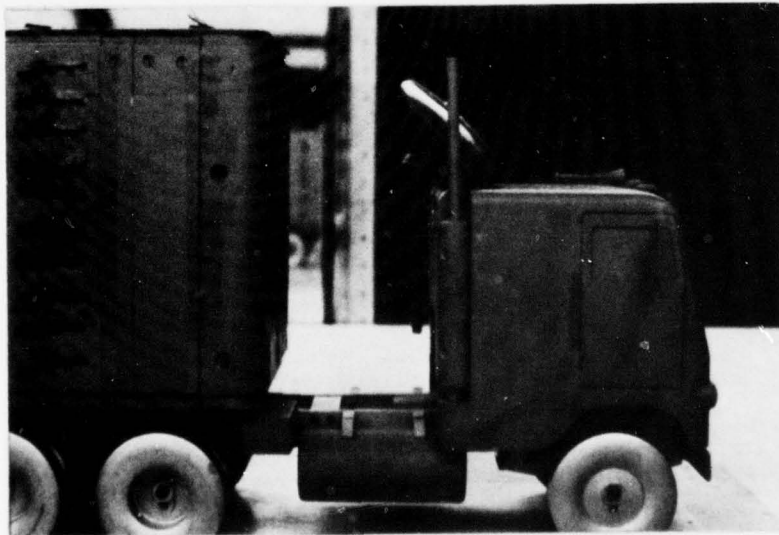


FIG. 10: UNIVERSITY OF MARYLAND DEFLECTOR.



TYPICAL OF CURRENT
PRACTICE



ANGLE OFFERING IMPROVED
PERFORMANCE

FIG. 11: ORIGINAL AND IMPROVED DEFLECTOR ANGLES.

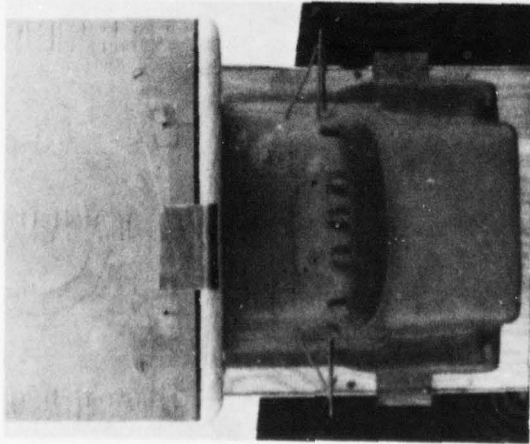
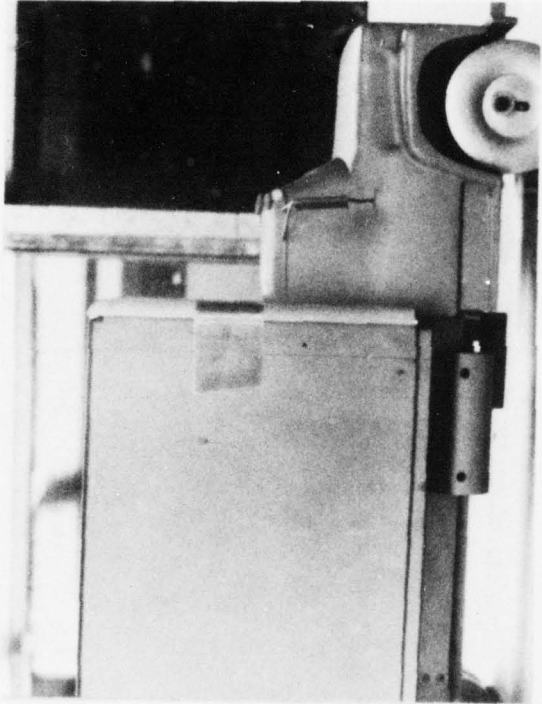
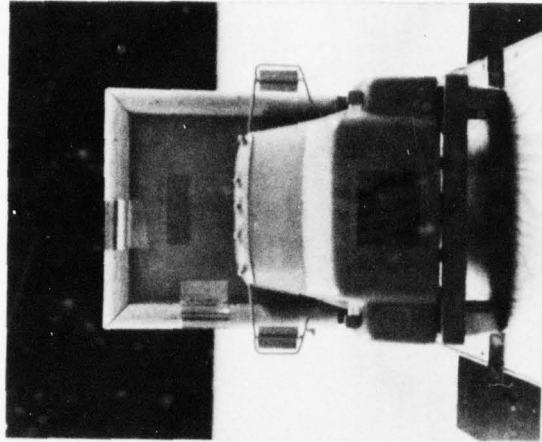
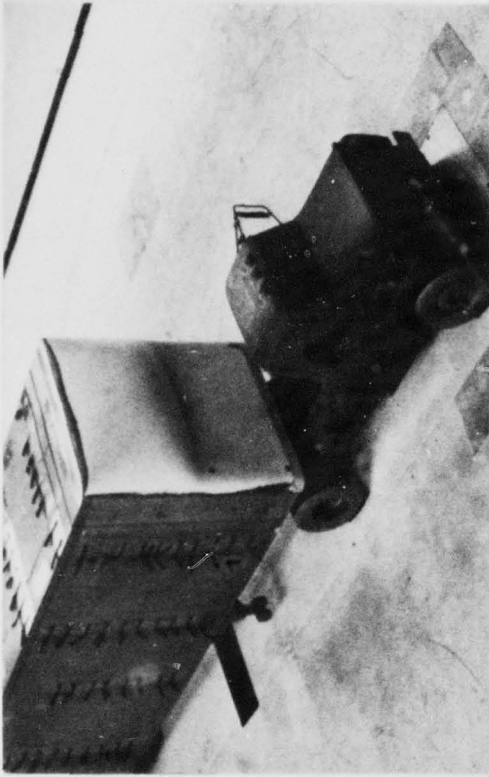
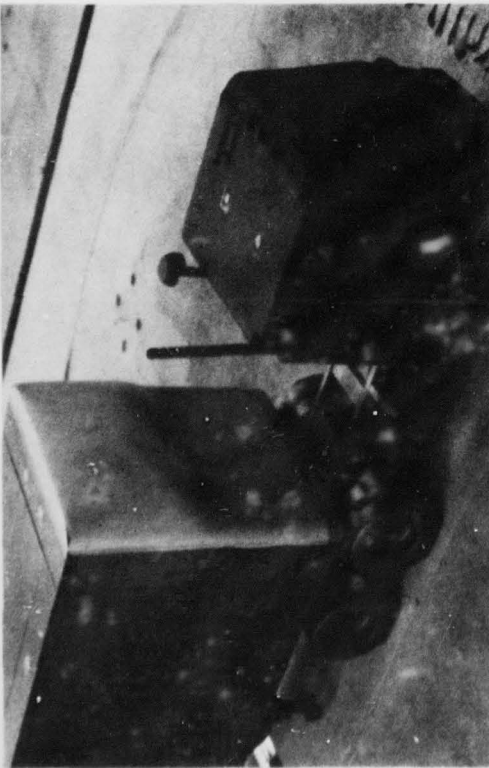


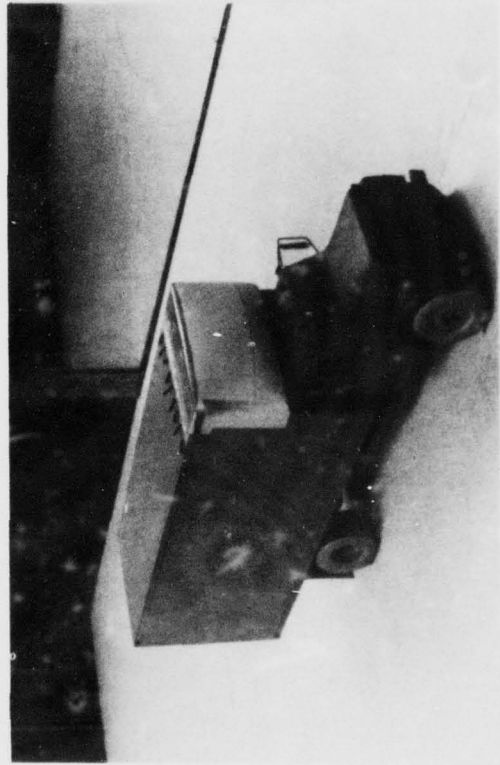
FIG. 12: AEROBOOST CORNER FAIRINGS.



IHC 1800

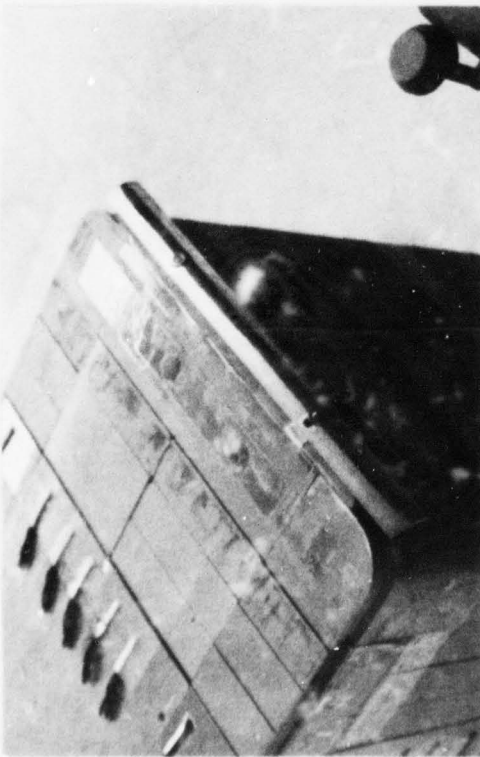


FREIGHTLINER

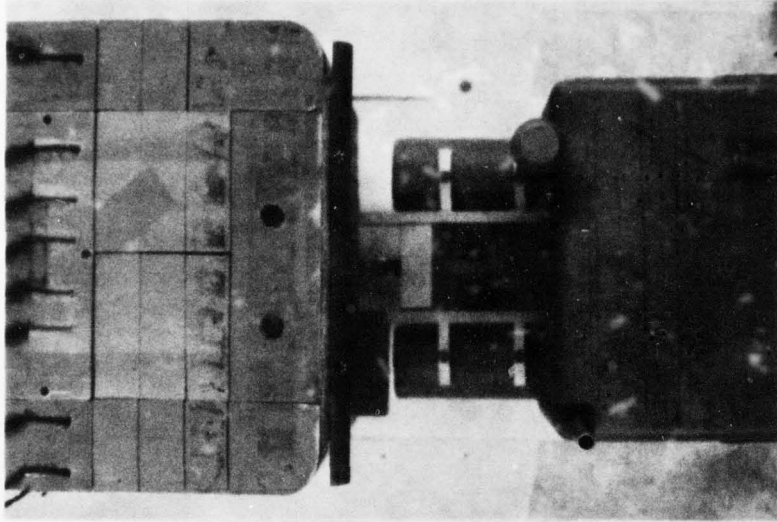


STRAIGHT TRUCK

FIG. 13: NOSE CONE.



TRAILER MOUNTED

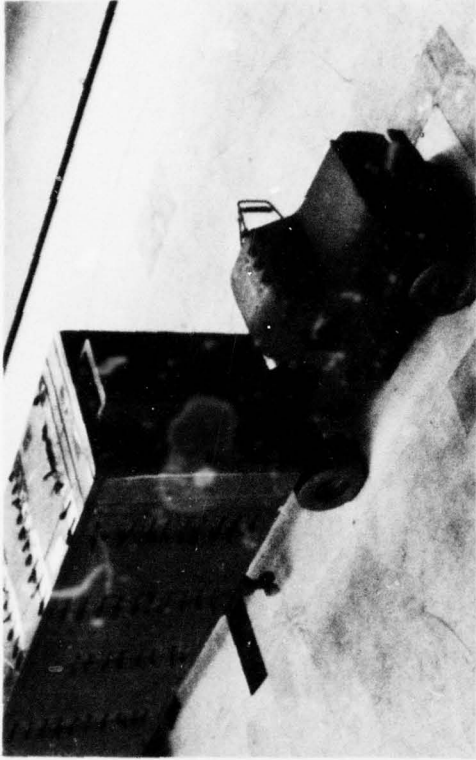


TRAILER MOUNTED



STRAIGHT TRUCK

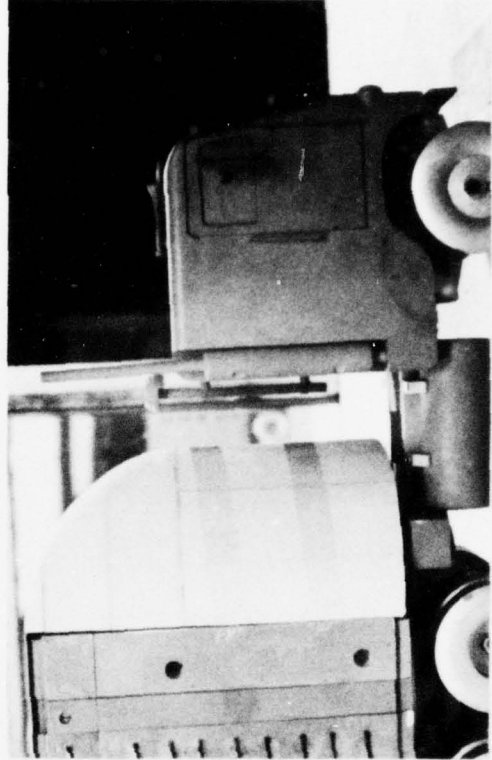
FIG. 14: SYSTEMS SCIENCE AND SOFTWARE (S³) AIRVANE.



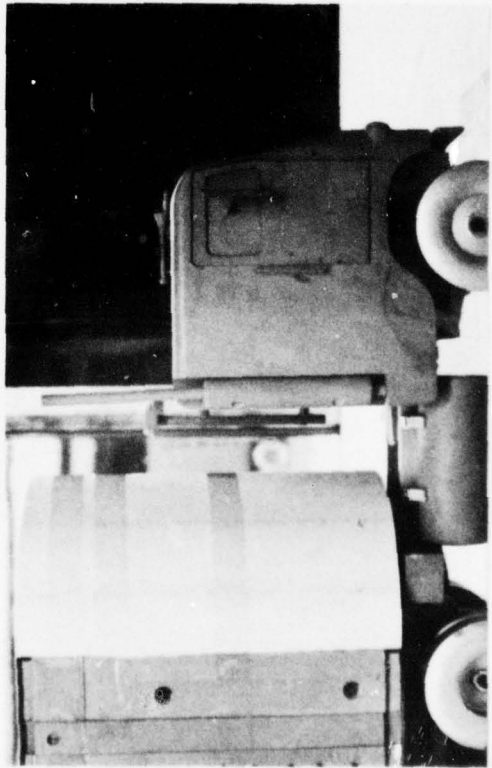
REFRIGERATION UNIT



BEVELLED ("BULL") NOSE

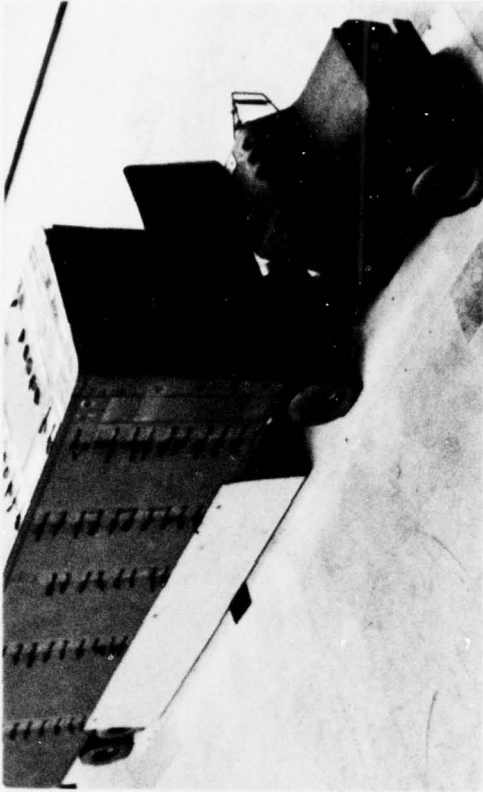


FAIRED CYLINDRICAL NOSE

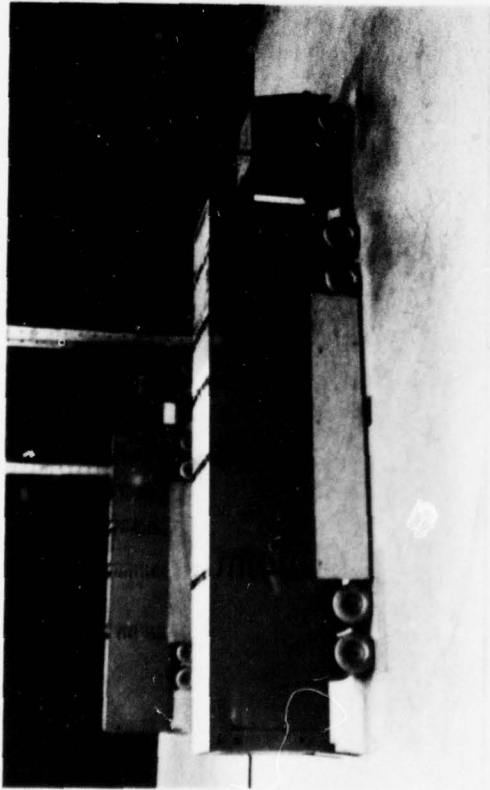


CYLINDRICAL NOSE

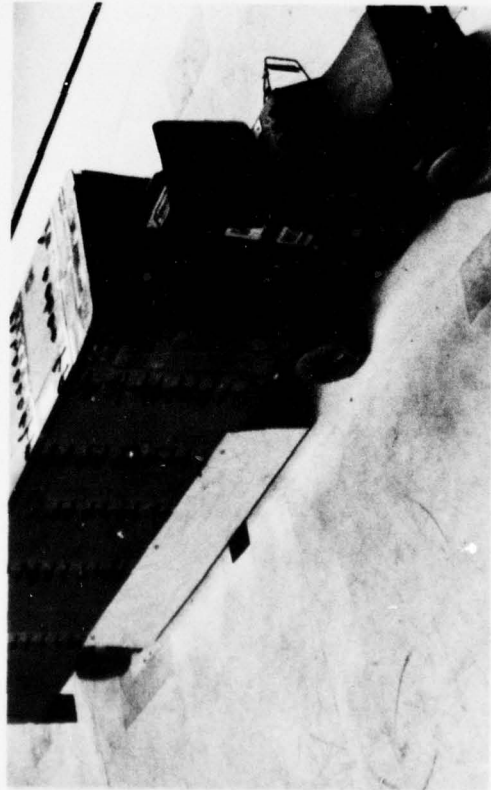
FIG. 15: TRAILER FRONT FACE MODIFICATIONS.



SKIRTS + AIRSHIELD

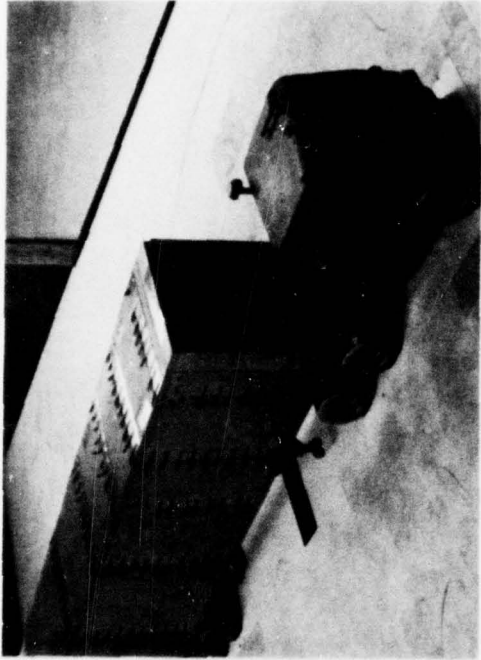


TRAILER SKIRTS (6" CLEARANCE FULL SCALE)



SKIRTS + AIRSHIELD + GAP SEAL

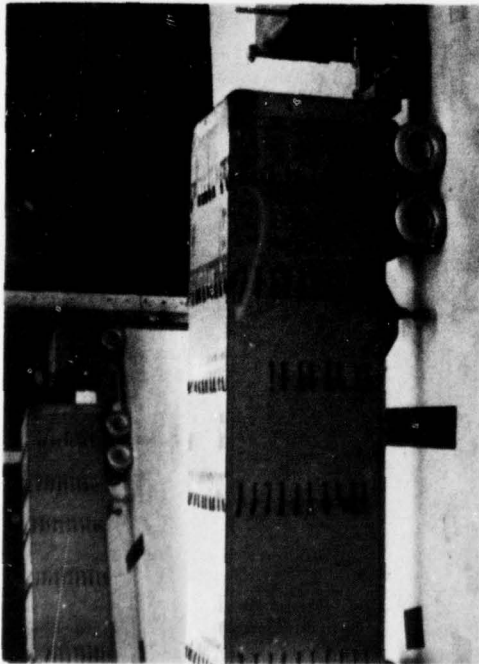
FIG. 16: TRAILER SKIRT CONFIGURATIONS



SQUARE CORNERS



STREAMLINED TRAILER TAIL



12-IN. RADII ON THREE FRONT CORNERS



18-IN. RADIUS REAR CORNERS

FIG. 17: CORNER RADIUS AND TAIL MODIFICATIONS.

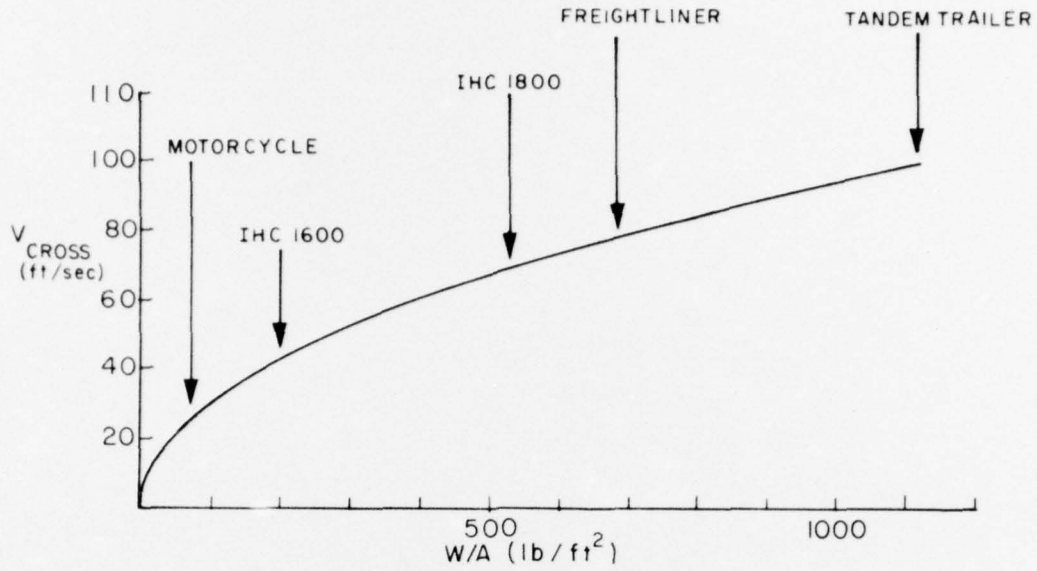


FIG. 19: SPEED AT WHICH AERODYNAMIC AND ROLLING DRAGS ARE EQUAL.

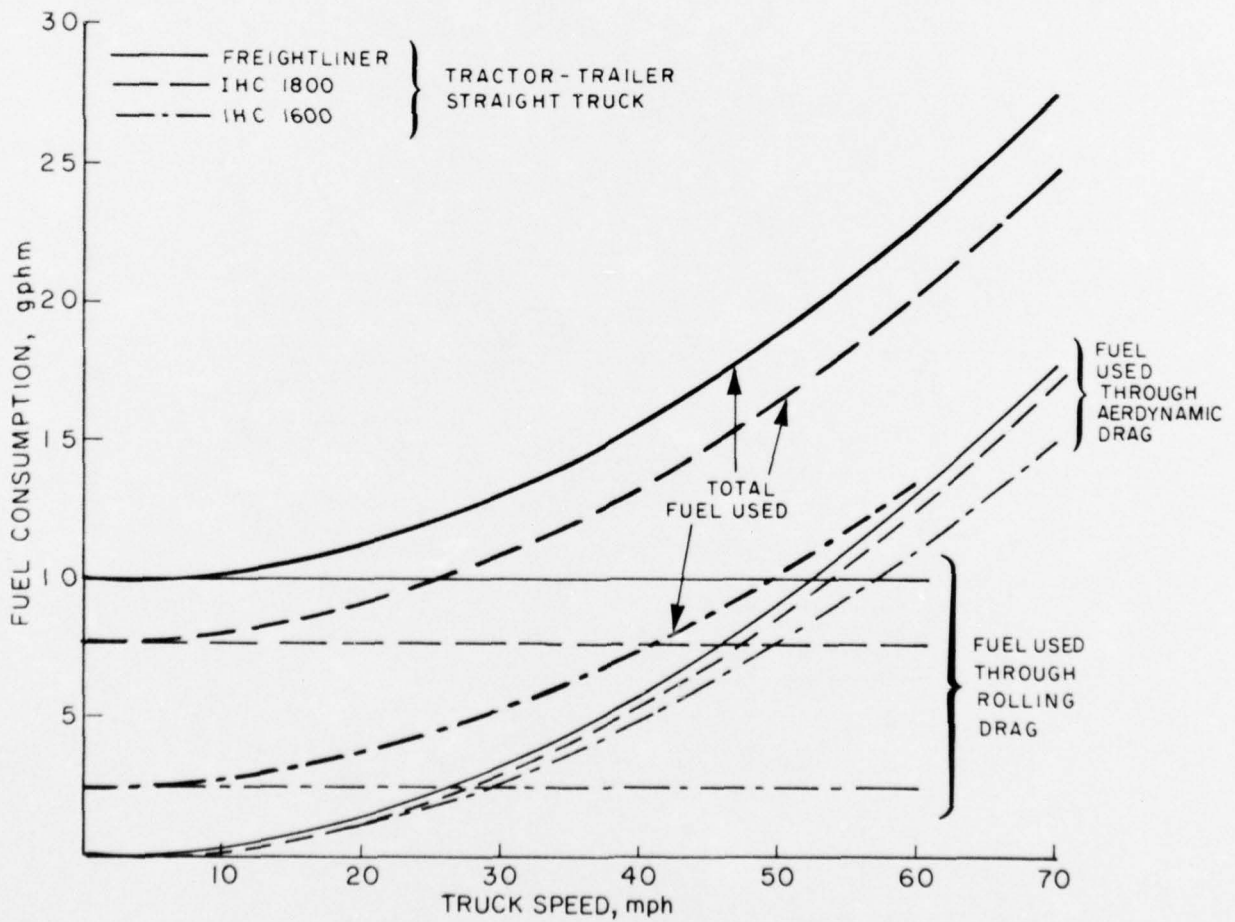


FIG. 20: FUEL REQUIREMENTS.

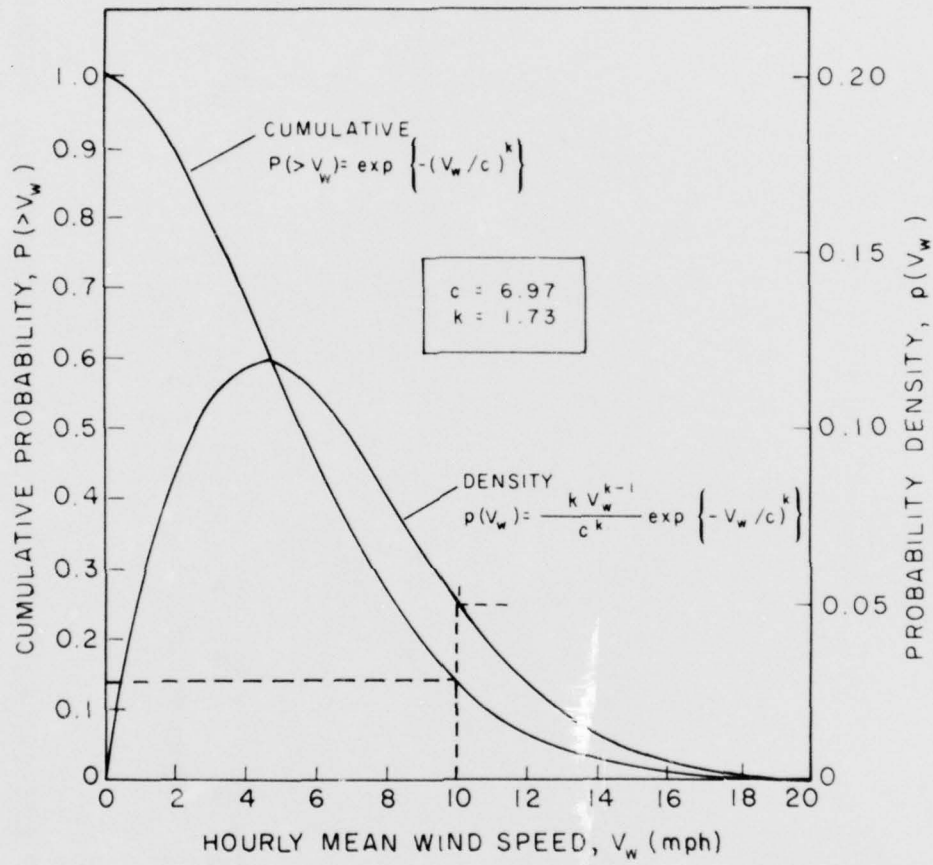


FIG. 21: AVERAGE CANADIAN WIND PROBABILITIES AT 10 FT. ABOVE THE ROAD.

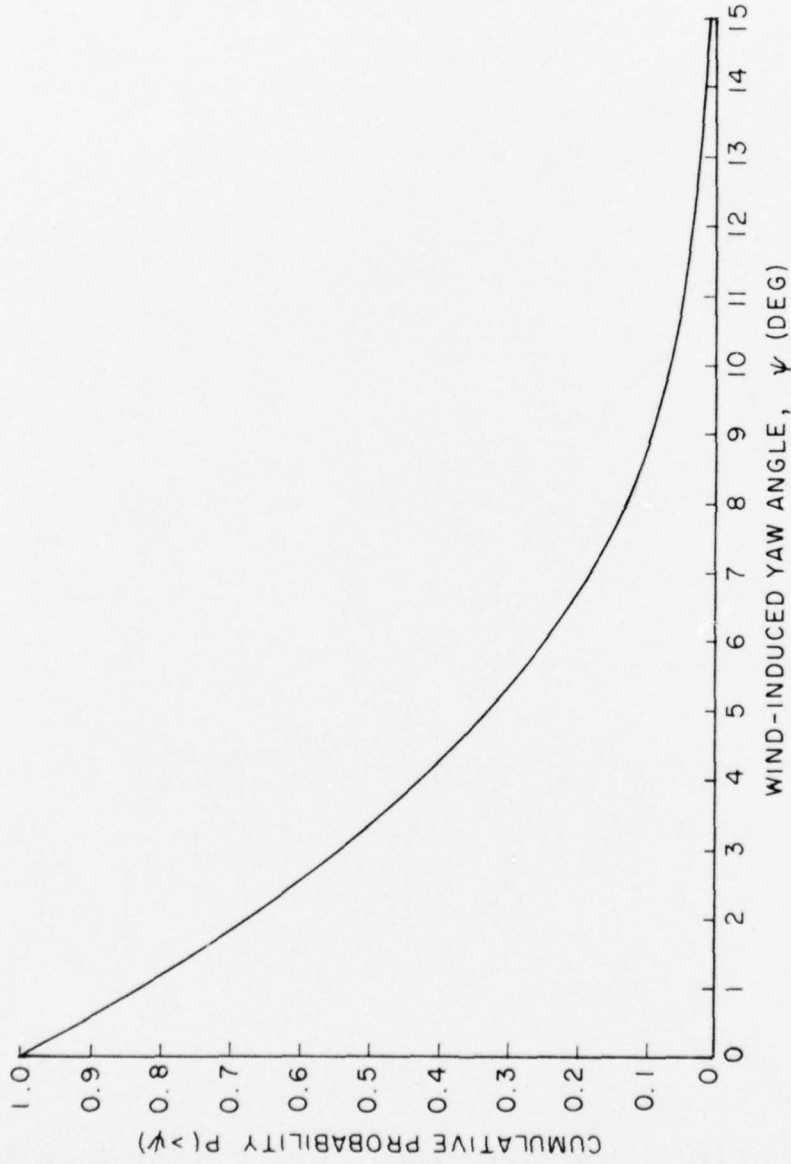
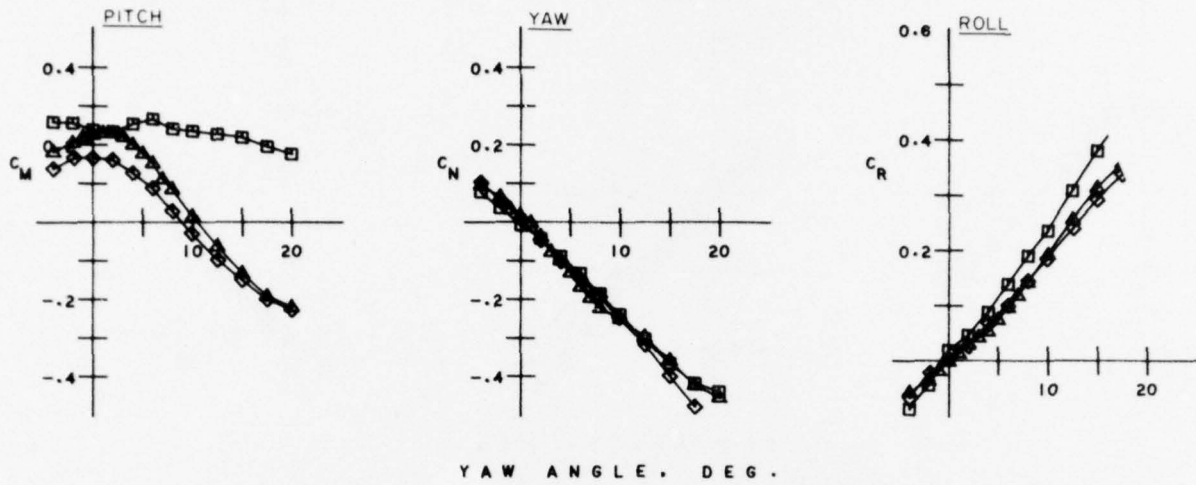


FIG. 22: PROBABILITY OF EXCEEDING A GIVEN YAW ANGLE FOR A TRUCK TRAVELLING 55 MPH.



\bar{C}_D	CONFIGURATION	} $x = 53$ in.
△ 0.99	WHITE FREIGHTLINER WFT 8664	
◇ 0.92	IHC 1800 LOADSTAR	
□ 0.88	IHC 1600 STRAIGHT TRUCK	

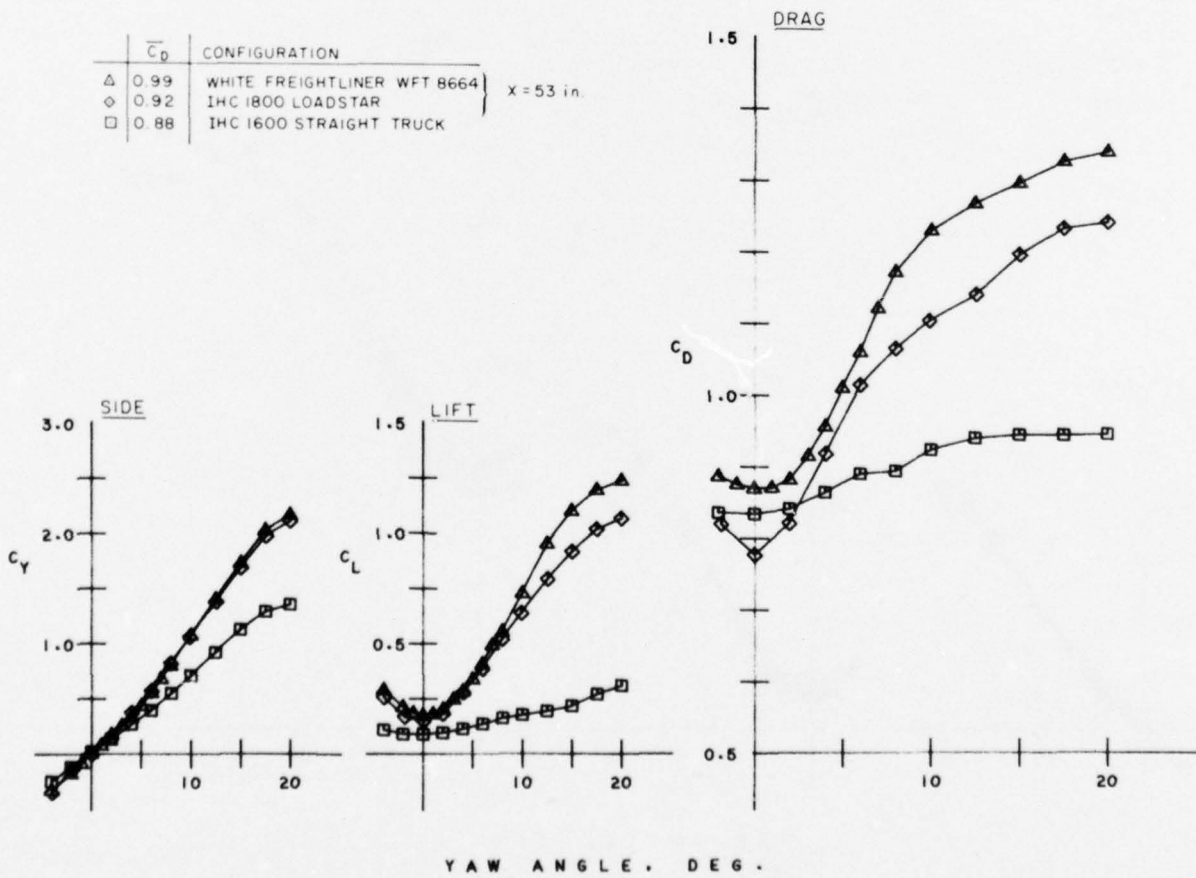
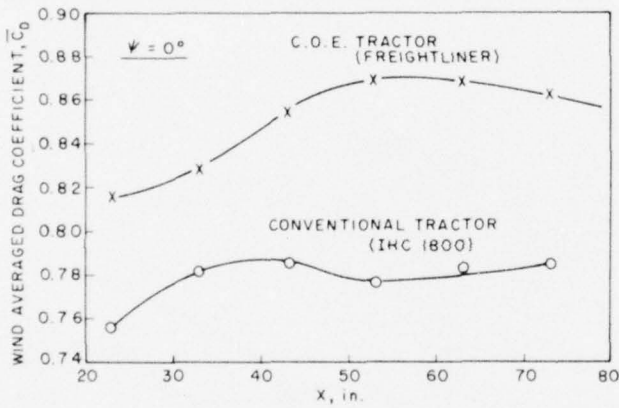
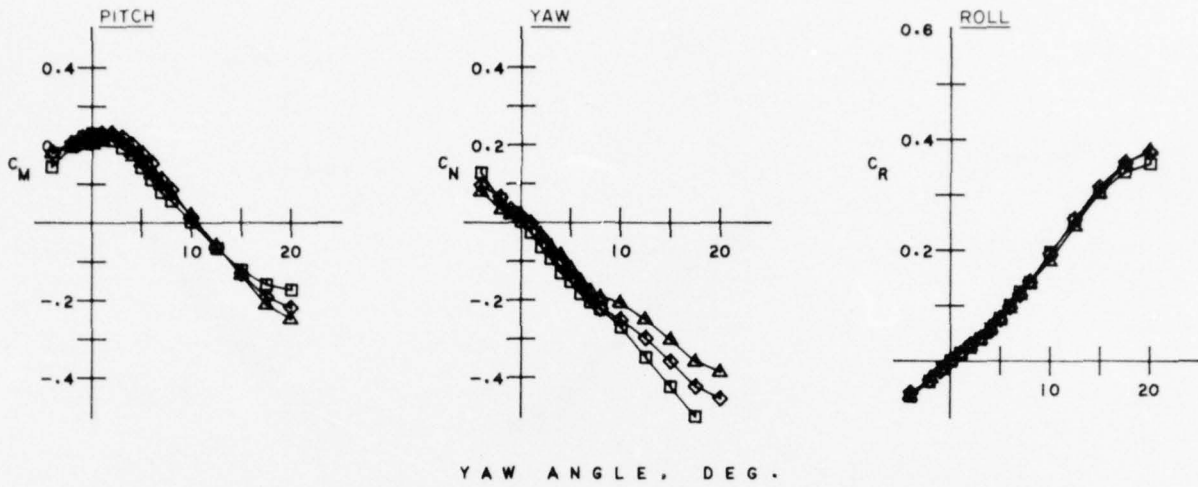


FIG. 23: CHARACTERISTICS OF THE THREE BASELINE TRUCKS ($V = 225$ FT./SEC.).



	C_D	X (in)
Δ	0.94	33
\diamond	0.99	53
\square	1.00	73

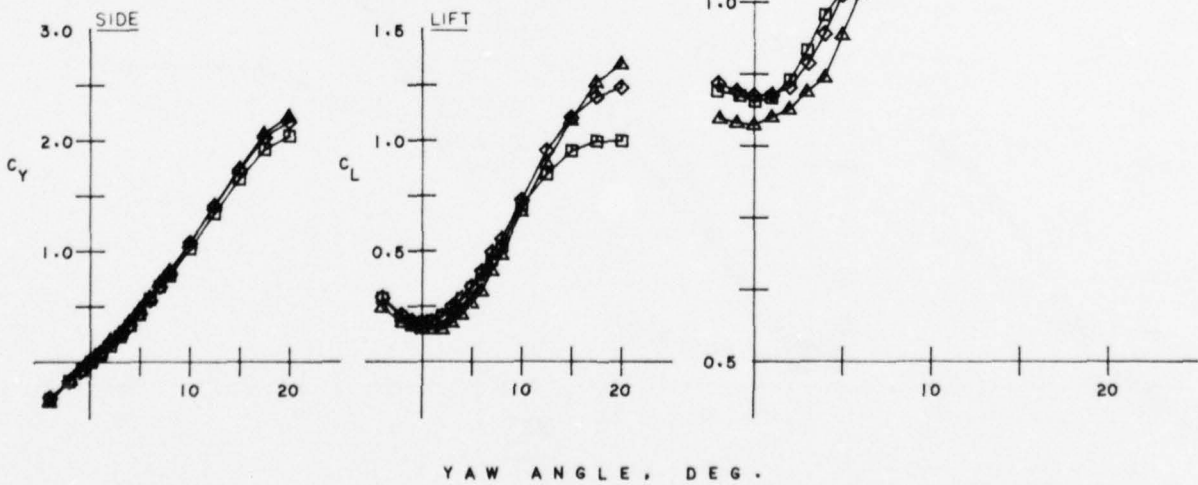


FIG. 24: EFFECT OF TRACTOR-TRAILER SEPARATION FOR THE FREIGHTLINER ($V = 225$ FT./SEC.).

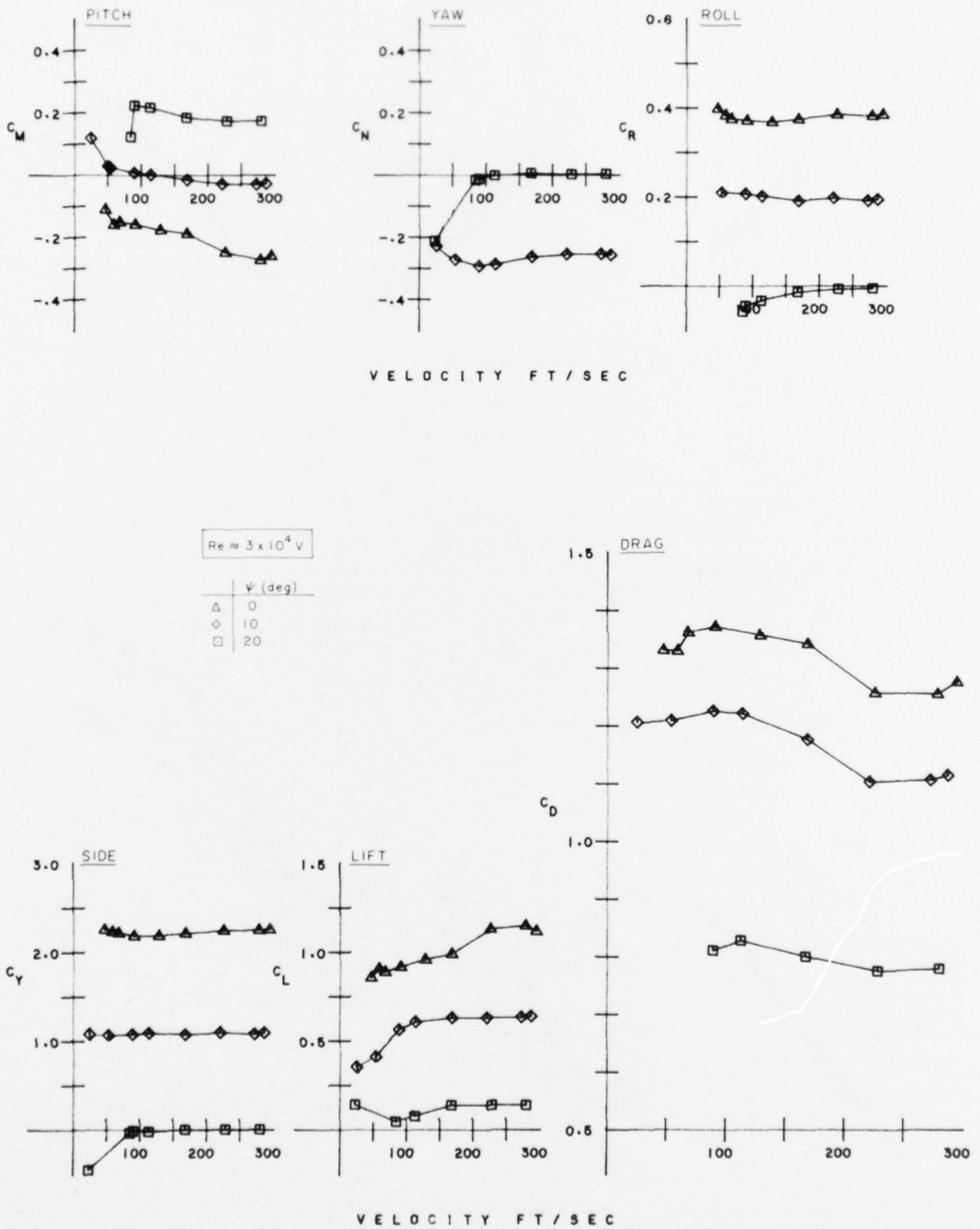


FIG. 25: EFFECT OF REYNOLDS NUMBER FOR THE IHC 1800 LOADSTAR
(X = 53 IN., V = 225 FT./SEC.).

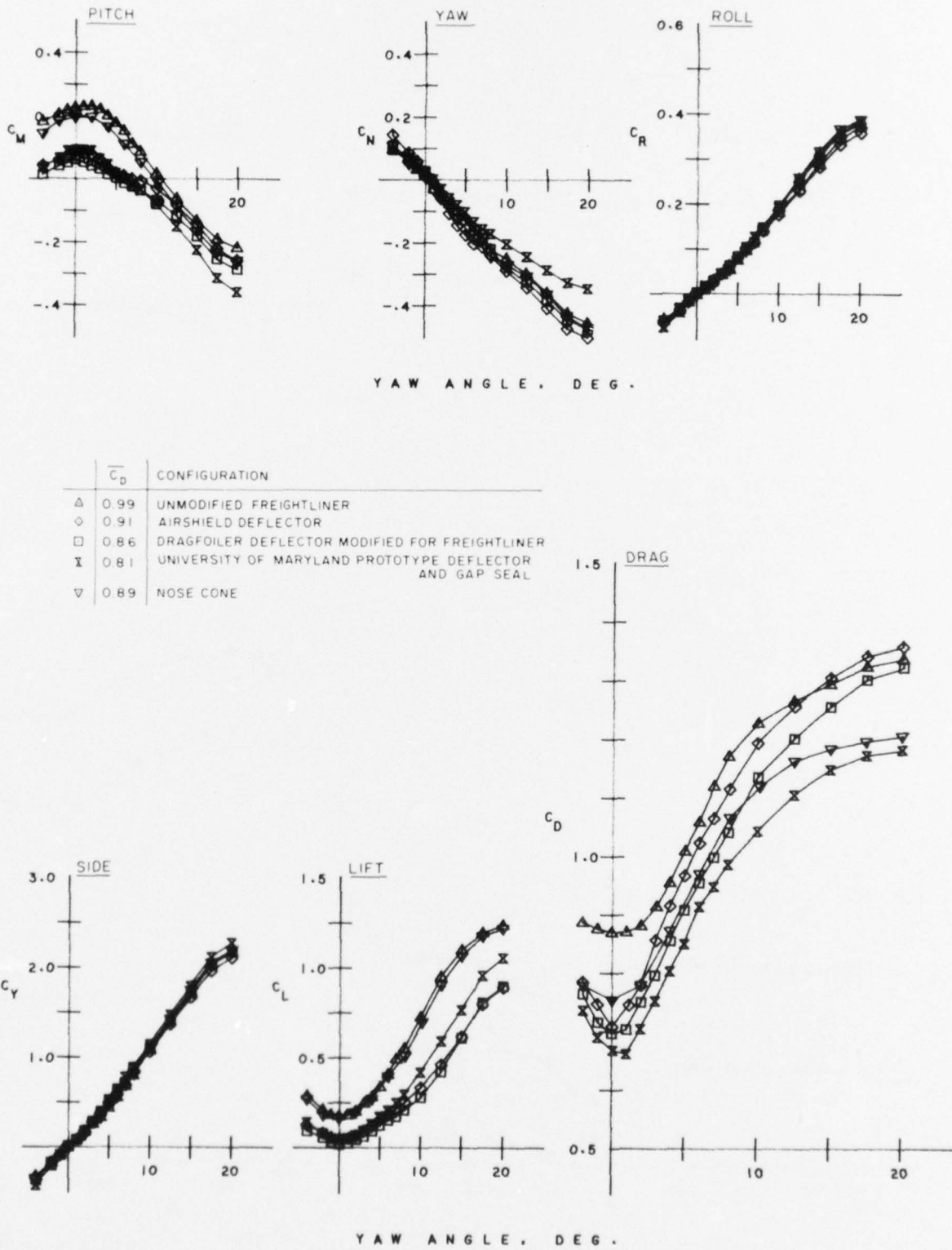


FIG. 26: WHITE FREIGHTLINER WFT8664 WITH ADD-ON DEVICES
(X = 53 IN., V = 225 FT./SEC.).



\bar{C}_D	CONFIGURATION
△	0.92 UNMODIFIED IHC 1800 LOADSTAR
◇	0.88 AIRSHIELD DEFLECTOR
□	0.84 AIRSHIELD DEFLECTOR AND GAP SEAL
×	0.78 AIRSHIELD DEFLECTOR AND TRAILER SKIRTS
▽	0.84 NOSE CONE

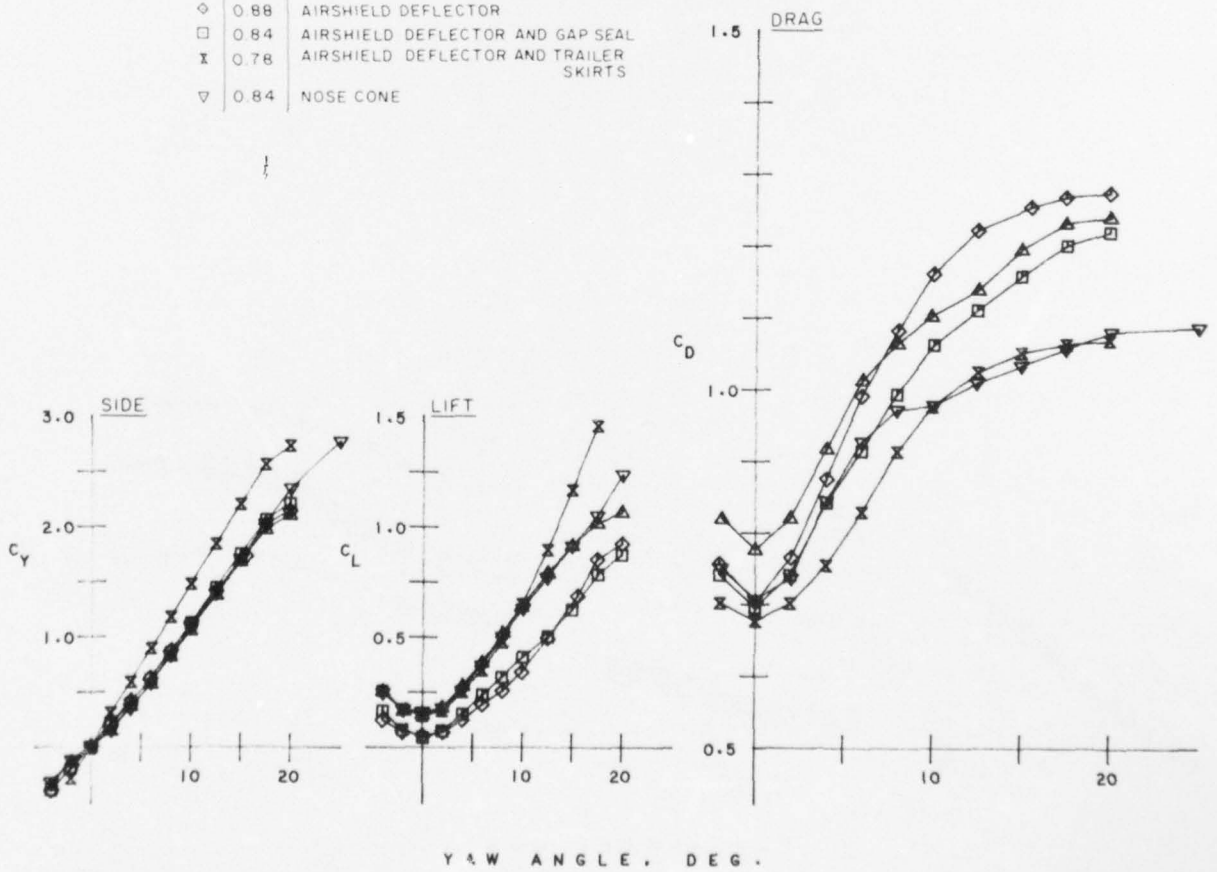
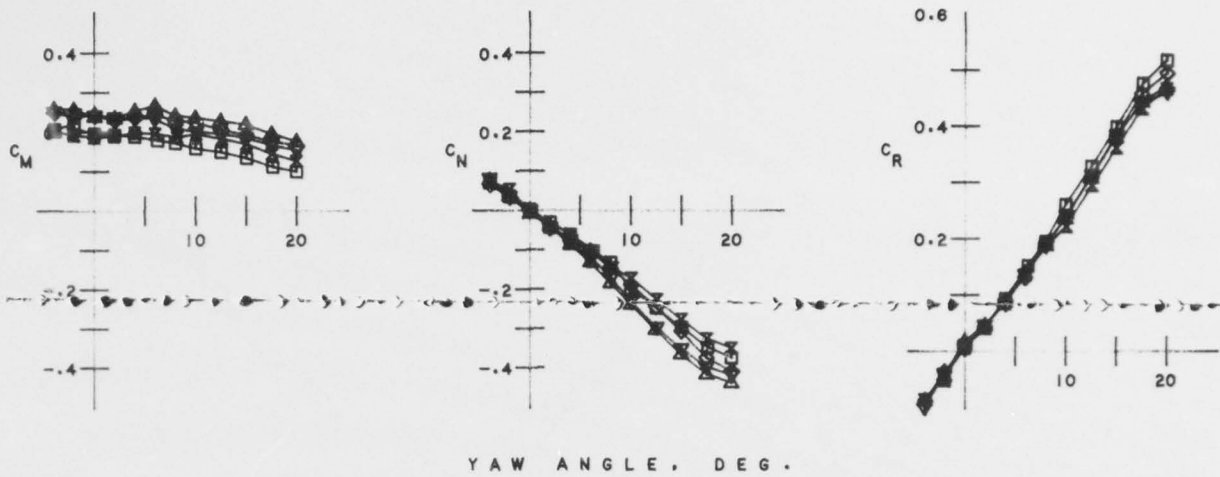


FIG. 27: IHC 1800 LOADSTAR WITH ADD-ON DEVICES (X = 53 IN., V = 225 FT./SEC.).



	$\overline{C_D}$	CONFIGURATION
△	0.88	UNMODIFIED IHC 1600 STRAIGHT TRUCK
◇	0.76	AEROBOOST (APPROXIMATION TO)
□	0.68	NOSE CONE
⊗	0.73	AIRSHIELD AND GAP SEAL
▽	0.80	AIRVANE (TOP FRONT CORNER ONLY)

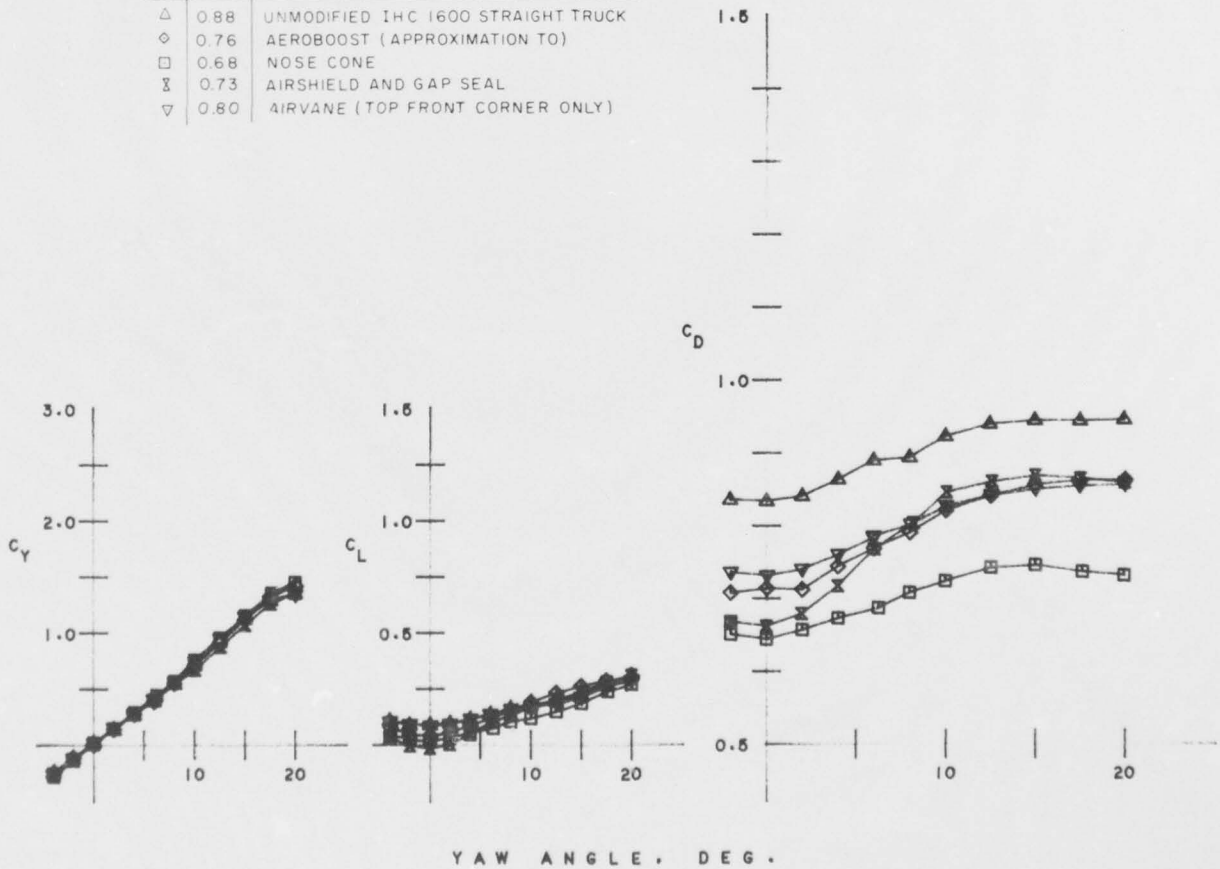


FIG. 28: IHC 1600 STRAIGHT TRUCK WITH ADD-ON DEVICES (V = 225 FT./SEC.).

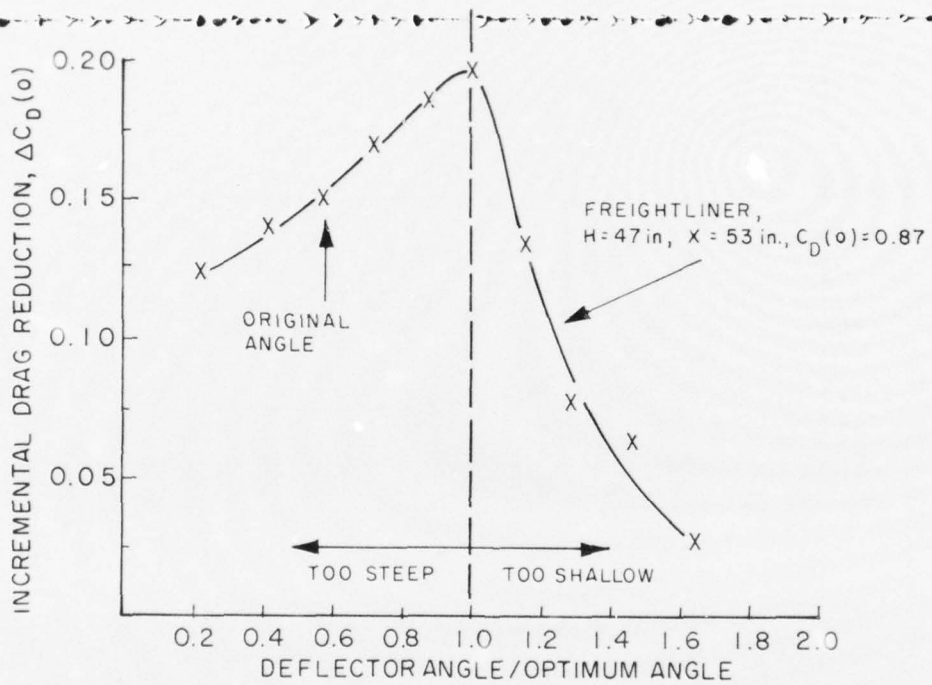


FIG. 29: EFFECT OF DEFLECTOR INCLINATION AT ZERO YAW ANGLE.

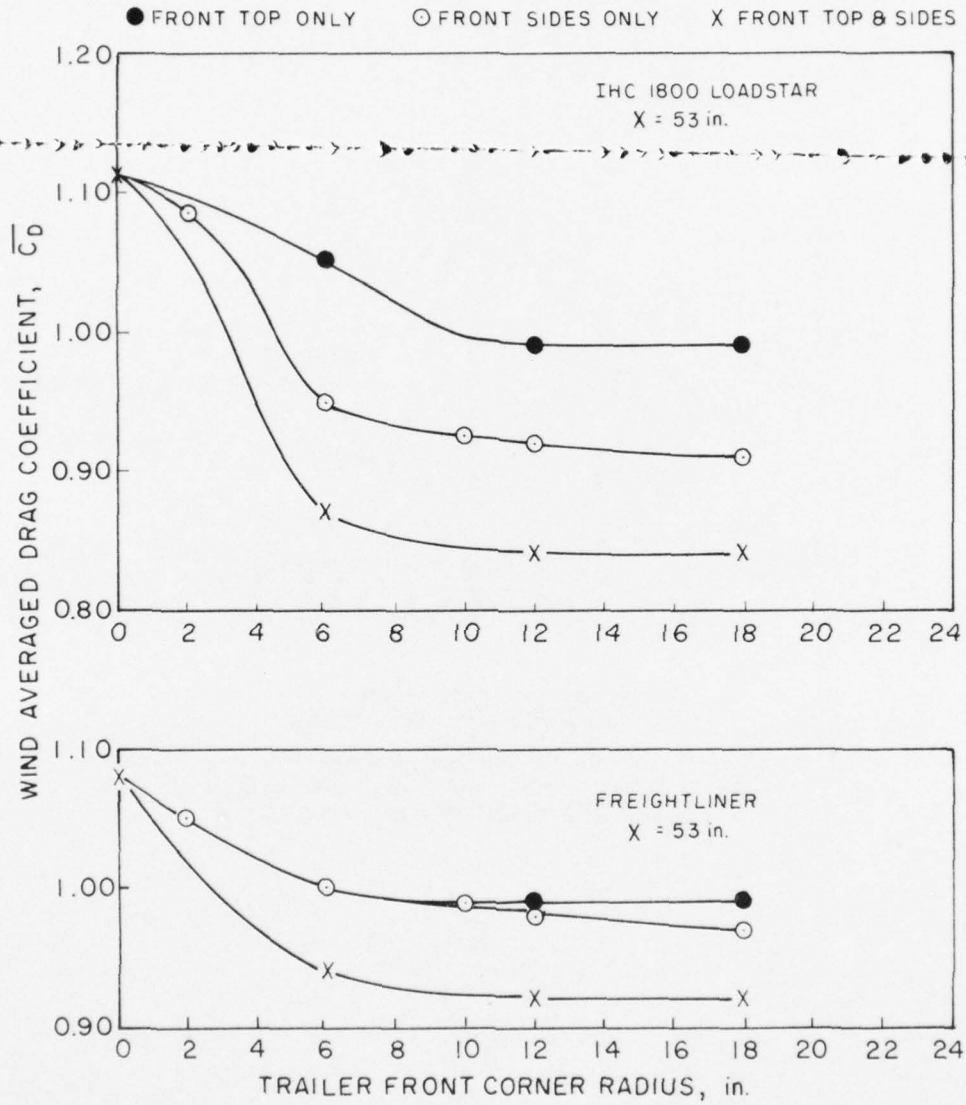
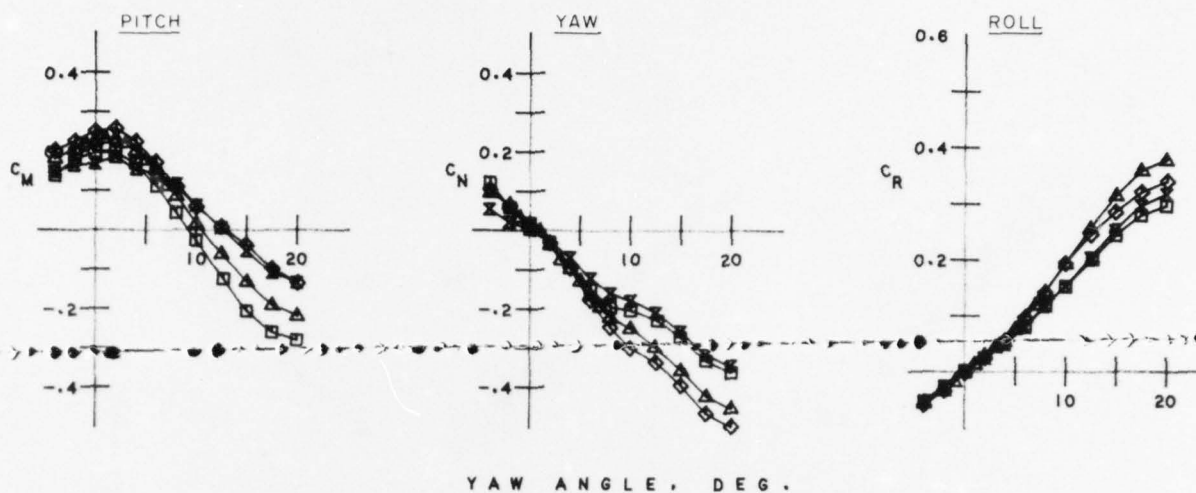


FIG. 30: EFFECT OF CORNER RADIUS.



	C_D	CONFIGURATION
△	0.99	UNMODIFIED FREIGHTLINER
◇	1.07	SQUARE CORNERED TRAILER
□	0.91	12-INCH RADIUS ON FRONT TOP AND SIDE CORNERS
⊗	0.80	AS ABOVE + 18-INCH RADIUS ON REAR TOP AND SIDE CORNERS

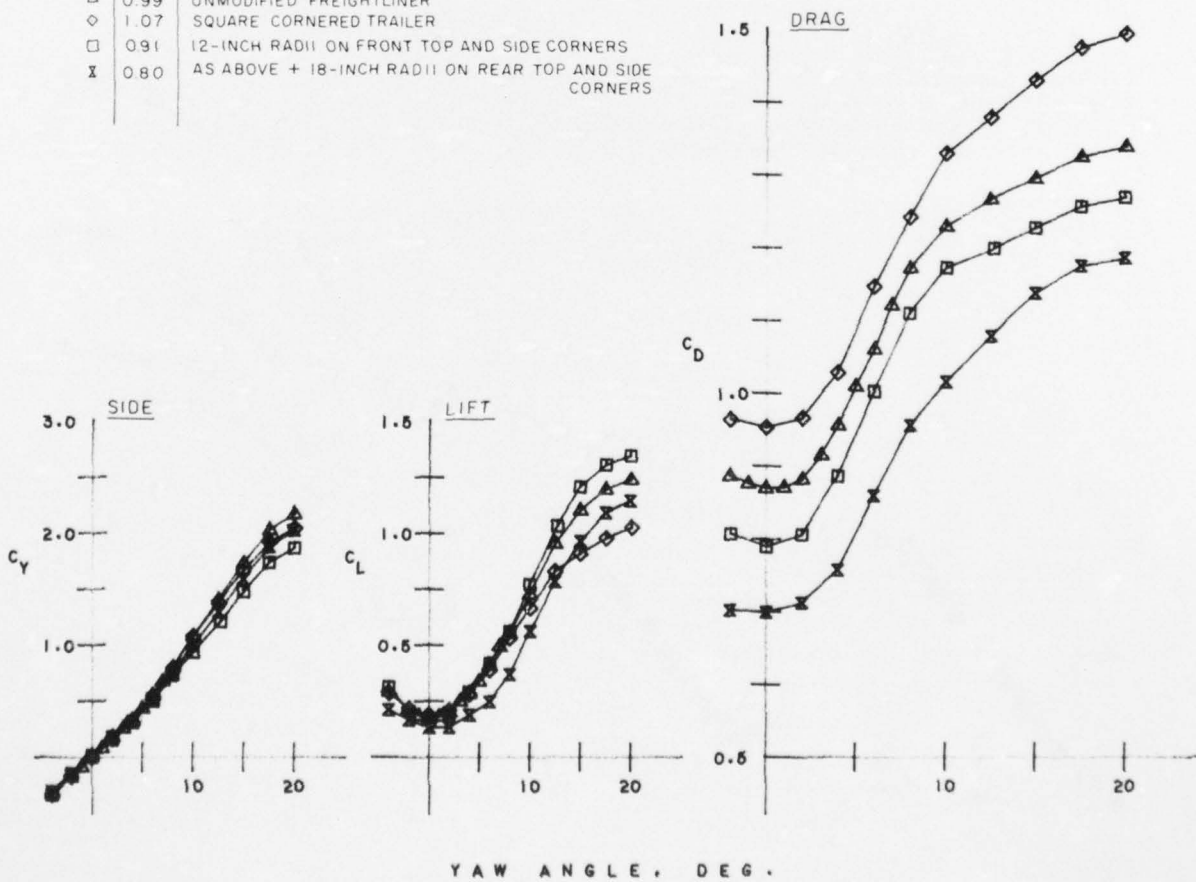
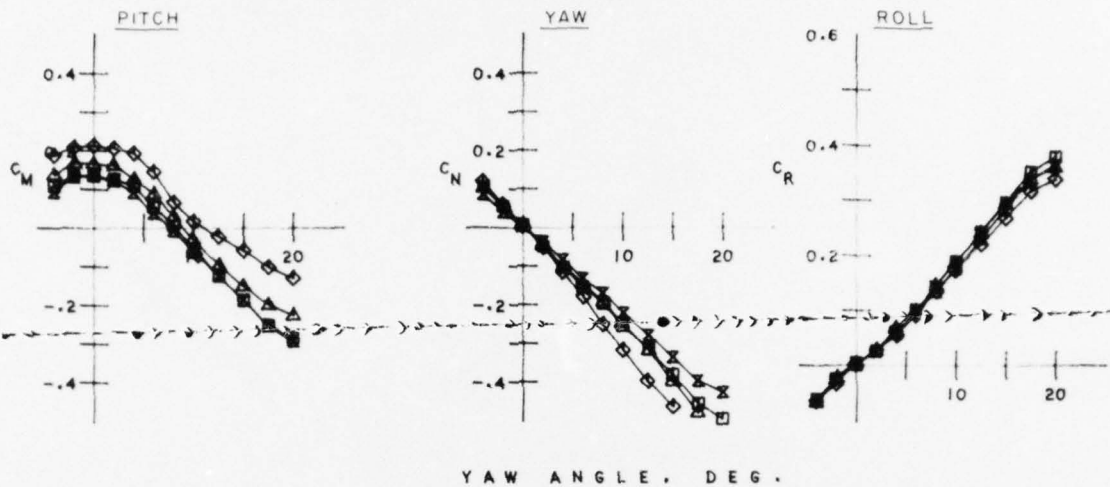
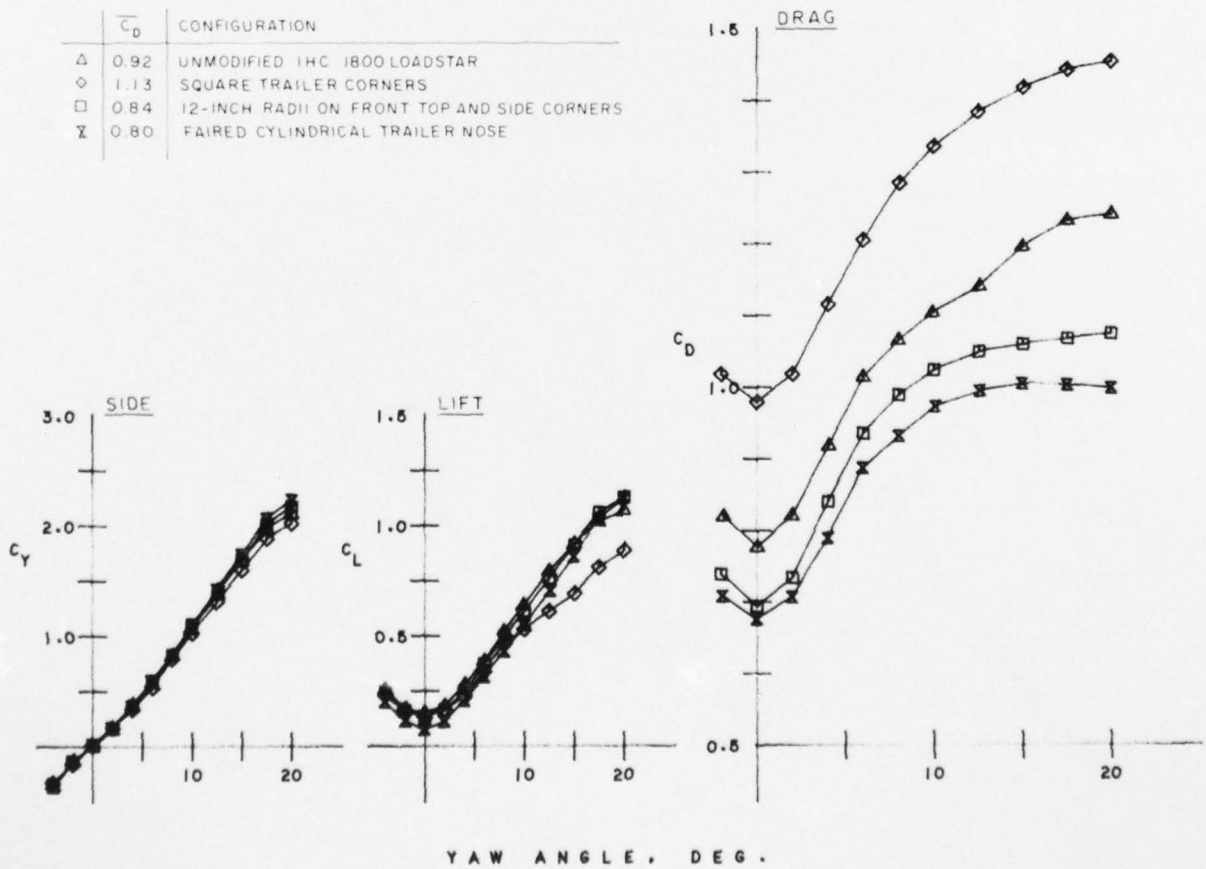


FIG. 31: TRAILER MODIFICATIONS WITH THE FREIGHTLINER TRACTOR
(X = 53 IN., V = 225 FT./SEC.)



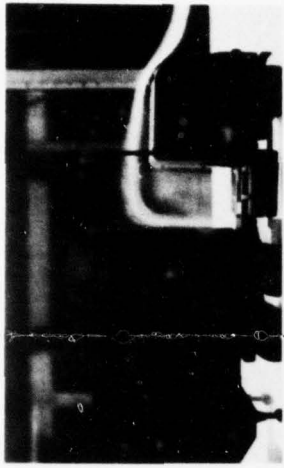
YAW ANGLE, DEG.

\overline{C}_D	CONFIGURATION
△	0.92 UNMODIFIED IHC 1800 LOADSTAR
◇	1.13 SQUARE TRAILER CORNERS
□	0.84 12-INCH RADI ON FRONT TOP AND SIDE CORNERS
×	0.80 FAIRED CYLINDRICAL TRAILER NOSE



YAW ANGLE, DEG.

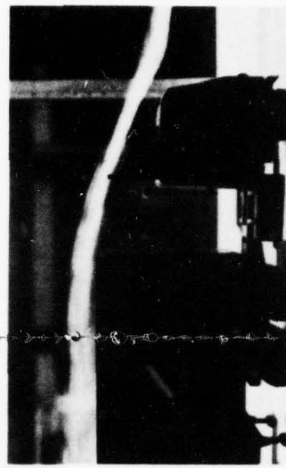
FIG. 32: TRAILER MODIFICATIONS WITH THE IHC 1800 LOADSTAR TRACTOR
 (X = 53 IN., V = 225 FT./SEC.).



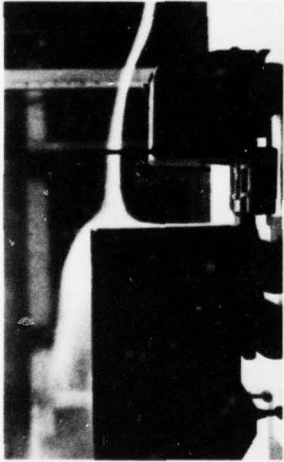
BASELINE FREIGHTLINER



AIRSHIELD



CURVED DRAG FOILER



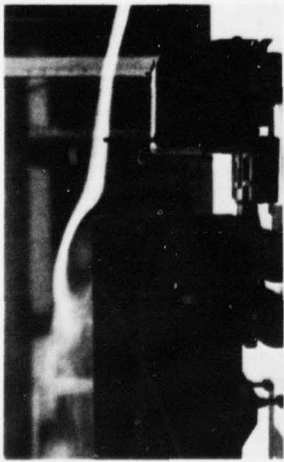
BASELINE FREIGHTLINER



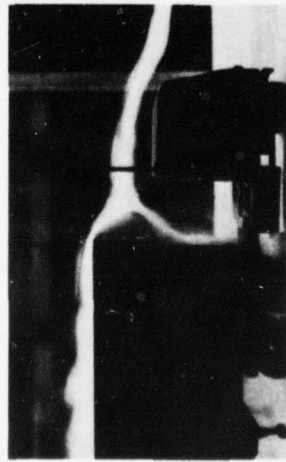
AIRGLIDE



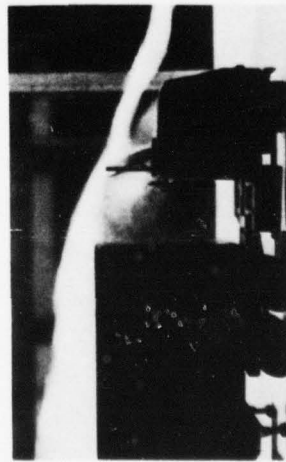
INCLINED UNIROYAL



BASELINE FREIGHTLINER



NOSE CONE

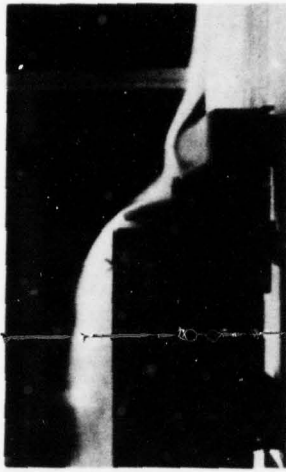


UNIROYAL

FIG. 33a: FLOW VISUALIZATION OF BASELINE AND MODIFIED TRUCKS USING SMOKE ($V = 50$ FT./SEC, $\psi = 0$ DEG.).



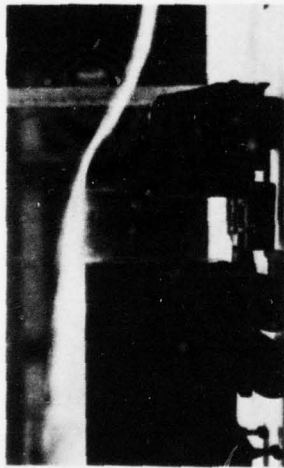
BASELINE IHC 1600



UNIROYAL



NOSE CONE



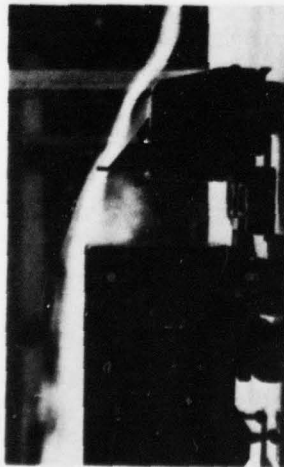
UNIVERSITY OF MARYLAND



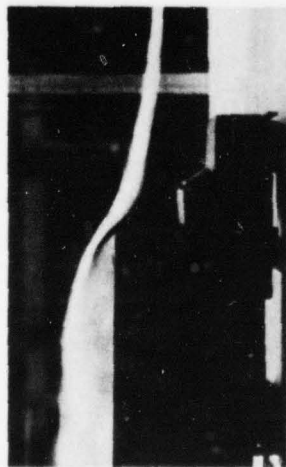
AIRVANE



AIRSHIELD



STRAIGHT DRAG FOILER



BASELINE IHC 1600



AIRGLIDE

FIG. 33b: FLOW VISUALIZATION OF BASELINE AND MODIFIED TRUCKS USING SMOKE ($V = 50$ FT./SEC, $\psi = 0$ DEG.).

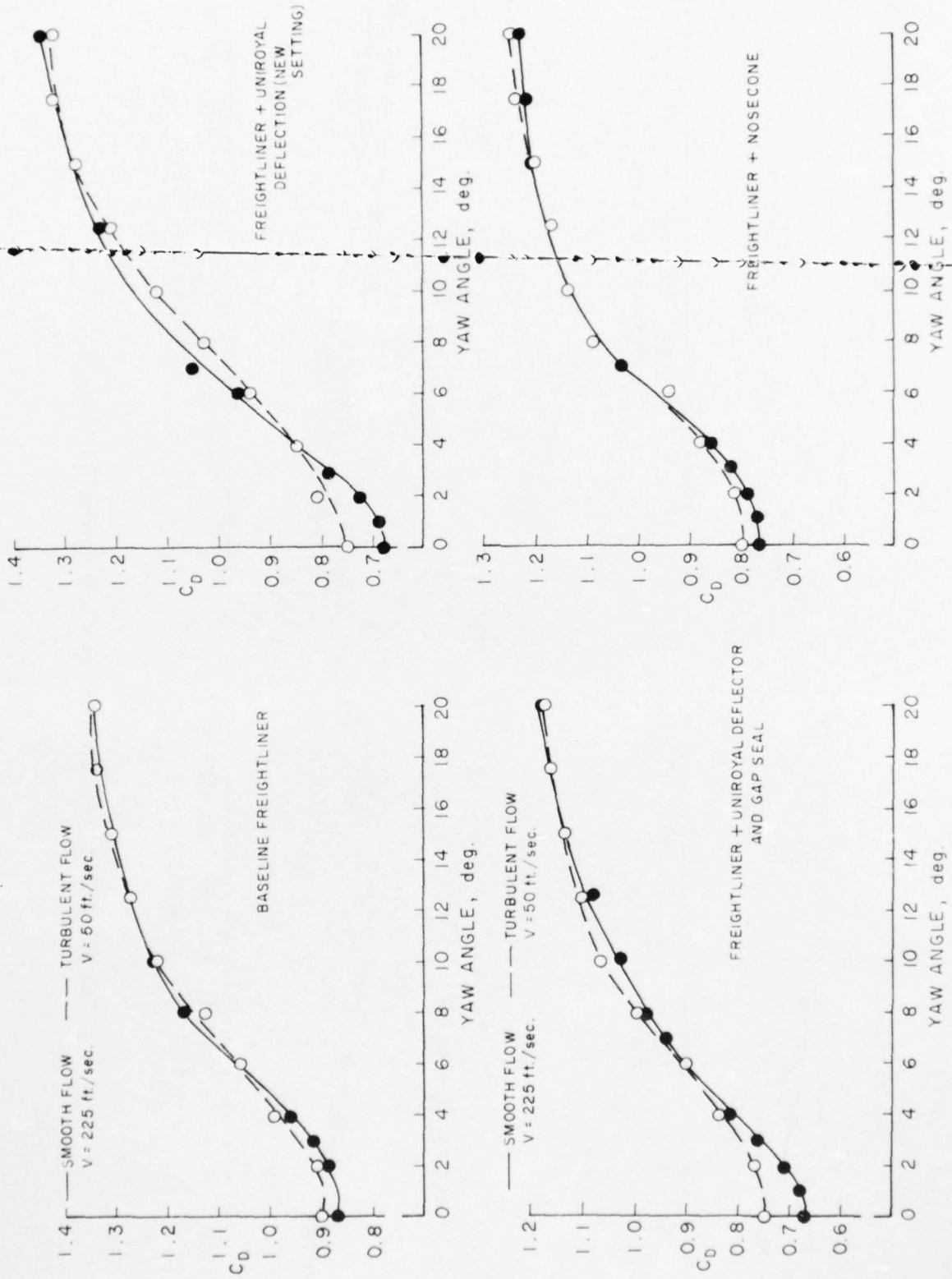


FIG. 34: EFFECT OF TURBULENCE ON THE FREIGHTLINER (X = 53 IN.).

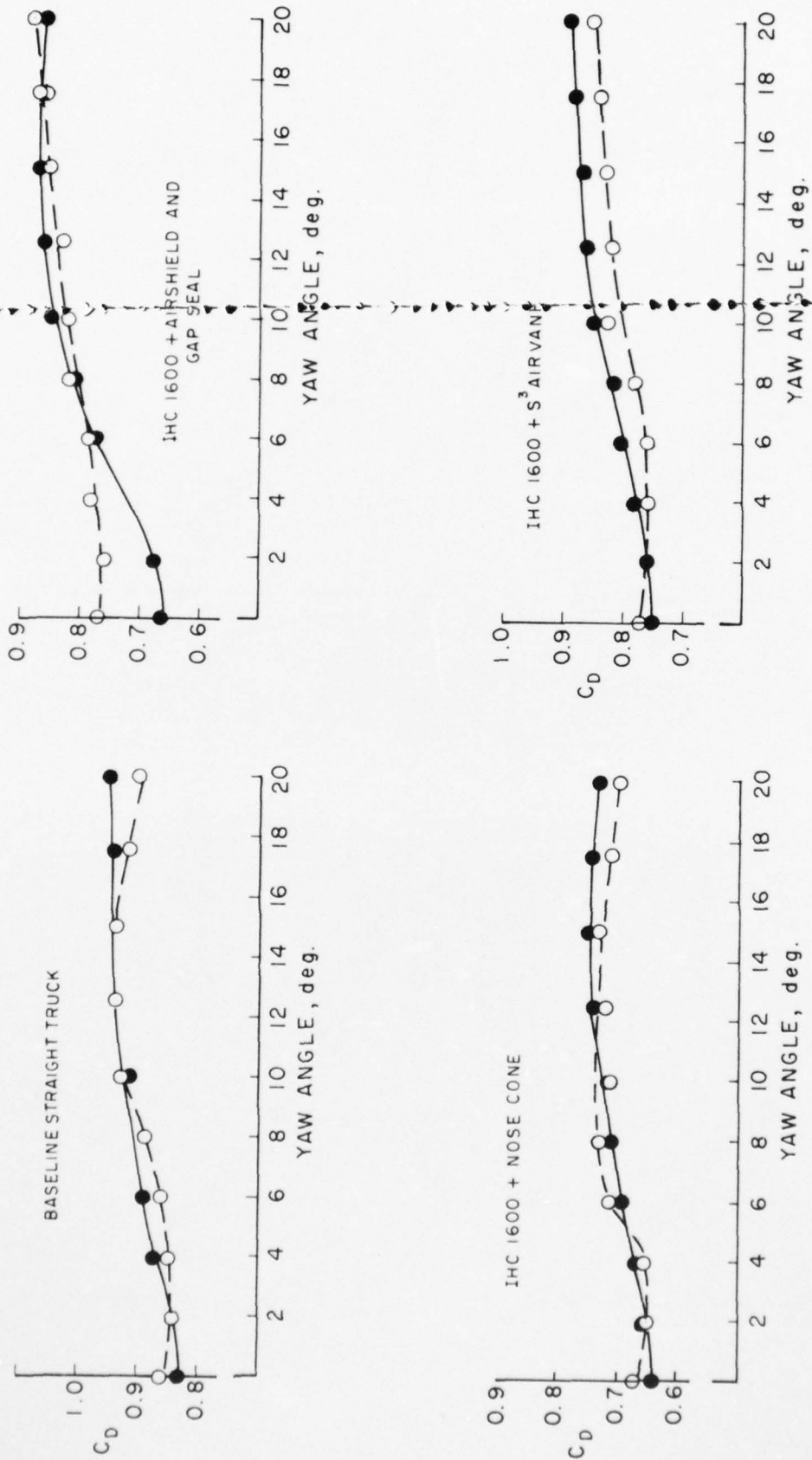


FIG. 35: EFFECT OF TURBULENCE ON THE STRAIGHT TRUCK.

CURRENT PROJECTS

Much of the work in progress in the laboratories of the National Aeronautical Establishment and the Division of Mechanical Engineering includes calibrations, routine analyses and the testing of proprietary products; in addition, a substantial volume of the work is devoted to applied research or investigations carried out under contract and on behalf of private industrial companies.

None of this work is reported in the following pages.

ANALYSIS LABORATORY

AVAILABLE FACILITIES

This laboratory has analysis and simulation facilities available on an open-shop basis. Enquiries are especially encouraged for projects that may utilize the facilities in a novel and/or particularly effective manner. Such projects are given priority and are fully supported with assistance from laboratory personnel. The facilities are especially suited to system design studies and scientific data processing. Information is available upon request.

EQUIPMENT

1. An Electronic Associates 690 HYBRID COMPUTER consisting of the following:
 - (a) PACER 100 digital computer
 - 32 K memory
 - card reader
 - high speed printer
 - disc
 - digital plotter
 - (b) Two EAI 680 analogue computer consoles
 - 200 amplifiers including 60 integrators
 - 120 digitally set attenuators
 - non-linear elements
 - x-y pen recorders
 - strip chart recorders
 - large screen oscilloscope
 - (c) EAI 693 interface
 - 24 digital-to-analogue converters
 - 48 analogue-to-digital converters
 - interrupts, sense lines, control lines

2. Hewlett Packard Model 3960 FM instrumentation tape recorder. IRIG standard, 4-track, 1/4-inch tape. Speeds: 15/16, 3-3/4 and 15 inches per second.

GENERAL STUDIES

A computer package called BUGOFF to assist in the on-line debugging of hybrid computer programs has been developed.

A study of the equations of motion for n coupled flexible bodies is being carried out.

APPLICATIONS STUDIES

In collaboration with the Low Speed Aerodynamics Laboratory of NAE, a hybrid computer model of the large vertical axis wind turbine, to be installed in collaboration with Hydro Quebec, has been assembled and is being used for dynamical studies.

In collaboration with United Aircraft of Canada Ltd., a hybrid computer model of an advanced turbo-fan engine is being put together in order to investigate the expected performance of the engine and its control system.

In collaboration with the Instruments Laboratory, a pilot hybrid computer model of the NRC roller rig for railway vehicle testing is being built as an aid in the design of the roller rig and its controls.

In collaboration with the British Gas Council, TransCanada Pipelines Ltd. and G.F. Crate Ltd., a study of the station controls for the St. Fergus terminal gas compressor station, location on the North Sea coast, is being undertaken.

In collaboration with the Control Systems and Human Engineering Laboratory and the Quebec Iron and Titanium Co., interactive computer model of an iron smelter is being developed to study scheduling of cranes and tracked vehicles and to improve materials handling in the smelter.

In collaboration with Aviation Electric Ltd., modelling work is underway in support of their advanced control concepts for both the small business jet engine and the helicopter engine. At present, a validation of a detailed model of a twin engine helicopter model is complete.

In collaboration with the Control Systems and Human Engineering Laboratory and the International Nickel Co., Ontario Division, an interactive computer model of a copper-nickel smelter is being developed to study material handling and scheduling in the plant.

In collaboration with the Engine Laboratory, a data reduction program has been put together for the hybrid computer which accepts tape recorded transducer data gathered during transient engine tests of the J85 program. The program is currently being used to process data from the test program.

In collaboration with the Control Systems and Human Engineering Laboratory and R.L. Crain Ltd., an interactive order streaming program for a print shop is being developed for use by the press-co-ordinators.

In collaboration with Canadian Westinghouse Ltd. and G.F. Crate Ltd., a study is being made of the fuel controller requirements for a new family of 35,000 HP gas turbines. A hybrid computer model is being assembled to be used in the development.

APPLICATIONS STUDIES BY OTHERS

Forest R. Livingstone Ltd. and the Maritime Equipment Engineering Group of the Department of National Defence are using the hybrid computer for a study of the propulsion system on the DDH280 Navy destroyer. A final report is being prepared.

Kendall Associates, under contract to SPAR Aerospace Products Ltd., have assembled a hybrid computer model of the proposed joint design of the remote manipulator arm for the space shuttle. Two joints have been modelled, and the arm flexibility effects on the design have been evaluated.

CONTROL SYSTEMS AND HUMAN ENGINEERING LABORATORY

INDUSTRIAL CONTROL PROBLEMS

Industrial systems and agricultural applications of fluidic circuits.

Fluid sensor and control component research and development.

Investigation of the process dynamics and control characteristics of copper converters including the development of optimal process scheduling strategies.

Interactive computer modelling applied to scheduling of large scale metallurgical plants.

Development of CAMAC instrumentation for industrial control applications.

Engineering support to specific firms for the implementation of schemes for control and mechanization.

HUMAN ENGINEERING — BEHAVIOURAL STUDIES

Investigation of the control characteristics of the human operator and the basic phenomena underlying tracking performance.

Investigation of the nature of sensory interaction in human perceptual-motor performance.

Investigation of the factors involved in the presentation and processing of information, particularly in relation to simulator design.

HUMAN ENGINEERING — MEDICAL AND SURGICAL

Investigation of the implementation of feedback control in living organisms with particular reference to the control of temperature and pressure in the spinal cord.

Investigation of non-ionizing electromagnetic radiation as means of controlling living processes with particular reference to controlled wound healing.

Measurement of in-vivo tensile strength characteristics of skin.

Development of models of tissue sections, organs, and whole organisms.

Development of stereo-taxic and allied apparatus for neurosurgical procedures.

PATTERN RECOGNITION AND IMAGE PROCESSING

Investigation of the fundamentals of pattern recognition.

Application of pattern recognition techniques to identification and classification problems with particular reference to image enhancement and computer analysis of human chromosome material from electron micrographs.

ENGINE LABORATORY

HOSPITAL AIR BED

A hospital air bed designed and built by NRC has been delivered to the Hotel Dieu Hospital in Kingston, Ontario for clinical evaluations of treatment of burn patients. The function and performance specifications of the bed were devised in collaboration with Canadian medical authorities to satisfy Canadian needs.

A second air bed was purchased in England by the Victoria Hospital in London, Ontario, and was adapted by NRC to meet Ontario Hydro requirements.

Both beds are now being used for experimental work and clinical evaluations in the two hospitals.

GAS TURBINE OPERATIONS

An investigation of aircraft gas turbine engine operating characteristics is being conducted in conjunction with the Canadian Forces.

Assistance has been given to the Canadian Forces in the development of an inlet protective system for sea-borne gas turbines operating in icing environments.

Prototype instrumentation for an in-flight thrust meter has been verified on a test-bed installed turbojet engine.

DUCTED FAN AEROACOUSTICS

A 12-inch diameter ducted fan model has been tested aerodynamically for the purpose of making performance comparisons between a standard 19-bladed stator and a 19-bladed stator with stepped leading edges. Comparative noise studies of the same configurations in an acoustically treated test cell are now underway.

These experiments are made by the Engine Laboratory in co-operation with the Division of Applied Physics with the intent of exploring special noise reducing features in ducted fan design.

ENGINE COOLING SYSTEM AERODYNAMICS

An experimental study of the aerodynamics related to automotive power plants has been initiated in collaboration with Canadian industry.

ROTOR DYNAMICS

An experimental rig is being constructed to investigate techniques for improved vibration signal diagnosis from rotating machinery under a variety of operating and support conditions. A literature review of the dynamic stiffness and damping parameters of fluid film bearings has been undertaken. The operating range of the laboratory's torsional vibration transducer calibrator is being extended to meet new requirements from industry.

AIR CUSHION VEHICLES

The first CASPAR program, on the Multicell skirt has been completed. A report on this program will be issued shortly.

AD-A034 552

NATIONAL RESEARCH COUNCIL OF CANADA OTTAWA (ONTARIO) --ETC F/6 13/6
QUARTERLY BULLETIN OF THE DIVISION OF MECHANICAL ENGINEERING AN--ETC(U)
SEP 76

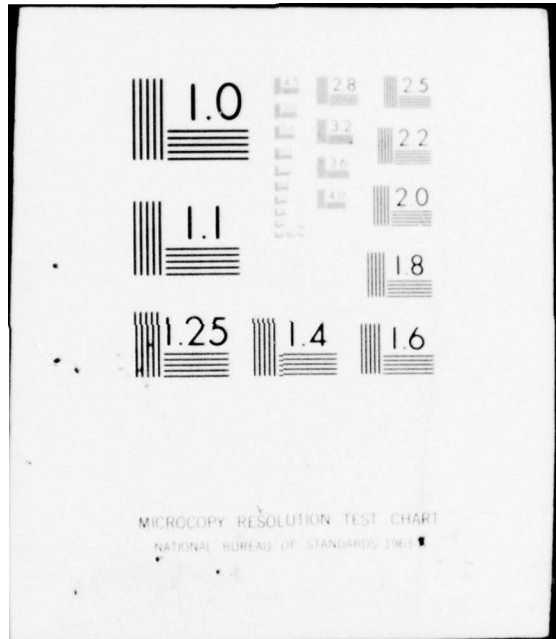
UNCLASSIFIED

DME/NAE-1976(3)

NL

2 OF 2
AD
A034552





An analytical study of ACV drag overland is continuing. Advances in the theory have been formulated, and an experimental program is in progress, to explore the validity of these theories and provide numerical values for the coefficients proposed.

An associated study of skirt element structural stability and response to transient disturbances during forward motion is proceeding.

A new (HDL) type skirt system has been built onto research vehicle HEX-1B, and this test program is in progress.

Research vehicle HEX-3 is being completely rebuilt to the HEX-4 configuration. It will be used for high-speed skirt-wear experiments, with particular reference to on-road A.C. assisted transports, and later for over-snow drag tests related to icebreaking problems. Special instrumentation for this work is being incorporated.

HYDROSTATIC BEARINGS

A design study of a hydrostatic bearing support system for the railroad roller test rig is in progress.

AEROACOUSTICS

A study of the noise characteristics of centrifugal blowers is in progress. An existing laboratory centrifugal fan has been tested to investigate the relation between flow characteristics and noise generation and to determine appropriate test procedures. The effect of certain changes in casing geometry on the noise generated by a commercial blower have been investigated.

AIR BEARINGS

Experimental and analytical work on air lubricated bearings and seals is continuing. Attention is being focused on aerostatic thrust bearings with one compliant surface.

INDUSTRIAL AERODYNAMICS

In conjunction with the Gas Dynamics Laboratory further studies are being carried out on the internal gas flow distributions in an industrial furnace.

FLIGHT RESEARCH LABORATORY

AIRBORNE REMOTE SENSING OF MAGNETIC PHENOMENA

Experimental and theoretical studies relating to the further development and use of magnetic airborne detection equipment. Equipment under development is installed on a North Star aircraft, which is used as a flying laboratory. Surveys requested by various Government Departments and other agencies are carried out periodically using an advanced navigation system based on very low frequency (VLF) radio signals and doppler, for recovery of survey tracks. A Convair 580 aircraft is being equipped to replace the North Star on its retirement from service with the Flight Research Laboratory.

INVESTIGATION OF PROBLEMS ASSOCIATED WITH V/STOL AIRCRAFT OPERATIONS

The Laboratory's two variable stability helicopters, a Bell 47G3B1 and a Bell 205A1, are being employed in programs to investigate terminal area operational problems which are most severe for or peculiar to aircraft capable of low approach speeds. The Bell 47 program is aimed at an investigation of optimum energy management to reduce the effects of atmospheric disturbances on the ride characteristics of low speed aircraft. The 205, which is capable of measuring and recording the magnitude of the three components of motion of the atmosphere through which it flies, is employing this capability in a program of terminal area wind and turbulence documentation at the Rockcliffe STOLport. In a related program the 205 is being configured to simulate the flight characteristics and handling qualities of a "good" powered-lift STOL transport aircraft; the effects of severe turbulence and strong wind shears on the approach handling qualities and *operational envelope* of such an aircraft are being evaluated by flying the simulated vehicle through naturally occurring atmospheric disturbances.

INVESTIGATION OF ATMOSPHERIC TURBULENCE

A T-33 aircraft, equipped to measure wind gust velocities, air temperature, wind speed, and other parameters of interest in turbulence research, is used for measurements at very low altitude, in clear air above the tropopause, in the neighbourhood of mountain wave activity, and near storms. Records are obtained on magnetic tape to facilitate data analysis. The aircraft also participates in co-operative experiments with other research agencies, in particular, the Summer Cumulus Investigation (see below). A second T-33 aircraft is used in a supporting role for these and other projects.

AIRCRAFT OPERATIONS

The Flight Recorder Playback Centre is engaged in the recovery and analysis of information from the various flight data recorders and cockpit voice recorders used on Canadian military and civil transport aircraft. The military systems are being monitored on a routine basis. Civil aircraft recorders are being replayed to investigate incidents or accidents at the request of the Ministry of Transport. Technical assistance is being provided during incident and accident investigations and relevant aircraft operational problems studied.

INDUSTRIAL ASSISTANCE

Assistance is given to aircraft manufacturers and other companies requiring the use of specialized flight test equipment or techniques.

INVESTIGATION OF SPRAY DROPLET RELEASE FROM AIRCRAFT

Theoretical and experimental studies of spray droplet formation from a high speed rotating disc have been conducted. Flight experiments utilize a Harvard aircraft modified to carry external spray tanks. Automatic flying spot droplet and particle analysis equipment is in operation for processing samples obtained in the laboratory and in the field by various agencies. The equipment has potentialities for the analysis of many unusual configurations provided that these may be photographed with sufficient contrast.

AUTOMOBILE CRASH DETECTOR

There is a need for a sensing device to activate automobile passenger restraint systems in incipient crash situations. Investigations are in progress to determine the applicability of C.P.I. technology to this problem.

SUMMER CUMULUS INVESTIGATION

At the request of the Department of the Environment flight studies of Cumulus cloud formations over Quebec and Ontario were instituted during the Summer of 1974. Instrumented T-33 and Twin Otter aircraft are being used to determine the properties of Cumulus clouds which extend appreciably above the freezing level. These measurements are being made to assess the feasibility of inducing precipitation over forest fire areas by seeding large cumulus formations. During 1975 a variety of cloud physics instruments were added to the Twin Otter, and special pods for burning silver iodide flares were attached beneath the wing of the T-33 turbulence research aircraft. The effects of seeding on the microstructure of individual cumulus clouds were studied in the Yellowknife area during the Summer of 1975. This project is planned to continue for several years.

FUELS AND LUBRICANTS LABORATORY

FUNDAMENTAL STUDIES OF FRICTION, LUBRICATION, AND WEAR PROCESSES

Investigations of friction and wear processes including the mechanism of adhesion between non-conforming metal surfaces.

PRACTICAL STUDIES ON LUBRICATION, FRICTION AND WEAR

Investigation of means of improving sharpness retention of wood cutting tools.

Laboratory simulations of wide range of practical sliding contact and bearing conditions to obtain the friction and wear characteristics of specific lubricants and materials.

COMBUSTION RESEARCH

Experiments on fuel spray evaporation.

Investigation of handling and combustion problems involved in using hydrogen as a fuel for mobile prime movers.

Study of possible methods for destruction of oxides of nitrogen in engine exhaust gas.

Evaluation of the use of mixtures of methane and carbon dioxide as automobile fuels.

EXTENSION AND DEVELOPMENT OF LABORATORY EVALUATION

Development of new laboratory procedures for the determination of the load carrying capacity of hypoid gear oils under high speed conditions and under low speed high torque conditions.

Evaluation of filter/coalescer elements for aviation turbine fuels.

Evaluation of longlife filter/coalescer elements from aviation turbine fuel service.

PERFORMANCE ASPECTS OF FUELS, OILS, GREASES, AND BRAKE FLUID

Co-operative investigation covering used oil analysis and inspection of engines from Ottawa Transportation Commission buses to establish realistic oil and filter change periods.

Investigation of laboratory methods for predicting flow properties of engine and gear oils under low temperature operating conditions.

Investigation of laboratory methods for predicting low temperature flow properties of diesel and heating fuels and assessment of their suitability.

Co-operative investigation covering test procedure for the evaluation of thermal oxidation stability of hypoid gear lubricants.

Evaluation of performance of experimental engine lubricants to determine their effect on ring sticking, wear, and accumulation of deposits under high speed, supercharged conditions.

Development of a laboratory method for the evaluation of oil performance in air-cooled two-stroke engines.

Investigation of the electrostatic charging tendency of distillate fuels.

Evaluation of static dissipator additives for distillate fuels.

Evaluation of properties of re-refined oils and surveys of problems in the oil re-refining industry.

Investigation of the use of anti-icing additive in aviation gasoline.

MISCELLANEOUS STUDIES

The preparation and cataloguing of infra-red spectra of compounds related to fuels, lubricants, and associated products.

The application of Atomic Absorption spectroscopy to the determination of metals in petroleum products.

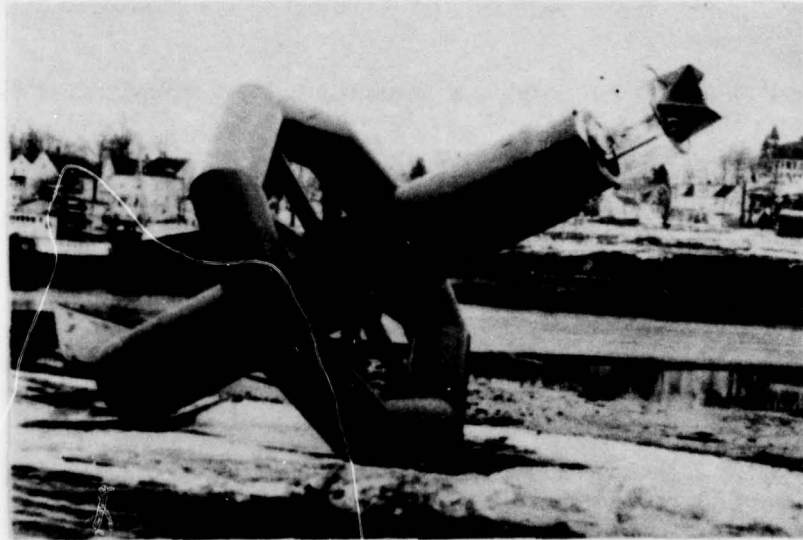
Investigation of the stability of highly compressed fuel gases.

Analytical techniques for analysis of engine exhaust emissions.

Participation in the Canadian (CGSB), American (ASTM) and International (ISO) bodies to develop standards for petroleum products and lubricants.

The design and development of an internal combustion engine/hydraulic transmission hybrid power plant for the energy conserving car.

Further developments of specialized pressure transducers for engine health diagnosis and the development of diagnostic techniques.



Ice Formation on Navigation Buoys is a Serious Problem Off Canada's East Coast. This Buoy - Developed Jointly by Division of Mechanical Engineering and the Ministry of Transport - Uses the Thermosiphon Principle to Transport Heat from the Sea to the Superstructure to Prevent Ice Formation. The Central Cylinder is Charged with Ammonia (Mostly Vapour with a Small Quantity of Liquid). When Ice Begins to Form the Vapour is Condensed in the Upper Section. The Condensate Film Falls into the Underwater Section where it Evaporates, and the Vapour Flows to the Upper Section. This Cycle of Condensation and Evaporation is an Effective Means of Transferring Heat, Even at Small Temperature Differences. The Prototype Buoy is Now in the Sea Off Halifax for Testing.

SELF DE-ICING NAVIGATION BUOY

GAS DYNAMICS LABORATORY
DIVISION OF MECHANICAL ENGINEERING

GAS DYNAMICS LABORATORY

V/STOL PROPULSION SYSTEMS

A general study of V/STOL propulsion system methods with particular reference to requirements of economy and safety.

INTERNAL AERODYNAMICS OF DUCTS, DIFFUSERS AND NOZZLES

An experimental study of the internal aerodynamics of ducts, bends, diffusers and nozzles with particular reference to the effect of entry flow distortion in geometries involving changes of cross-sectional area, shape, and axial direction.

SHOCK PRODUCED PLASMA STUDIES

A general theoretical and experimental investigation of the production of high temperature plasma by means of shock waves generated by electromagnetic and gasdynamic means, and the development of diagnostic techniques suitable for a variety of shock geometries and the study of physical properties of such plasmas.

NON-DESTRUCTIVE SURFACE FLAW DETECTION IN HOT STEEL BILLETS

An eddy-current surface flaw detector is being developed, using a special coil system by which a three-phase modulated R.F. signal is being electrically rotated round the billet at a rate given by the modulation frequency. The system displays the angular position of the flaw on a polar oscilloscope sweep or numerically, while the signal amplitude represents the depth of the flaw.

HIGH PRESSURE LIQUID JETS

Water Jets ranging in size from 0.002 inch to 0.150 inch, generated by pressures in the range of 10,000 to 100,000 psi, are capable of cutting materials such as paper, cloth, plastics, wood, ice, masonry, and even some metals.

Laboratory work is directed towards commercial exploitation of this phenomenon by various industries (e.g. paper, lumber, leather, garments, plastics, fruit, etc.) and to the detailed study of the phenomenon itself in order to improve the efficiency of the process. Experimental studies directed towards the production of intermittent jets for obtaining higher stagnation pressures are continuing.

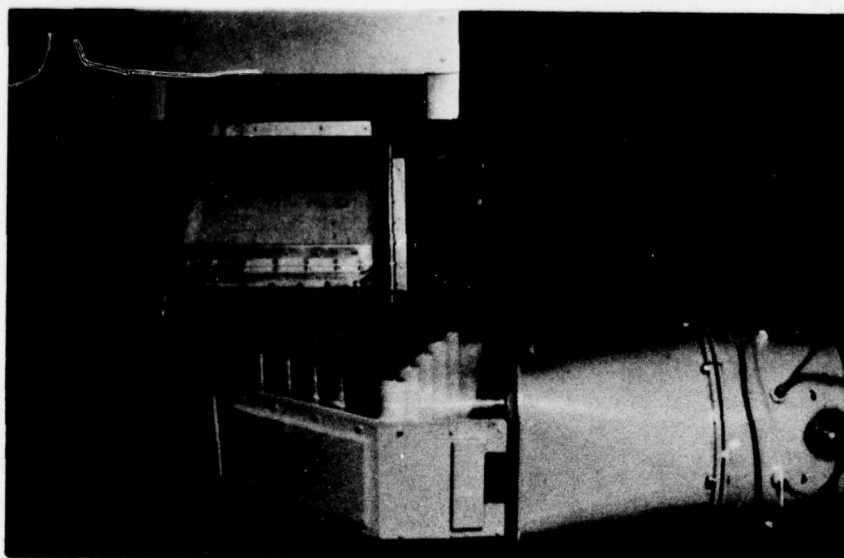
Experimental studies of rock cutting using water jets have been started and a prototype rotating rock drill is being developed.

A seal arrangement has been developed which enables a small jewel orifice to be used as a nozzle which can be operated at pressures up to 60,000 psi. Development for specific applications in collaboration with industry is continuing.

Research and development work on nozzles to produce cavitating jets (jets containing vapour bubbles) is in progress. These nozzles will be used in the investigation of rock fracturing and cutting other hard materials. Experimental work has begun on the use of water jets for clearing ice off runway surfaces and for cutting through thick ice ridges.

HEAT TRANSFER STUDIES

Initial development of a temperature control thermosiphon for an electronic package has been successfully concluded. Life testing of this device has commenced.



**INTERNAL FLOW STUDIES FOR LOW ENERGY LOSSES AT EXTREME
GEOMETRIES: APPLICATION TO A SPECIFIC INDUSTRIAL DUCT**

**GAS DYNAMICS LABORATORY
DIVISION OF MECHANICAL ENGINEERING**

COMPUTATIONAL FLUID DYNAMICS

To support the experimental work, numerical simulations are being developed in three areas.

Single-pulse jets from vertically-accelerated liquid-filled rotating cones. This is a two-dimensional, axisymmetric, unsteady, incompressible flow problem with a free surface, where the liquid is subjected to large body accelerations.

Fluid dynamics of laser-produced plasmas. The phenomena are considered as two-dimensional, axisymmetric, unsteady, compressible flow problems in which real gas behaviour is considered. The approach, which uses Lagrangian formulation, has been used to calculate two cases:

- (a) The fluid dynamics of a laser breakdown plasma, with the objective of explaining the mechanism of beam re-entry into the plasma when beam intensity is reduced.
- (b) The interaction of a CO₂ laser beam with magnetically confined plasmas. This major problem is currently being studied numerically as part of a co-operative effort with the Aerospace Research Laboratory of the University of Washington.

Shock dynamics and fluid dynamics resulting from synchronized spark discharges on the axis and discharges on the perimeter of a cylindrical vessel containing hydrogen, to achieve high gas temperatures on the axis of the vessel.

GAS TURBINE BLADING STUDIES

A program on the theoretical and experimental study of the performance of highly loaded gas turbine blading has been undertaken as a collaborative program with industry and universities.

INDUSTRIAL PROCESS, APPARATUS, AND INSTRUMENTATION

There is an appreciable effort, on a continuing basis, directed towards industrial assistance. This work is of an extremely varied nature and, in general, requires the special facilities and capabilities available in the laboratory.

Current co-operative projects with manufacturers and users include:

- (a) Flow problems associated with industrial gas turbine exhaust systems (Foster Wheeler).
- (b) Combustion studies for industrial gas turbine applications (Westinghouse and Rolls-Royce).
- (c) Application of thermosiphon as an energy conserving device in industrial applications (Dept. of Agriculture, Ministry of Transport and Farinon Electric).
- (d) Scaled model studies on steel and copper converters to establish relative performance and ceramic liner deterioration rates (Canadian Liquid Air and Noranda).
- (e) High pressure water jet applications in industry (High Pressure Systems Ltd.).
- (f) Power turbine nozzle vane studies (Westinghouse).

HIGH SPEED AERODYNAMICS LABORATORY

CONTROL OF TURBULENT BOUNDARY LAYER IN A THREE-DIMENSIONAL SHOCK WAVE/BOUNDARY LAYER INTERACTION

The investigation of the three-dimensional interaction between a swept shock wave and a turbulent boundary layer along a flat wall at freestream Mach number of 2 and 4 in the 5-in. \times 5-in. blow-down wind tunnel has been completed. Some parts of the work were reported at the AGARD Specialists meeting on 'Flow Separation' at Göttingen, W. Germany, May 1975, and have been published in the Conference Proceedings, AGARD CP-168. A fuller report will be available as NRC LR-592.

SETTLING CHAMBER STUDY IN 5-IN. \times 5-IN. WIND TUNNEL

Revisions to the settling chamber of the 5-ft. \times 5-ft. wind tunnel are under consideration to improve the flow distribution and to decrease the level of pressure fluctuation at the entry to the stilling section. Model tests will be conducted in the NAE pilot facility.

TWO-DIMENSIONAL TRANSONIC FLOW STUDIES

Efficient computer programs based on finite difference procedures are available for the design of supercritical airfoils and for the analysis of supercritical flow. The possibility of using finite element methods are being explored with the aim of extending into three-dimensional flow cases.

HIGH REYNOLDS NUMBER PIPE FLOW

This investigation is carried out at the request of and in co-operation with Laval University, Quebec.

The object is to obtain turbulent skin friction data at very high Reynolds number (Re_d up to 20×10^6) in a pipe. The investigations to date include calibration of a range of Preston and razor blade surface pitot tubes and mean velocity traverses. Direct skin friction measurements with a floating element balance is awaiting the commissioning of the balance at Laval University. Turbulence and noise measurements are also being considered. Analysis of the Preston tube calibration data has been carried out and the results agree well with semi-empirical theory based on the logarithmic wall law.

THEORETICAL AND EXPERIMENTAL STUDY OF JET NOISE

Further investigations of internal noise in a low speed jet are in progress. More detailed studies of the interaction of the transmitted sound with the jet flow and some statistical investigation of the multiple wave scattering by the turbulent eddies will be carried out. Some experiments on co-axial jets have been performed and measurements of pressure fluctuations in the turbulent shear layer will be undertaken.

Wave-like large scale eddies have been shown to be the basic characteristic of free turbulent shear flows. For circular jets, measurements of the wave development have been made for the axisymmetric mode of propagation. Recent experiments show that the jet can also support wave propagation in helical modes. Some detail measurements have been performed. A report on the helical mode study will be presented in the 10th ICAS Congress in Ottawa, October 1976.

THREE-DIMENSIONAL WALL INTERFERENCE EFFECTS

The wall effects in a rectangular wind tunnel test section with perforated walls is being evaluated using the finite difference method. The effort is concentrated on analysis of the measurements recently performed on the ONERA calibration models in the NAE 5-ft. X 5-ft. wind tunnel.

HIGH REYNOLDS NUMBER SUBSONIC FLOW SEPARATION

In preparation for final design of a dual pitot/hot wire traversing probe, several probe shapes have been tested in a water tunnel. The shape which gave the least flow disturbance (as shown by flow visualization) when the probe head was near the wall is now being tested in the tunnel wall boundary layer in order to check out signal processing.

REYNOLDS NUMBER EFFECTS ON TWO-DIMENSIONAL AEROFOILS WITH MECHANICAL HIGH LIFT DEVICES

An iterative solution of the compressible boundary layer flows about multi-element aerofoils is being developed. Measurements have recently carried out in the NAE high Reynolds number two-dimensional test facility on a multi-element high lift aerofoil, where various configurations were made possible by varying the gap between and the angular settings of the elements. A pitot probe rake survey of the upper surface flow at the main flap trailing edge was included. Preliminary analysis of this survey shows regions of reversed flow well before stall.

TESTS IN THE 5-FT. X 5-FT. BLOWDOWN TUNNEL FOR OUTSIDE ORGANIZATIONS

SAAB-Scania, Sweden

Investigations were completed on four different test objects; a 1/30 scale model of a current aircraft, a series of missile configurations and a 1/13 and a 1/25 scale model of a swept wing aircraft.

Canadair Limited, Montreal

An investigation of a 1/3 scale model of a reconnaissance drone was commenced.

HYDRAULICS LABORATORY

ST.LAWRENCE SHIP CHANNEL

Under the sponsorship of the Ministry of Transport, a study to improve navigation along the St.Lawrence River, using hydraulic and numerical modeling techniques.

NUMERICAL SIMULATION OF RIVER AND ESTUARY SYSTEMS

Mathematical models have been developed to simulate tidal propagation in estuaries, wave refraction in shallow water and littoral drift processes.

DEVELOPMENT OF SPECTRAL ANALYSIS PROGRAMS

For use in the analysis of wave records and on-line analysis of turbulent diffusion data produced in the laboratory.

WAVE FORCES ON OFF-SHORE STRUCTURES

Wave flume study to determine design criteria for off-shore mooring structures.

RANDOM WAVE GENERATION

A study of random waves generated in a laboratory water wave flume by signals from a computer.

CHURCHILL HARBOUR MODEL STUDY

A hydraulic model study to determine effects of extending wharf facilities at Churchill, Man. on local flow pattern and the effect of diversion of upland discharge on salinity distribution in estuary.

MIRAMICHI CHANNEL STUDY

A hydraulic model study to determine the feasibility of deepening the navigation channel of the Miramichi River, N.B.

LOCK MODEL STUDY ON VESSEL SIZE

In co-operation with the Marine Dynamics and Ship Laboratory a model study has been undertaken to determine the effect of vessel and lock dimensions on the entrance and exit speeds of ships in locks of the St.Lawrence Seaway.

STABILITY OF RUBBLE MOUND BREAKWATERS

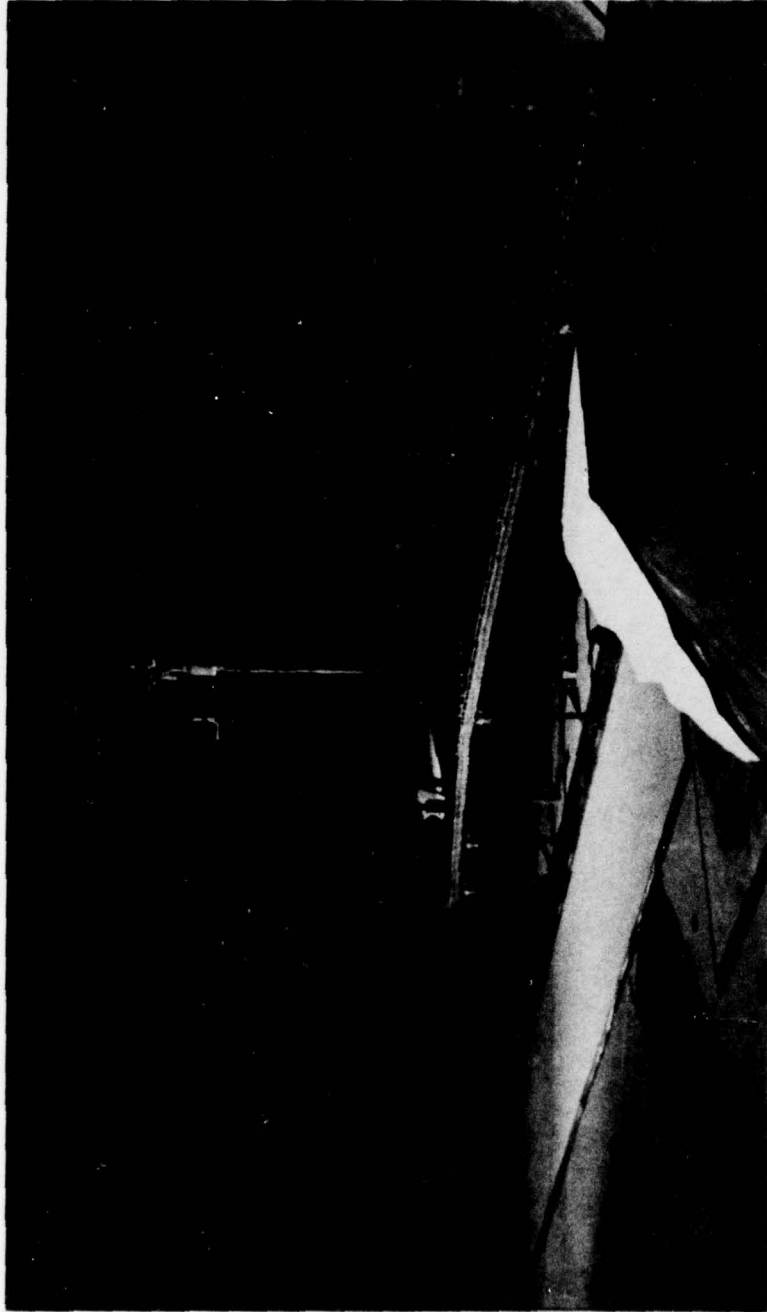
A flume study for the Department of Public Works to determine stability coefficients of armour units and the effect of a number of wave parameters on the stability of rubble mound breakwaters.

WAVE LOADS ON CAISSON TYPE BREAKWATERS

A flume study for the Department of Public Works to determine the overall loading, as well as the pressure distribution on various Caisson-type breakwaters.

WAVE POWER AS AN ENERGY SOURCE

A general study to assess the wave power available around Canada's coast and to evaluate various proposed schemes to extract this energy. International co-operation is taking place through the International Energy Agency of OECD.



AEROELASTIC MODEL OF THE LIONS' GATE BRIDGE
IN THE 30-FT. X 30-FT. WIND TUNNEL

LOW SPEED AERODYNAMICS
NATIONAL AERONAUTICAL ESTABLISHMENT

LOW SPEED AERODYNAMICS LABORATORY

WIND TUNNEL OPERATIONS

The three major wind tunnels of the Laboratory are: the 15-ft. diameter, open jet, vertical tunnel; the 6-ft. \times 9-ft. closed jet, horizontal tunnel; and the 30-ft. V/STOL tunnel. During the quarter, 15 programs were undertaken which included work for Canadair Ltd., DeHavilland Aircraft of Canada Ltd. and Irvin Industries Canada Ltd. Adapter stands for the 30-ft. wind tunnel balance have been made which now enable the Laboratory to undertake full scale automobile aerodynamic testing.

WIND ENGINEERING

Dynamic sectional model tests of the Lions' Gate Bridge have been completed in the 3-ft. \times 3-ft. wind tunnel at the same Reynolds number as for the full aeroelastic model tests done in the 30-ft. wind tunnel. The road deck dynamic behaviour was similar in the two experiments. The investigation was made for Buckland and Taylor Limited.

One-tenth scale models of highway tractor trailers in the 6-ft. \times 9-ft. wind tunnel were used to calibrate anemometer locations for full scale fuel consumption road tests. A water tunnel flow visualization program was completed to complement the previous experiments in the 6-ft. \times 9-ft. tunnel into commercially available drag reduction devices for tractor trailers.

Spectral analysis of field measurements to determine natural frequencies and damping coefficients of I-beam road deck hangers on the Burton Bridge were completed for the Department of Transport of New Brunswick.

A wind tunnel investigation was completed in the 15-ft. vertical wind tunnel for the proposed Polar VII Icebreaker. Smoke funnel effectiveness and airflow quality at the helicopter landing deck were examined. The Polar VII would be the world's largest icebreaker. It will be 650 ft. long and will be powered by diesel and gas turbine engines with a total rating of 90,000 horsepower. The work has been done for German and Milne, Marine Transportation Consultants and Naval Architects.

Surface pressure measurements on a variety of building configurations are to be undertaken in the 6-ft. \times 9-ft. wind tunnel as part of a collaborative program with the Division of Building Research on the prediction of air infiltration. The models are now being constructed.

Force measurements were made in the 3-ft. \times 3-ft. wind tunnel for Fathom Oceanology Limited on a streamlined fairing for underwater circular pipes.

Consultation has taken place with Atlantic Bridge Company Limited concerning the design of unloaders for fishing vessels. The fish are propelled through pipes by a high velocity airstream. Calculations of the velocity time history of the fish have been completed.

FLUIDICS

Co-operative studies with D.G. Instruments of a 3-axis air velocity sensor are continuing using both NRC and industry developed concepts. Studies of vortex excitation of velocity sensor probes have been carried out in co-operation with Fluidynamic Devices Ltd. A program of applications of laminar flow in thin passages is being carried out in co-operation with the Control Systems and Human Engineering Laboratory of DME.

NUMERICAL METHODS

A correlational theory for the prediction of boundary layer transition has been devised and successfully demonstrated in some simple cases which are of interest for the design of airfoils.

The numerical methods are applicable to compressible flows involving heat and mass transfers at the boundaries.

VERTICAL AXIS WIND TURBINE

Dominion Aluminum Fabricating, Ltd. has delivered six 15-ft. diameter wind turbines to NRC, who in turn has shipped these units to interested federal agencies for field trials. These units are now in operation. DAF are now marketing two sizes (a 15-ft. diameter (4kW) and a 20-ft. diameter (6kW) turbine). Fabrication of the 200kW demonstration unit is proceeding at DAF. Dynamic tests of a 1/4 scale model of this turbine, in the 30-ft. V/STOL wind tunnel, have been completed.

AERIAL SPRAYING OF PESTICIDES

A co-operative program between NAE and the University of New Brunswick, to determine the droplet size distribution of standard nozzle configurations, has been completed. The experimental method consisted of photographing droplets in the 50- to 250-micron range using a narrow depth of focus, and a high intensity flash. An electronic detector was also placed in the spray; its function was to count the number of droplets in a given size range. The second stage of the experiment is currently underway with measurements of droplet emissions from a Micronair rotary atomizer being made.

A new spray boom design has been tested in co-operation with Con-Air Aviation (Abbotsford, B.C.). This configuration will have significantly less aerodynamic drag than the present installation which is used on the DC-6B aircraft and is expected to save several hundred horsepower.

Theoretical and experimental studies are continuing on the effects of the vortex wake and other factors on the swath width of spray left by a low flying aircraft.



PROPOSED POLAR VII ICEBREAKER IN THE 15-FT. VERTICAL WIND TUNNEL

LOW TEMPERATURE LABORATORY

RAILWAY CLIMATIC PROBLEMS

Under the auspices of the NRC Associate Committee on Railway Problems, Sub-Committee on Climatic Problems, a variety of analytical and experimental work is conducted on a continuing basis.

THERMAL PROTECTION OF TRACK SWITCHES

The use of heat to eliminate switch failures from snow and ice is a standard approach to this problem. Work has been carried out on improving the efficiency of forced convection combustion heaters and the means of distributing heat to the critical areas of a switch.

HORIZONTAL AIR CURTAIN SWITCH PROTECTOR

A non-thermal method of protecting a switch from failure due to snow has been undergoing development and evaluation. This method consists of high velocity horizontal air curtains designed to prevent the deposit of snow in critical areas of a switch. The tests conducted to date are especially encouraging with respect to yards and terminals. Additional evaluation is required for the line service application.

NEW RAILWAY SWITCH DEVELOPMENT

The ultimate solution to the existing problem of snow and ice failure of the point switch would appear to be replacement by a new design that is not subject to failure in this way. A switch has been designed, fabricated, laboratory tested and has now completed one winter season of field trials. The design involves only shear loading from snow and ice.

LOCOMOTIVE SANDING EQUIPMENT

An investigation into the various possible modes of failure of a locomotive sanding system resulting from low temperature has been undertaken. In addition to the expected failures resulting from moisture freezing in various parts of the pneumatic equipment, two other modes of failure are being investigated further.

HELICOPTER DE-ICING

A study of helicopter icing protection involving the evaluation of various systems (thermal, fluid, and self-shedding materials) and the development of de-icing control systems including ice detectors. The principles for a dynamic ice detector with high sensitivity to be used on helicopters are being investigated. Investigation of methods of establishing a rate function with the dynamic icing detection principle is being conducted.

MISCELLANEOUS ICING INVESTIGATIONS

Analytical and experimental investigations of a non-routine nature, and the investigation of certain aspects of icing simulation and measurement.

TRAWLER ICING

In collaboration with Department of Transport, an investigation of the icing of fishing trawlers and other vessels under conditions of freezing sea spray, and of methods of combatting the problem.

AIR CUSHION VEHICLE ENVIRONMENTAL PROBLEMS

A study has been started on the deposition of snow on sections representing possible tracks for guided ACV's. Snow and ice deposits are being measured and recorded during each winter storm.

A study of snow removal by unconventional methods is being undertaken for high speed transit systems.

AIRBORNE SNOW CONCENTRATION

To provide statistical data on the airborne mass concentration of falling snow in order to define suitable design and qualification criteria for flight through snow, measurements of concentration and related meteorological parameters are being made.

SEA ICE DYNAMICS

Analytical and experimental work on the techniques of forming low-strength ice from saline solutions is being carried out in connection with proposed modelling studies of icebreaking ships and arctic port facilities.

MARINE DYNAMICS AND SHIP LABORATORY

HIGH SPEED CRAFT

Several models in a systematic series have been studied and others are being prepared to determine their performance in still water and in waves.

YACHTS

A program of yacht model studies is underway using equipment and techniques developed in the laboratory.

POLAR ICEBREAKER

A model of a polar icebreaker has been constructed in the laboratory. Extensive studies and development of its design are being made, including power, wake, manoeuvring, seakeeping and icebreaking performance.

BULK CARRIER

A model of a dry cargo vessel has been constructed in the laboratory and a careful investigation is being made to determine the feasibility of its unique design.

CABLE FAIRING

Various types of cable fairings have been investigated for their sway, drag, stacking forces and alignment properties.

FOIL PROGRAM

An experiment program is to be conducted on a model of a hydrofoil main foil, for which program a special dynamometer has been built by the laboratory.

HYDROFOIL DESIGN SERIES

A series of five hydrofoil models is being considered and two have been built for investigation of their hull lift and drag, foil lift and drag seakeeping.

BEHAVIOUR OF SHIPS IN LOCKS

Three radio-controlled Great Lakes cargo vessel models with varying length beam ratios are being built in the laboratory. A study of their behaviour is to be carried out in a Seaway lock model in co-operation with the Hydraulics Laboratory. Investigation will be made of the hydrodynamic forces acting on the vessels during approach and passage through the locks with a view to recommending modifications to the existing lock structures.

OIL DRILLING PLATFORM

Studies on a model are to be made to determine towing forces, joint loading and rotation over a range of wave lengths, speeds, and ballast conditions both in still water and in waves.

RAILWAY LABORATORY

RAILWAY STUDIES

Development of a laser system for measuring angle of attack of the axle to the track.

Assistance to Canadian railroads and T.D.A. (Transport Development Agency) in an investigation of the mechanics of the formation of corrugations on the surface of rail in curves under heavy usage. A short report has been produced. Further tests are being carried out at the Uplands Laboratory on a grain car loaned by the Canadian Government.

Rebuilding of dynamometer car supplied by CP Rail for use as a mobile instrument car and improvements to the present test caboose.

Design and development of a transducer to measure surface movement of wheel and rail during rolling.

RAILWAY DYNAMICS BUILDING (U-89)

The building has been completed.

A rail access road bed to the building has been completed. An experimental switch has been installed with the assistance of CP Rail.

Development of a computer simulation program for the roller rig in conjunction with the Analysis Laboratory. A model of the gear box and motor drive system has been implemented.

Design of control room, rail support, and associated structures to be incorporated in the new building. The weigh scale has been installed.

Development and construction of the control systems for the drive and position motors of the track simulator roller stands continuing.

Development of a vehicle vibration stand. Orders have been placed for electro-hydraulic vibrators and controllers.

NON-CONTACTING LEVEL GAUGE

Development of a non-contacting servo gauge using stepping motor drive for the measurement of tidal levels in hydraulic models.

MEDICAL AIDS TO SURGERY

Continued technical support to two local hospitals in the use of prototype and commercial vessel suturing instruments for clinical surgery, and to their Departments of Experimental Surgery in organ transplant procedures, arterio-venous surgery, etc.

A new form of driving mechanism devised to give reduced actuating forces on the larger sizes of vessel suturing instruments has been proven effective in surgery.

Assistance to Control Systems and Human Engineering Laboratory in the manufacturing of electrodes to improve the recording of electrospinograms.

GENERAL INSTRUMENTATION

The laboratory is co-operating with the Marine Dynamics and Ship Laboratory in the development of the micro-processor controlled ship motion analyzer.

MECHANICAL AIDS TO THE HANDICAPPED

A pocketbook page turner has been developed; one model has been evaluated in the Ottawa Children's Hospital and will now be sent to Toronto for a trial period with young adults.

INSTRUMENTATION AIDS TO INDUSTRY

Adaptation of the automatic passenger counting system for individual vehicles for use with a fluorescent light source.

Development of a multi-channel signal conditioning unit for general use and loan to industry.

Modification of the numerical control (N.C.) editor 'NCEDIT' (LTR-IN-300) to suit a fixed block format of punched tape information for N.C. machines.

The development of a computer assisted programming aid which will allow N.C. tape for a recently acquired N.C. machining centre to be produced economically and accurately using a mini computer and tele-typewriter with paper tape reader/punch.

Continued development of manual programming and N.C. machining techniques to demonstrate the advantages of N.C. machining, e.g. automatic tool changing, simple fixturing and the use of a tape controlled indexer for rotation of the work piece.

Proposals made for measurements of rail tie down forces on sea going vessels are being prepared in collaboration with M.O.T.

A pocket calculator "chip" has been tested in a low cost metric conversion system for machine tool readouts. The present generation of the calculator chips has been demonstrated to be too slow for such applications. A micro-processor based equivalent system is now under development.

STRUCTURES AND MATERIALS LABORATORY

FATIGUE OF METALS

Studies of the basic fatigue characteristics of materials under constant and variable amplitude loading; fatigue tests on components to obtain basic design data; fatigue tests on components for validation of design; studies of the statistics of fatigue failures; development of techniques to simulate service fatigue loading.

RESPONSE OF STRUCTURES TO HIGH INTENSITY NOISE

Study of excitation and structure response mechanisms; study of panel damping characteristics and critical response modes; investigation of fatigue damage laws; industrial hardware evaluation; investigation of jet exhaust noise.

AIRCRAFT AND INDUSTRIAL HYDRAULICS

Cognizance of state of the art maintained in all branches of hydraulics and pneumatics; physical properties of hydraulic fluids and aspects of high pressure, high velocity fluid phenomenon under continuous study.

OPERATIONAL LOADS AND LIFE OF AIRCRAFT STRUCTURES

Instrumentation of aircraft for the measurement of flight loads and accelerations; fatigue life monitoring and analysis of load and acceleration spectra; full-scale fatigue spectrum testing of airframes and components.

ELECTRON FRACTOGRAPHY

Qualitative determination of fracture mechanisms in service failures; fractographic studies of fatigue crack propagation rates and modes.

METALLIC MATERIALS

Structure-property relationships in cast and wrought nickel-base superalloys. Studies of the consolidation and TMT processing of superalloy powders and compacts by hot isostatic pressing, hot extrusion and upset forging; studies on mechanical properties. Mechanics of cold isostatic compaction of metal powders, properties of hydrostatically extruded solids and compacts, extruded at pressures up to 1600 MN/m². Studies of the oxidation/hot corrosion behaviour of coated and uncoated refractory metals and superalloys.

MECHANICS AND THEORY OF STRUCTURES

Stresses in multi-cell caissons for marine structures. Stress concentrations at corners of box structures. Behaviour of plates under high-speed impact, with reference to bird resistance of aircraft windshields.

FLIGHT IMPACT SIMULATOR

Simulator developed and calibrated to capability of accelerating a 4-lb. mass to velocity of 1000 ft/sec and an 8-lb. mass to velocity of 760 ft/sec; operation on year-round basis achieved and includes use of temperature controlled enclosure from -40° to $+130^{\circ}$ F; in addition to airworthiness certification program includes assessment of resistance to impact for materials and structural design for most types of viewing transparencies.

CALIBRATION OF FORCE AND VIBRATION MEASURING DEVICES

Facilities available for the calibration of government, university, and industrial equipment include deadweight force standards up to 100,000 lb., dynamic calibration of vibration pick-ups in the frequency range 10 Hz to 2000 Hz.

COMPOSITE MATERIALS

Studies of composites including resins, crosslinking compounds, polymerization initiators, selection of matrices and reinforcements, application and fabrication procedures, material properties, and structural design.

FINITE ELEMENT METHODS

Development and application of finite element methods to structural problems. Development of refined elements with curved edges. Development of methods for non-linear problems.

MOTOR VEHICLE SAFETY

The mathematical model of the redirection of a vehicle by a cable barrier has been validated experimentally and effort is now being concentrated on the development of a facility for the dynamic measurement of the inertial properties of automobiles by suspending them on air bearings. Engineering charts for the design of flexible road barriers are being prepared.

In collaboration with Ministry of Transport, Road and Motor Vehicle Traffic Safety Branch, studies to determine the performance of headlights in the driver passing task are being carried out. Work is continuing on a system for studying driver performance and traffic quality by the analysis of automatically recorded vehicle control input and response data.

POLICE EQUIPMENT STANDARDS

The NRC/CACP Technical Liaison Committee on Police Equipment is a bilateral arrangement for bringing together police and government personnel to review police equipment requirements, equipment performance specifications, and conformance testing procedures. Work of the Committee is expedited by a permanent Secretariat which has a primary responsibility for continuity in the activities of a number of Sections, each dealing with a particular area of expertise, and for co-ordinating work and specialist contributions from various participating Departments and organizations.

UNSTEADY AERODYNAMICS LABORATORY

DYNAMIC STABILITY OF AIRCRAFT

Development of new techniques for dynamic stability experiments (for NASA).

Determination of cross-derivatives on an aircraft-like configuration at high angles of attack.

Exploratory measurements of vertical acceleration derivatives at transonic and supersonic speeds.

Development of an electro-mechanical calibrator for the existing dynamic cross-derivative apparatus.

ATMOSPHERIC DISTRIBUTION OF POLLUTANTS

Analysis of the downwind vertical spread of gaseous and aerosol pollutants from sources near the ground, with special emphasis on the effect of atmospheric stability.

Instrumentation of a small mobile laboratory for measurements of the concentration and particle size of airborne pollutants.

Application of the above detection system to experiments designed to assess the reliability of analytical methods of dispersion prediction.

TRACE VAPOUR DETECTION

Development of highly sensitive gas chromatographic techniques for detection of trace quantities of vapours of pesticides, explosives and fluorocarbons.

Sensitivity evaluation of commercially available explosive detectors.

Airborne and ground-vehicle based measurements of the spread and distribution of various aerosols and tracer gases.

WORK FOR OUTSIDE ORGANIZATIONS

Wind tunnel experiments for the Defence Research Establishment, Valcartier, involving static force- and-moment measurements, hinge-moment measurements and high-speed cine-camera experiments.

Development and construction of a four-component control-surface balance for the above.

Dynamic moment measurements and flow visualization studies for NASA, using wind tunnel facilities at NAE and at NASA Ames.

Feasibility and design studies for NASA.

Gas-chromatographic experiments for the Department of Transport.

PUBLICATIONS

The following unclassified reports were released during the quarter:

AERONAUTICAL REPORTS

LR-591 CONTROLLED AND UNCONTROLLED FLOW SEPARATION IN THREE DIMENSIONS.

Peake, D.J., National Aeronautical Establishment, July 1976.

The advantages of swept, sharp edges that generate controlled (or fixed) three-dimensional flow separations on a vehicle — because of the qualitatively unchanging flowfield developed throughout the range of flight conditions — are promoted in preference to allowing uncontrolled (or unfixed) separations.

The three-dimensional viscous flowfields and vortical interactions about typical components such as delta wings and bodies at incidence are discussed, in apposition to their use on selected examples of current flight vehicles.

LR-592 THREE-DIMENSIONAL SWEEP SHOCK/TURBULENT BOUNDARY-LAYER SEPARATIONS WITH CONTROL BY AIR INJECTION.

Peake, D.J., National Aeronautical Establishment, July 1976.

Experimentally determined wall pressure distributions, local surface shear stresses and their directions, and detailed turbulent boundary-layer traverses in near zero heat transfer conditions, are presented through skewed shock/boundary-layer interaction regions generated by a wedge standing normal to a test wall. The mainstream Mach numbers were 2 and 4, while the Reynolds number based on the undisturbed test boundary-layer thickness of 0.2-in., growing along the nozzle side-wall of the NAE 5 × 5-in. blowdown wind tunnel, was $\sim 2 \times 10^5$.

Tangential air injection at a jet exit Mach number of 3 was then introduced into the 3D shock separated Mach 2 boundary layer, to control the separation. The optimum direction of blowing was found to be along a line somewhere between the deflected surface of the wedge and the line of the oblique shock wave.

MECHANICAL ENGINEERING REPORTS

ME-243 MODEL STUDY OF A PROPOSED ENGINEERING ACOUSTIC RESEARCH FACILITY.

Johnston, G.W., Rueter, F., Chappell, M.S., Division of Mechanical Engineering, July 1976.

A one-twelfth scale aeroacoustic model of a proposed engineering acoustic research facility has been tested to assess the background noise levels in the anechoic measurement area, and to develop a suitable exhaust collector for deflected jet conditions. The facility comprises an open circuit, open jet wind tunnel with an anechoic space surrounding the test section.

Collector configurations with acceptably low background noise and low sensitivity to jet deflection have been defined, but these features were achieved at the expense of some aerodynamic efficiency.

MECHANICAL ENGINEERING REPORTS (Cont'd)

MP-70 **STUDY OF MIXTURES OF METHANE AND CARBON DIOXIDE AS FUELS IN
A SINGLE CYLINDER ENGINE (CLR)**

Wong, J.K.S., Division of Mechanical Engineering, September 1976.

A single cylinder four stroke engine (CLR) was used to investigate the feasibility of using mixtures of methane and carbon dioxide as an alternate fuel. Effects of fuel quality on engine power output and brake specific fuel consumption were investigated at 800, 1600, 2400, 2800 and 3200 rpm using full throttle setting with various spark timing, equivalence ratio and maximum load. Results indicated that using fuel mixtures having quality of 65/35 or better in methane and carbon dioxide ratio along with optimum spark timing and operating equivalence ratio corresponding to maximum fuel economy, engine power losses and brake specific fuel consumption increases could be kept below 10% compared to the maximum power produced with pure methane fuel.

LABORATORY TECHNICAL REPORTS

National Aeronautical Establishment

- LTR-FR-52 MacPherson, J.I., Bobbitt, N.R.

 A Weather Modification Experiment for Forest Fire Control. NAE Participation
 and Results for 1975.
 April 1976.
- LTR-UA-35 Anstey, C.R.

 Feasibility Study of a 2.5 Inch Diameter High-Load Dynamic Apparatus for Moment
 Derivatives Due to Rolling.
 July 1976.
- LTR-UA-37 Crabbe, R.S.

 Examination of Gradient-Transfer Theory for Vertical Diffusion Over Mesoscale
 Distances Using Instrumented Aircraft.
 August 1976.

Division of Mechanical Engineering

- LTR-AN-30 Gagne, R.E., Inrig, C.M.L.

 BUGOFF — An On-Line Interactive Debugging Package for Digital and Hybrid
 Computers.
 September 1976.
- LTR-CS-156 Isnor, C.D.

 Video Camera and Storage System: Checkout Set Up and Operations Manual.
 May 1976.
- LTR-CS-157 Meunier, C.

 Redesigned Positive Stop Feature for Surgical Pneumatic Drill.
 July 1976.

LABORATORY TECHNICAL REPORTS (Cont'd)

Division of Mechanical Engineering (Cont'd)

- LTR-CS-159 Schwartz, J.-L.
An Electronic Current-Voltage Processor for Membrane Voltage-Clamp Experiments.
August 1976.
- LTR-ENG-50 Krishnappa, G., Bassett, R.W.
Some Aerodynamic and Noise Measurements on Two Centrifugal Blowers.
July 1976
- LTR-GD-42 Savic, P.
Heat Generation in Elastomeric Roll Covers During Pressing Operation. Part 2 —
The Four-Parameter Body.
September 1976.
- LTR-GD-43 Tyler, R.A.
A Novel Industrial Duct: Model Test Results.
September 1976.
- LTR-HY-52 Funke, E.R., Haines, S.A.
Production of Model Armour Units for Scale Breakwaters.
August 1976.
- LTR-HY-53 Modgridge G.R., Baird, W.F.
Estimates of the Power of Wind-Generated Water Waves at Some Canadian Coastal
Locations.
August 1976.
- LTR-IN-352 Aero Photo Inc., Ste Foy, P.Q.
Calibration (July 22, 1976)
- LTR-LT-65 Coveney, D.B., Lane, J.F.
The "Cyclone Switch Heater" for Railway Track Switches.
May 1976.
- LTR-LT-69 Stallabrass, J.R.
Supercooled Fog and Rime Icing Conditions at Ottawa on 25 and 26 February 1976.
August 1976.
- LTR-LT-72 Lane, J.F., Shulhan, G.M., Martin, R.A.
Sea Ice Dynamics Project — First Progress Report.
June 1976.

MISCELLANEOUS PAPERS

- Cooper, K.R., Irwin, H.P.A.H., Wardlaw, R.L. Aerodynamic Investigations of In-line Slender Towers for Heavy Water Plants. Proceedings of the National Structural Engineering Conference — Methods of Structural Analysis, Madison, Wisconsin, 22-25 August 1976.
- Cooper, K.R. Wind Tunnel Investigations of Eight Commercially Available Devices for the Reduction of the Aerodynamic Drag on Trucks. Proceedings of the Annual Conference of the Roads and Transportation Association of Canada, Quebec City, 15 September 1976.
- Cooper, K.R., Holmes, B. Article on Aerodynamic Drag Reducing Devices for Trucks — Motor Truck, September 1976.
- Cooper, K.R. "Motorcycle Aerodynamics", Cycle, Vol. XXVII, No. 9, December 1976.
- Gagne, R.E. Computer-Aided Study of the Scheduling of a BOF Shop. DME Newsletter, Computers, Vol. 6, No. 1, July 1976.
- Gagne, R.E. Computer-Aided Design of a Satellite Attitude Control Systems. DME Newsletter, Computers, Vol. 6, No. 2, July 1976.
- Gould, D.G. Measurements of the Aerodynamic Stability Derivatives of the T-33 Aircraft. Part A — Longitudinal Tests. NAE Lab. Memo FR-75, August 1976.
- Graefe, P.W.U., Nenonen, L.K., Neimanis, M.V., Woodside, C.M. Matte Allocation in a Copper Smelter. Proc. 2nd IFAC Symposium on Automation in Mining, Mineral and Metal Processing. Johannesburg, South Africa, September 1976.
- Hughes, P.C., Abdel-Rahman, T.M. Nonlinear Attitude Control of Very Flexible Communications Satellites. Institute for Aerospace Studies, University of Toronto, Final Report DSS Contract OSU5-0103, July 1976.
- Immarigeon, J.-P., Wallace, W., Van Drunen, G.* The Hot Working Behaviour of Mar M200 Superalloy Compacts. Presented at the Third International Conference on Superalloys, held in Champion, Penn., September 12-15, 1976. Superalloys-Metallurgy & Manufacture Proceedings of the 3rd International Symposium, published by Claitors Publishing Div., Baton Rouge, Louisiana, p. 463.
- Krzymien, M., Elias, L. A Continuous-flow Trace Vapour Source. Journal of Physics E: Scientific Instruments, Vol. 9, No. 7, 1976, pp. 584-586.
- Lau, J., Margerum, J. Application of Pulsed Plasma Accelerators in Thermal Spraying. 8th International Thermal Spraying Conference, Miami Beach, Florida, U.S.A., September 27-October 1, 1976.
- Lee, B.H.K. Near-Field Studies of a Choked Jet Seeded with Upstream Sound. AIAA Journal, Volume 14, No. 2, February 1976.
- Lee, B.H.K. Some Measurements of Spatial Instability Waves in a Round Jet. AIAA Journal, Volume 14, No. 3, March 1976.

* Westinghouse, Canada

MISCELLANEOUS PAPERS (Cont'd)

- MacHattie, L.B.**, Isaac, G.A.*, Bobbitt, N.R. Prospects for Economic Suppression of Large Forest Fires by Induced Showers. Inf. Rep. FF-X-59, Forest Fire Research Institute, June 1976.
- McLean, P.D., Scott, R.F. Preactivation of Epoxide Resins. Presented at the 22nd Meeting of TTCP Panel TP3 Organic Materials, Boston, Mass., July 1976. To be Published in Proceedings.
- McLean, P.D., Scott, R.F., Krichew, L.*** A Position Statement by Canada on Composite Material. Presented at the 22nd Meeting of TTCP Panel TP3 Organic Materials, Boston, Mass., July 1976. To be Published in Proceedings.
- Moellenkamp, G.E., Scott, J.N., Farmer, F.H. A Compressor Station Mini-Computer System for Control, Monitoring and Telemetry. Proc. 13 World Gas Conference, London, England, 1976. (International Gas Union, 17 Grovenor Cres. London, SW1X 7ES)
- Mogridge, G.R., Jamieson, W.W. Wave Forces on Square Caissons. Proc. 15th Coastal Engineering Conference, Honolulu, Hawaii, July 1976.
- Neimanis, M.V., Woodside, C.M., Graefe, U., Nenonen, L.K. Matte Allocation in a Copper Smelter. Proceedings of the Second IFAC Symposium on Automation in Mining, Mineral and Metal Processing, Johannesburg, Republic of South Africa, 13-17 September 1976.
- Pratte, B.D. The Churchill River Salt-Water Tidal Model. Proc. 15th Coastal Engineering Conference, Honolulu, Hawaii, 11-17 July 1976.
- Rangi, R.S. Recent Canadian Activities in Wind Power, Vol. I. Proceedings of Joint Conference "Sharing the Sun" Sponsored by ISES and SESCI, Winnipeg, Man., 15-20 August 1976.
- Romero-Sierra, C., Tanner, J.A., Roomi, M.W., Bigu del Blanco, J. Bipolar Electromagnetic Field Applicator for Skin Wound Repair. Workshop presented at 11th International Conference on Medical and Biological Engineering. Published in Workshop Proceedings, August 1976, pp. 44-45.
- Rueter, F., Giroux, G.J., Fowler, H.S. Comparison of the Performance of Slotted and Solid Aerofoil Blades in a Centrifugal Impeller. NRC Engine Laboratory Memorandum NRC-ENG-88, July 1976.
- Savic, P., Kekez, M.M. Further Support of the Hypersonic and Volterra Models of Spark Channel Development. 4th International Conference on Gas Discharges, Swansea, U.K., September 1976, p. 129.
- Sherman, N.K., Lokan, K.H., Gellie, R.W. Photoneutrons from ¹⁹F. Published in Canadian Journal of Physics, Vol. 54, No. 11, 1976, pp. 1178-1189.
- Templin, R.J., South, P. Canadian Wind Energy Program. Proceedings of the Vertical-Axis Wind Turbine Technology Workshop, Albuquerque, New Mexico, 17-20 May 1976.
- Tucker, H.G. Directional Anemometer for Near-Ground Aircraft Vortex Wake Detection. DME Newsletter, Vol. 8, No. 2, July 1976.

* Atmospheric Environment Service

** Canadian Forestry Service

*** Dept. of National Defence, Ottawa, Ontario

MISCELLANEOUS PAPERS (Cont'd)

- Wallace, W., Trenouth, J.M., Daw, J.D.* Microstructural Instabilities in an Industrial Gas Turbine Engine Vane. Metallurgical Transactions, Vol. 7A, Issue 7, 1976, pp. 991-997.
- Wiebe, W. The Use of the TEM as a Diagnostic Tool for Metal Fracture. Presented at the Third Annual Meeting of the Microscopical Society of Canada, University of Ottawa, Ottawa, Ontario, 23 June 1976. Published in Proceedings.

UNPUBLISHED PAPERS

- Brierley, W.H., Vijay, M.M. Experimental and Theoretical Investigations of Hydraulic Rock Cutting. 31st Annual Petroleum Mechanical Engineering Conference, Mexico City, 19-23 September 1976.
- Caiger, B. The Recovery and Analysis of Accident Data from Flight Recorders in Canadian Transport Aircraft. Presented at AGARD Flight Mechanics Symposium on Operational Experience and its Impact on Safety and Survivability, Sandefjord, Norway, 31 May-3 June 1976.
- Chan, A.W. An Introduction to Industrial Engineering and Operations Research. Analysis Lab. Seminar, 29 September 1976.
- Cooper, K.R. Aerodynamic Investigations of Surface Vehicles. Canadian Wind Engineering Workshop, Toronto, 23-24 September 1976.
- Crabbe, R.S. A Study of Vertical Diffusion in the Atmosphere Using Airborne Gas-Chromatography and Numerical Modelling. Presented at the NBS Symposium on Methods and Standards for Environmental Measurement, Gaithersburg, Md., 20-24 September 1976.
- Elias, L. In-situ Quantification of Background Halo-Fluorocarbon Levels. Presented at the NBS Symposium on Methods and Standards for Environmental Measurement, Gaithersburg, Md., 20-24 September 1976.
- Graefe, P.W.U. Print Shop Order Streaming. Analysis Lab. Seminar, 8 September 1976.
- Hewitt, R.L., Wallace, W. A Model of Powder Compaction. Presented at the Canadian Metal Physics Conference, Kingston, Ontario, June 1976.
- Isaac, G.A.**, MacPherson, J.I., MacHattie, L.B.*** Cumulus Cloud Seeding for Forest Fire Control - Preliminary Seeding Experiments. Presented at Tenth Congress of the Canadian Meteorological Society, Laval University, Quebec City, 26-28 May 1976.
- Templin, R.J., South, P. Some Design Aspects of High-Speed Vertical-Axis Wind Turbines. Paper delivered to International Symposium on Wind Energy Systems, Cambridge, England, 7-9 September 1976. (To be Published in Proceedings).
- Templin, R.J. Wind Energy Research in Canada. Canadian Wind Engineering Workshop, Toronto, 23-24 September 1976.

* Westinghouse Canada, Hamilton, Ontario
** Atmospheric Environment Service
*** Canadian Forestry Service

UNPUBLISHED PAPERS (Cont'd)

Wardlaw, R.L.W. Problems in the Design of Structures Against Wind Action. Engineering Foundation Conference, Full-Scale Structural Testing, Rindge, New Hampshire, 19-23 July 1976.

TECHNICAL TRANSLATIONS

The following translations requested by NAE staff were published in our Technical Translation series in the quarter ending September 30, 1976.

TT-1883 U.S.S.R. Ministry of Railroads, All-Union Research Institute of Railroads.

\$2.20 Properties of Volume-Hardened Rails (Brinell Hardness 331-388) used on Soviet Railroads. (Svoistva ob'emno-zakalennykh rel'sov (s tverdost'yu poryadka 331-388 edinits po Brinellyu), ispol'zuemykh na zheleznykh dorogakh SSSR).

AERONAUTICAL AND MECHANICAL ENGINEERING LIBRARY

Statistical Summary for July 1 – September 30, 1976

Documents accessioned (including duplicates)	3821
Cards added to catalogue	6639
Books received	1135
Bound periodicals received	67
Loans to NRC staff (including Periodical circulation and Xerox and Microfiche copies in lieu of loans)	4520
Loans and distribution to outsiders	2892
Total circulation	7412
Information inquiries (quick references)	5360
Literature searches and bibliographies	402

NOTE: The Uplands Library is no longer a sub-branch of the Aero/ME Library. However, all documents for the Uplands Library are indexed and all document catalogue cards produced by the Aeronautical and Mechanical Engineering Library.

UPLANDS LIBRARY

Statistical Summary for July 1 — September 30, 1976

Regular loans made to NRC divisional staff	682
Loans to CISTI and NRC branch libraries	104
Loans to outside NRC:	
a. Universities	9
b. Industries	2
c. Govt. Depts	10
	21
Periodical rapid circulation	1017
Xeroxed copies supplied in lieu of loans	166
TOTAL LOANS FOR THE QUARTER	1990
Documents accessioned (including duplicates)	721
Cards added to catalogue:	
a. Book cat.	390
b. Document	3177
	3567
Books received	29
Bound periodicals received	33
Information inquiries (quick reference)	888
Literature searches	118

